UNIVERZITA KARLOVA
Přírodovědecká fakulta
Katedra buněčné biologie

Studijní program: Biologie
Studijní obor: Imunologie

Bc. Michal Kraus

Role mitochondriálního komplexu II v biologii nádorové buňky

The role of mitochondrial complex II in cancer cell biology

Diplomová práce

Školitel: prof. Ing. Jiří Neužil, CSc.

Praha, 2021

Prohlašuji, že jsem tuto diplomovou práci zpracoval samostatně pod vedením prof. Ing. Jiřího Neužila, CSc., a že jsem uvedl všechny použité informační zdroje a literaturu. Tato práce ani její podstatná část nebyla předložena k získání jiného nebo stejného akademického titulu.

V Praze dne ..... Podpis: .....

Acknowledgements

First and foremost, I would like to express my sincere gratitude to my supervisor Professor Jiří Neužil, the Head of the Laboratory of Molecular Therapy on the Institute of Biotechnology of the Czech Academy of Sciences, for giving me the opportunity to be part of such outstanding international research team. I also thank Professor Neužil for providing me guidance and feedback throughout the fascinating project of mitochondrial complex II biology.

Furthermore, I would like to give very special thanks to Dr. Jakub Rohlena and Dr. Kateřina Hadrava Váňová for all methods I learned from them, and for their valuable insights and advice that helped in the completion of this thesis.

My thanks also go to every member of the Laboratory of Molecular Therapy, especially to Dr. Šárka Dvořáková, Dr. Zuzana Nahácka and Mgr. Soňa Bálintová for their everyday invaluable help and support during work on the complex II project. I am also grateful to my friend, Bc. Michaela Vondráčková, who has supported me throughout this venture with her unceasing optimism and encouragement.

Last but not least, I thank my family for always being supportive and understanding. Finally, I owe my gratitude to my partner, Marek Ječmen, for all the love and hope he has given to me, for being always there and, especially, for the sacrifices he has made in order for me to pursue this Master's thesis.

Abstrakt

Mitochondrie jsou pro většinu eukaryotických buněk nezbytné organely, které obsahují řadu komplikovaných, vzájemně interagujících proteinových struktur. Mezi ně patří mimo jiné i komplexy elektron transportního řetězce, tedy komplexy I – IV. Mitochondriální komplex II hraje klíčovou roli v buněčném metabolismu, neboť leží na křižovatce mezi cyklem trikarboxylových kyselin a dýchacím řetězcem. Tento proteinový komplex, též zvaný sukcinát dehydrogenáza, zprostředkovává nejen oxidaci sukcinátu a přenos elektronů, ale také se podílí na tvorbě reaktivních forem kyslíku. Mitochondriální komplex II sestává ze čtyř podjednotek zvaných SDHA-D, navíc sestavení komplexu vyžaduje čtyři proteinové asemblační faktory SDHAF1-4. Mutace a epigenetické změny genů podjednotek a asemblačních faktorů sukcinát dehydrogenázy jsou spojeny s různými patologickými stavy, jako jsou například neurodegenerativní onemocnění, nebo mohou stát za vnikem nádorů. Mitochondriální nemoci způsobené vrozenými poruchami komplexu II nicméně nejsou tak dobře prostudovány jako například onemocnění vzniklá z důvodu nefunkčnosti ostatních mitochondriálních komplexů, zřejmě proto, že žádný protein komplexu II není kódován v mitochondriálním genomu. Nedávné studie ukázaly, že narušení funkce nebo skládání komplexu II vede k akumulaci alternativně asemblované formy komplexu, složené z podjednotky SDHA a asemblačních faktorů SDHAF2 a SDHAF4, která může mít signalizační funkci v rámci mitochondrií. Cílem této práce je objasnit roli sukcinát dehydrogenázy u nádorových onemocnění, především v případě nádorů, které se vyznačují mutacemi v podjednotkách tohoto komplexu, jež právě mohou dát vzniku jeho alternativně asemblované formě. Alternativní forma komplexu II je studována v buňkách s chybějícími asemblačními faktory SDHAF2 a SDHAF4, s důrazem na protein SDHAF4, jehož přesná funkce v rámci skládání komplexu II není zcela objasněna.

Klíčová slova: mitochondrie, elektronový transportní řetězec, mitochondriální komplex II, sukcinát dehydrogenáza, sukcinát, nádorová onemocnění

Abstract

Mitochondria are essential organelles for most eukaryotic cells, containing intricate networks of numerous proteins. These include, among others, complexes I–IV of the electron transport chain. Being at the crossroads of the tricarboxylic acid cycle and the respiratory chain, mitochondrial complex II plays a key role in cellular metabolism. The protein complex, also known as succinate dehydrogenase, is capable of not only succinate oxidation and electron transfer but also contributes to the production of reactive oxygen species. Mitochondrial complex II consists of four subunits, SDHA-D, and four dedicated protein assembly factors SDHAF1-4 that participate in complex II biogenesis. Mutations and epigenetic modulations of genes coding for succinate dehydrogenase subunits or assembly factors are associated with pathological conditions such as neurodegenerative diseases, or may result in tumor formation. However, inborn complex-II-linked mitochondrial pathologies are rather understudied, compared to diseases with causative errors of other mitochondrial complexes, presumably due to the fact that none of complex II subunits is encoded in the mitochondrial genome. Recent studies have shown that impairment of mitochondrial complex II function or assembly leads to accumulation of alternative assembly forms of the complex, comprising subunit SDHA and assembly factors SDHAF2 and SDHAF4, with potential signaling function in mitochondria. The overall aim of this thesis is to study the role of succinate dehydrogenase in cancer, primarily in tumors exhibiting mutations in genes encoding complex II subunits, which may result in the complex alternative assembly forms. The alternative forms are then studied in cells lacking SDHAF2 and SDHAF4, with particular emphasis on the SDHAF4 protein, whose role within complex II assembly has not been fully elucidated.

Keywords: mitochondria, electron transport chain, mitochondrial complex II, succinate dehydrogenase, succinate, cancer

Contents

List of abbreviations

5mC	5-methyl cytosine
AA	Amino acid
ADP	Adenosine diphosphate
ATP	Adenosine triphosphate
cAMP	Cyclic adenosine monophosphate
CII	Complex II
CII_{low}	Alternative assembly form of complex II
CoA	Coenzyme A
CoQ	Coenzyme Q, ubiquinone
CRISPR	Clustered regularly interspaced short palindromic repeats
crRNA	CRISPR RNA
CTLA-4	Cytotoxic T-lymphocyte antigen 4
DC	Dendritic cell
DCPIP	2,6-Dichlorphenol indophenol
DHODH	Dihydroorotate dehydrogenase
DIC	Dicarboxylate carrier
dKO	Double-gene knockout
DMSO	Dimethyl sulfoxide
DNA	Deoxyribonucleic acid
EDTA	Ethylenediaminetetraacetic acid
ERK1/2	Extracellular signal-regulated kinase 1/2
ETC	Electron transport chain
ETF-QO	Electron transfer flavoprotein-ubiqionone oxidoreductase
FA	Fatty acid
FAD	Flavin adenine dinucleotide
FBS	Fetal bovine serum
FH	Fumarate hydratase
GDP	Guanosine diphosphate
GIST	Gastrointestinal stromal tumors
GPR91	G-protein-coupled receptor 91
HIF	Hypoxia inducible factor
hPheo1	Human pheochromocytoma cell line 1
HSC20	DnaJ homolog subfamily C member 20
hrCNE	High resolution clear native electrophoresis
Hsp	Heat-shock protein
HSPA9	Heat shock 70 kDa protein 9
IDH	Isocitrate dehydrogenase
IGF1	Insulin-like growth factor 1
IGF1R	Insulin-like growth factor 1 receptor
IL	Interleukin
IMM	Inner mitochondrial membrane
IMS	Intermembrane space
ISC	Iron-sulfur cluster synthesis machinery
ISCU	Iron-sulfur cluster assembly, NifU-like protein
ISD11	Iron-sulfur protein biogenesis, desulfurase-interacting protein 11
JMJ	Jumonji
KIT	Tyrosine-protein kinase KIT

KO	Gene knockout
LPS	Lipopolysaccharide
MAX	MYC Associated Factor X
MCT1	Monocarboxylate transporter 1
MGMT	O6-methylguanine DNA methyltransferase
MitoTam	Mitochondrially-targeted tamoxifen
MM	Mitochondrial matrix
MPC	Mouse pheochromocytoma cell line
MPP	Mitochondrial processing peptidase
mRNA	Messenger RNA
mtDNA	Mitochondrial DNA
MEN-2	Multiple endocrine neoplasia 2 syndrome
MTS	Mitochondrial targeting sequence
MTT	Mouse tumor-tissue derived cell line
NADH	Nicotinamide adenine dinucleotide
NBGE	Native blue gel electrophoresis
NF1	Neurofibromatosis type 1
NFS1	Nitrogen Fixation 1 Homolog (*S. Cerevisiae*)
NK cell	Natural killer cell
NK-T cell	Natural killer T cells
NTB	Nitro tetrazolium blue
Oct1	Octapeptidyl aminopeptidase 1
OMM	Outer mitochondrial membrane
OXPHOS	Oxidative phosphorylation
PARP	Poly (ADP-ribose) polymerase
PBS	Phosphate buffer saline
PC	Pyruvate decarboxylase
PCC	Pheochromocytoma
PCR	Polymerase chain reaction
PD-1	Programmed cell death receptor 1
PDGFRA	Platelet Derived Growth Factor Receptor Alpha
PD-L1/2	Programmed cell death receptor ligand 1/2
PGL	Paraganglioma
PHD1-3	Prolyl hydroxylases 1-3
PMS	Phenazine methosulfate
PVDF	Polyvinylidene difluoride
RCC	Renal cell carcinoma
RET	Reverse electron transfer
RET gene	Rearranged during transfection' gene
RNA	Ribonucleic acid
RORγT	Retinoic-acid-receptor-related orphan nuclear receptor gamma
ROS	Reactive oxygen species
RT	Room temperature
SDH	Succinate dehydrogenase
SDHA-D	Succinate dehydrogenase subunit A-D
SDHAF1-4	Succinate dehydrogenase assembly factor 1-4
SDHAFx	Considering any of CII assembly factors
SDHx	Considering any of CII subunits or assembly factors
SDS	Sodium dodecyl sulfate

SDS-PAGE	Sodium dodecyl sulfate – polyacrylamide gel electrophoresis
sgRNA	Single guide RNA
SIRT	NAD-dependent protein deacetylase sirtuin
SQR	Succinate-ubiquinone oxidoreductase
STE	Sucrose-Tris-EDTA buffer
SUCL	Succinyl-CoA ligase
SUCNR1	Succinate receptor 1
TAE	Tris-Acetic acid-EDTA buffer
TAM	Tumor-associated macrophage
TBS	Tris buffer saline
TCA cycle	Tricarboxylic acid cycle
TET	Ten eleven translocation
T_H cell	Helper T cell
TIM	Translocase of the inner membrane
TMEM127	Transmembrane Protein 127
TOM	Translocase of the outer membrane
TRAP1	TNFR-associated protein 1
VDAC	Voltage dependent anion channel
VEGFA	Vascular endothelial growth factor A
VHL	Von-Hippel Lindau
WB	Western blotting
WT	Wild-type
α-TOS	a-Tocopheryl succinate

1. Introduction

1.1. Mitochondrion: a cell within a cell

1.1.1. Mitochondrial morphology, genome and proteome

With development of light microscopy in the 19th century, researchers observed various filamentous (mito) and granular (chondria) structures within the cytosol of eukaryotic cells. Advanced staining techniques and invention of electron microscopy led to the finding that both structures are homologous, hence named mitochondria [1]. Mitochondria are essential organelles for vast majority of eukaryotic cells, except for few protozoan anomalies completely lacking any mitochondria-like structures [2]. The generally accepted endosymbiont hypothesis explains the origin of the mitochondria as engulfment of a hydrogen-producing α-proteobacterium (mitochondrial ancestor) by a hydrogen-requiring amitochondrial cell (eukaryotic cell ancestor) [3, 4]. The organelles generally resemble few micrometres long bacteria, and a eukaryotic cell may contain from few hundreds to hundreds of thousands of individual mitochondria [5]. Notably, rather than individual organelles, mitochondria assemble into a network maintained by permanent fusion and fission [6]. Consistently with the endosymbiotic theory, a mitochondrion consists of two phospholipid bilayers - outer and inner mitochondrial membrane (OMM and IMM) – that highly diverge; whereas the OMM is similar to other eukaryotic membranes, proteins of the IMM more or less resemble those of bacteria. These two membranes then create intermembrane space (IMS) between them, with mitochondrial matrix (MM) bordered by the IMM. The IMM forms sheet-like or tubular invaginations called cristae, greatly increasing its surface [7].

Human mitochondrial genome is represented by 16,569 base pairs long circular molecule of mitochondrial DNA (mtDNA) within the MM [1]. The mitochondrial genome contains overall 36 genes – 13 protein encoding genes[1] for subunits of respiratory complexes I, III, IV and V [6], 2 ribosomal RNA sequences (12S and 16S) and 22 transfer RNAs employed in the translation process within the mitochondrion [10]. Noteworthy, mitochondrial genome is almost exclusively maternally inherited, as paternal mitochondria are degraded after the fertilization of the egg [11].

[1] Studies of last two decades revealed that mitochondrial 16S ribosomal RNA further contains a sequence, which is translated into peptide humanin when transported to cytosol, serving in oxidative stress resistance [8]; and 12S rRNA contains an ORF translated as MOTS-c peptide in cytosol, with the peptide participating in metabolic homeostasis [9].

In total, more than 1,000 genomic-DNA-encoded proteins, on top of 13 polypeptides encoded by mtDNA, constitute mitochondrial proteome that alters depending on individuals, tissues and cell types [6]. The proteins, alone or assembled into complexes, then contribute to mitochondrial morphology, homeostasis, or are involved in various metabolic processes such as the activity of respiratory complexes I-V in oxidative phosphorylation (see the chapter *Oxidative phosphorylation*) [12].

1.1.2. Maintenance of mitochondria

Mitochondria form continuous dynamic network by fusing and segregating via dynamin-related proteins [6], which is controlled by contact with the endoplasmic reticulum [6] and AMP-activated protein kinase (AMPK) [13]. Newly formed mitochondria carry the genome, whose replication is catalyzed by DNA polymerase γ, and are distributed along microtubules by means of Miro adaptors mediated via kinesin motors [6, 14]. Upon damage or decrease in mitochondrial membrane potential[2], mitochondria are degraded by autophagosomal engulfment by lysosomes in a process named mitophagy [17].

Mitochondrial genes are expressed using the organellar own machinery represented by polycistronic mRNA transcripts and slightly altered genetic code, distinct from the eukaryotic transcription and translation apparatus [18, 19]. The remaining 99% of mitochondrial proteins are encoded in the nuclear DNA, synthetized in the cytosol and transported into mitochondria. Majority of imported mitochondrial proteins carry mitochondrial targeting sequence (MTS), typically 15 – 50 amino acids in the N-terminus. Translocase of the outer membrane (TOM) complex recognizes the MTS and imports the pre-proteins across the OMM, and translocase of the inner membrane (TIM) complex transports the polypeptides further into the matrix [20]. The MTS is then cleaved by mitochondrial processing peptidase (MPP) or octapeptidyl aminopeptidase 1 (Oct1) [12, 21]. Proteins anchored in the membrane are either inserted via the oxidase assembly (OXA) insertase, or the translocation through the TIM channel is directly arrested due to a specific sequence, leaving the protein within the membrane. In addition, several other routes of mitochondrial protein transport exist [12]. Chaperones, such as mitochondrial Hsp70 and Hsp60, further help the imported proteins to fold properly [22, 23], since misfolded proteins may trigger the mitochondrial unfolded protein stress response, potentially resulting in mitophagy [17].

[2] Mitochondrial membrane potential (ΔΨm) is a gradient in electric potential and proton concentration across the IMM, maintained via proton-pumping action of respiratory complex I, III and IV (chapter *Oxidative phosphorylation*). ΔΨm is essential for cell viability, and, interestingly, cancer cells may exhibit higher level of ΔΨm [15, 16].

Correct protein folding is also important as many mitochondrial proteins assemble into intricate multi-subunit complexes, such as complexes I-V of oxidative phosphorylation machinery, additionally exploiting numerous dedicated assembly factors [24].

1.1.3. Indispensable roles of mitochondria

One of the key functions of mitochondria is execution of the tricarboxylic acid (TCA) cycle and electron transport chain (ETC) with subsequent adenosine triphosphate (ATP) production. However, anabolic rather than catabolic processes seem to be the fundamental role of mitochondria.

1.1.3.1. Anabolic processes

Certain anaerobic protozoans harbor reduced forms of mitochondria – hydrogenosomes or mitosomes – that may lack all known functions except for iron-sulphur (Fe-S) cluster synthesis [25, 26]. Highly conserved Fe-S cluster synthesis machinery (ISC) plays an indispensable role in most organisms, originating in bacteria (encoded by the *isc* operon) [27]. The ISC complex generates inorganic cofactors for many enzymes employed in the ETC, the TCA, and DNA metabolism [28]. Another iron-containing prosthetic group, heme, is also synthesized via a multi-step process within mitochondrial matrix, further serving as a prosthetic group in many hemoproteins. It is necessary for numerous essential processes, such as gasses transport, detoxification and the activity of the ETC [29].

Ribonucleotides and deoxyribonucleotides are synthesized via two pathways, either salvage pathway or *de novo* biosynthesis. Interestingly, pyrimidine synthesis requires the enzyme dihydroorotate dehydrogenase (DHODH) embedded in the IMM, which passes electrons to the ETC [30]. Mitochondria also harbor enzymes involved in several amino acid (AA) synthesis pathways – glutamate, glutamine, aspartate, alanine and proline. Ammonia, generated during AA catabolism, is incorporated into the ornithine molecule within the MM, contributing to the ornithine (urea) cycle. Furthermore, mitochondria mediate the initiating step of gluconeogenesis [31]. Most lipids are synthesized in the endoplasmic reticulum, cardiolipin and phosphatidylethanolamine originate predominantly in mitochondrial membrane [32]. Mitochondria also produce coenzyme Q (CoQ, ubiquinone) that plays a key role as an electron carrier in the ETC [12].

1.1.3.2. Mitochondria-mediated signaling

Besides an indispensable role of a metabolic hub, mitochondria participate in signaling pathways essential for cell survival. Most notably, mitochondrial outer membrane permeabilisation (MOMP) is a step triggered by distinct intrinsic stimuli, leading to cytochrome *c* release, apoptosome formation and caspase-3-dependent apoptosis [33].

Reactive oxygen species (ROS) are byproducts mostly generated by aerobic metabolism of the ETC. While ROS cause mainly detrimental oxidative stress, the molecules are also capable of modulating gene expression [34] and some cancer cells are directly dependent on elevated ROS levels [35]. Importantly, in immunocompetent cells, ROS promote and mediate both innate [36] and adaptive immune responses [37].

1.1.3.3. Catabolic pathways

Energy of the chemical bonds is yielded via the TCA cycle and the ETC, using various 'input' molecules. Glucose catabolism, glycolysis, is traditionally depicted as a cascade of ten subsequent enzymatic reactions within the cytosol, leading to two three-carbon molecules of pyruvate, with production of two molecules of ATP and two molecules of reduced nicotinamide adenine dinucleotide (NADH) from one glucose molecule. Under anaerobic conditions, pyruvate may be reduced to lactate using NADH via lactate dehydrogenase (LDH) [38]. Under normoxia, pyruvate enters the mitochondrion via its carrier in the IMM for further aerobic utilization [39]. However, some cells rely almost entirely on glycolysis even under aerobic environment (typically cancer cells or activated T lymphocytes) with elevated production of lactate, which is called Warburg effect [40, 41]. Within mitochondria, pyruvate is a substrate for the pyruvate dehydrogenase complex (PDC). The complex catalyzes reactions that generate acetyl-coenzyme A (acetyl-CoA), which enters the TCA cycle; CO_2 and NADH. The complex therefore serves as a gatekeeper of many metabolic pathways and is strictly regulated by kinases and phosphatases [42]. Alternatively, pyruvate may be utilized via pyruvate decarboxylase (PC), producing oxaloacetate, an intermediate of the TCA cycle [43].

The process of AA breakdown begins with transamination, i. e. transfer of the NH_3 group from the α-carbon of AA onto an α-keto acid. Respective de-aminated intermediates then follow individual degradation pathways, resulting in either glucogenic molecules (pyruvate, α-ketoglutarate, succinyl-CoA, fumarate, oxaloacetate), ketogenic molecules (acetyl-CoA, acetoacetate), or both. Breakdown products then may serve for further synthesis of glucose, ketone bodies or enter the TCA cycle [38]. Interestingly, some cancer cells or activated T cells fuel the TCA cycle primarily by glutamine breakdown [44, 45].

Fatty acids (FAs) 'preserve' considerable amount of energy. The OMM enzyme carnitine palmitoyltransferase 1 (CPT1) links carnitine to fatty acyl-CoA, forming acyl-carnitine which may now be transported into the mitochondrial matrix where the CPT2 enzyme releases carnitine and links FA to CoA [31].

FA-CoA within the MM then undergoes the β-oxidation process, wherein each reaction cycle shortens the FA chain by two carbons, yielding one acetyl-CoA, one NADH and one $FADH_2$. Thus, FA oxidation is able to fuel both the TCA cycle (acetyl-CoA) and the ETC, directly (NADH) and indirectly ($FADH_2$)[3] [38].

1.1.4. Tricarboxylic acid cycle

As far back as in 1937, Hans Krebs first observed that adding three-carbon pyruvate or lactate to muscle tissue leads to production of four-carbon acids, such as succinate, and proposed that occurs due to oxidation of citric acid. Other researchers then described several reactions that completed cyclic sequence of the reactions - tricarboxylic acid (TCA; citric acid, Krebs) cycle [47]. Acetyl-CoA from various sources mainly fuels the TCA cycle, which comprises several enzymes within the MM, with the exception of the IMM-anchored succinate dehydrogenase, exerting eight following reactions (depicted in *Introduction figure 1*) [1, 38]:

1. Citrate synthase (CS) condensates acetyl-CoA with oxaloacetate and H_2O, forming citrate (tricarboxylic acid).
2. Aconitase[4] (ACO) catalyzes conversion of citrate to isocitrate via intermediate cis-aconitate.
3. Isocitrate dehydrogenase (IDH) mediates decarboxylation of isocitrate, producing α-ketoglutarate (α-KG), CO_2 and NADH.
4. α-Ketoglutarate dehydrogenase (α-KGDH) links a carbon chain to CoA, generating succinyl-CoA and releasing again CO_2 and NADH.
5. Succinyl-CoA ligase (SUCL) cleaves the high energetic bond and utilizes the energy to form GTP (or ATP) from GDP (ADP)[5] and inorganic phosphate, releasing succinate.
6. Succinate dehydrogenase (SDH) oxidizes succinate to fumarate, forming $FADH_2$ and passing the electrons onto CoQ within the ETC.
7. Fumarate hydratase (FH) catalyzes H_2O addition, converting fumarate into malate.
8. Malate dehydrogenase (MDH) oxidizes malate into oxaloacetate with NADH generation.

[3] Electrons from $FADH_2$ are transferred via electron transfer flavoprotein-ubiqionone oxidoreductase (ETF-QO) onto ubiquione, contributing to the ETC [46].
[4] Cytosolic portion of the enzyme aconitase serves as an iron-responsive protein. When iron is scarce, aconitase binds to iron-responsive elements of mRNA encoding ferritin and transferrin receptor, attenuating and promoting its translation, respectively [48].
[5] Two-subunit enzyme succinyl-CoA ligase (SUCL) comprises α subunit SUCLG1 and one of two β subunits – SUCLG2 binding GDP and SUCLA2 specific for ADP [49].

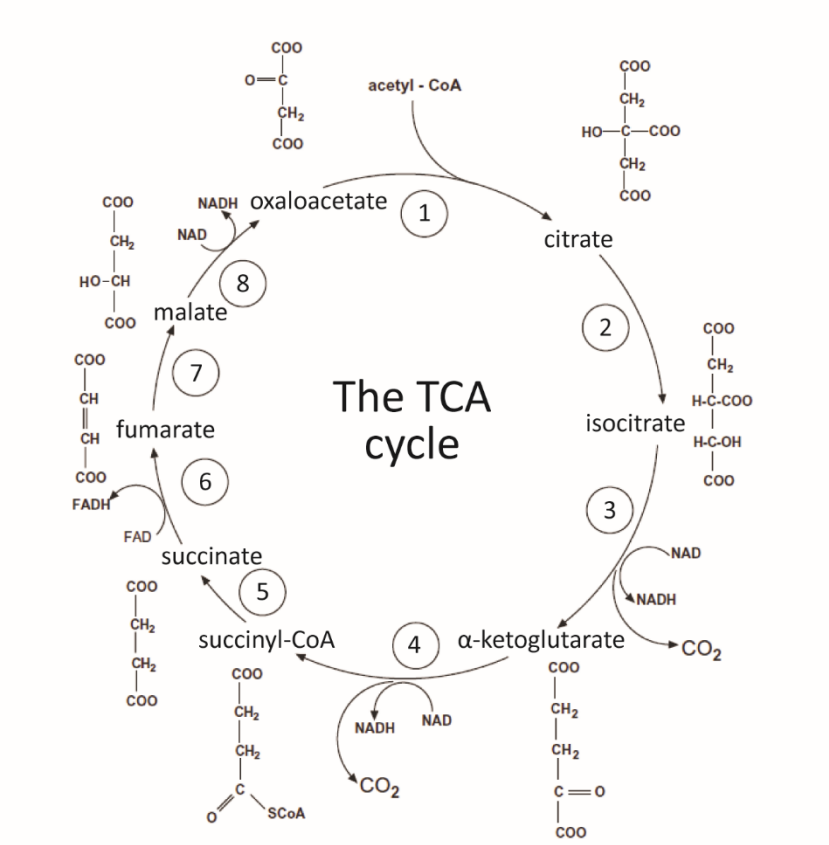

Introduction figure 1 – The tricarboxylic acid (TCA) cycle diagram. The reaction cycle employs eight enzymes, with the numbers corresponding to the TCA cycle description above. Adapted from [1].

Taken together, the reaction summary of the TCA cycle is [1, 38]:

$$\text{Acetyl-CoA} + 3\text{NAD}^+ + \text{CoQ} + \text{GDP (ADP)} + \text{P}_i \rightarrow \text{CoA} + 3\text{NADH} + \text{CoQH}_2 + \text{GTP (GDP)} + 2\text{CO}_2$$

The TCA cycle is an intricately regulated metabolic process, readily adapting to changing conditions and meeting the energetic requirements. Several cycle intermediates act as allosteric and competitive inhibitors or activators of other TCA cycle enzymes; for example, oxaloacetate attenuates the function of succinate dehydrogenase [50]. Moreover, in case of disrupted ETC, accumulated NADH impedes several TCA cycle enzymes. Likewise, ATP accumulation allosterically inhibits PDH and IDH [51].

Fundamental function of the TCA cycle is to oxidize acetyl-CoA to CO_2. Nonetheless, various catabolic and anabolic processes participate in input and output of the intermediates, respectively, depending on the cell type or specific metabolic requirements. For instance, citrate is cleaved in the cytosol by ATP citrate lyase (ACLY) to oxaloacetate and to acetyl-CoA, which is further used for FA synthesis [52]. Phosphoenolpyruvate carboxykinase (PEPCK) exploits oxaloacetate for generation of phosphoenolpyruvate (PEP), which is exported from mitochondria and further utilized for gluconeogenesis; as well as malate may also serve for glucose production. The process of outflow of the TCA cycle intermediates

necessitates simultaneous influx of the molecules in order to maintain a balance of the TCA cycle reactions. This ensures the enzyme PC, converting pyruvate to oxaloacetate. Importantly, AA breakdown generates several TCA cycle intermediates, thus replenishing the cycle [53]. Taken together, the TCA cycle acts as a roundabout on a bustling highway of mitochondrial metabolism with carefully maintained balance between individual traffic participants entering and leaving the cycle.

1.1.4.4. The signaling role of tricarboxylic acid cycle metabolites

In addition to the metabolic utilization, the TCA cycle intermediate metabolites play a significant part in signaling in physiology, pathology or immune system function. A cell strictly maintains its acetyl-CoA pool, since the molecule is essential for major posttranslational protein modification, acetylation. Thus, high level of cytosolic acetyl-CoA leads to a shift in gene expression (due to histone acetylation) mostly toward proliferation, as seen in some cancer cells [54] and activated T cells [55], or to pro-inflammatory responses in macrophages [56]. Anti-microbial activity of macrophages necessitates itaconate, a molecule generated from cis-aconitate that further supports anti-inflammatory environment [57]. Enzymes employed in another protein modifying process, hydroxylation, use molecules of α-ketoglutarate and O_2. Certain level of the TCA cycle intermediate is needed for maintenance of normoxic phenotype due to the enzymes prolyl hydroxylases (see the chapter *Pseudohypoxia*). Nevertheless, α-ketoglutarate may be metabolized to 2-hydroxyglutamate, especially due to gain-of-function mutations in the *IDH* gene [58] or in high level of NADH (e. g. caused by ETC disruption). 2-Hydroxyglutamate then acts as a typical oncometabolite that promotes cancer formation by inhibiting DNA demethylation and subsequent altered gene expression [59]. Other two TCA cycle oncometabolites, succinate and fumarate, are discussed in detail in the chapter *Mechanisms of tumorigenesis*.

1.1.5. Oxidative phosphorylation

Electrons formed in the TCA cycle (or glycolysis and FA breakdown) are transferred via NADH into the ETC. It comprises multimeric respiratory complexes I–IV that transport electrons along increasing redox potential of metal centres of the complexes, with two freely moving electron carriers – ubiquinone (CoQ)[6] and cytochrome *c*, shuttling electrons between the respiratory complexes. Energy of electron transfer between complex I, III and IV is used to pump protons from the MM into the IMS, generating mitochondrial membrane potential ($\Delta\Psi m$).

[6] In addition, DHODH and ETF-QO also contribute to the ETC by reducing ubiquinone [30, 46].

Respiratory complex V then utilizes the proton gradient to synthetize ATP. The whole process of oxidative phosphorylation (OXPHOS) hence constitutes a series of oxidation-reduction reactions of the ETC and phosphorylation of ADP (see *Introduction figure 2*) [1, 38].

Complex I (NADH-ubiquinone oxidoreductase) is the largest complex, composed of 45 protein subunits. The MM-pointing part of complex I oxidizes NADH, transferring electrons via flavin mononucleotide (FMN) and several Fe-S clusters to the ubiquinone-binding site, reducing the ubiquinone molecule present in the IMM. Energy from oxidation-reduction transition of electrons results in conformational changes in four proton channels within the IMM part of complex I, mediating unidirectional flow of protons from the MM into the IMS [60, 61]. The complex-I-catalyzed reaction can be described as follows [1, 62]:

$$NADH + CoQ + 5H^+ (MM) \rightarrow NAD^+ + CoQH_2 + 4H^+ (IMS)$$

Complex II (succinate dehydrogenase, SDH), is the smallest OXPHOS complex, comprising only four subunits. Interestingly, all subunits are encoded within the nuclear genome, unlike other complexes, which have 1–7 subunits encoded by mtDNA [1]. Complex II catalyzes oxidation of succinate to fumarate, thus participates in the TCA cycle; however, electrons from the reaction are used for ubiquinone reduction within the ETC. Respiratory complex II harbors several cofactors as flavin adenine dinucleotide (FAD), Fe-S clusters and a heme group. Although complex II does not contribute to proton transfer across the IMM, the complex plays a pivotal role in mitochondrial metabolism, being part of both the TCA cycle and the ETC [63]. Respiratory complex II is analyzed in detail in the chapter *Mitochondrial complex II*. Complex II catalyzes the following reaction [1, 62]:

$$succinate + CoQ \rightarrow fumarate + CoQH_2$$

Complex III (ubiquinol-cytochrome *c* oxidoreductase or cytochrome bc_1 complex) with its 11 subunits accepts electrons from the pool of reduced ubiquinone (from complex I and II or other enzymes[6]) on the IMS side. Electrons are then transferred in two pathways – via Fe-S clusters onto cytochrome *c*, and simultaneously via two heme groups again to a ubiquinone molecule (on the MM site). This cyclic oxidation and reduction of ubiquinone on the opposite sides of the IMM (Q-cycle) results in proton transfer across the membrane [64, 65]. Reduced cytochrome *c*, which moves freely within the IMS or bound to a cardiolipin molecule, passes electrons further to complex IV [66]. The overall reaction catalyzed by the complex is:

$$2CoQH_2 (IMS) + 2cyt\ c^{3+} + CoQ (MM) + 2H^+ (MM) \rightarrow 2CoQ + 2cyt\ c^{2+} + CoQH_2 + 4H^+ (IMS)$$

Complex IV (cytochrome *c* oxidase) is formed by 13 or 14 subunits [67] and constitutes the last step of the ETC. Cytochrome *c* binds to complex IV, transferring electrons via various metal centers and heme cofactors into the active site of the complex, where the reaction of final transfer of the electrons to O_2 molecule occurs, forming H_2O [68, 69]. Part of the protons from the MM is utilized for H_2O generation, part is also pumped out to the IMS by complex IV via three proton channels, similarly as in complex I [69]. The overall complex IV reaction is the following [1, 62]:

$$4\text{cyt } c^{2+} + 8H^+ (\text{MM}) + O_2 \rightarrow 4\text{cyt } c^{3+} + 2H_2O + 4H^+ (\text{IMS})$$

Complex V (ATP synthase or F_oF_1-ATPase) is an exceptionally elaborate molecular machine, comprising 29 subunits of 18 different types, forming two distinct domains [70]. The F_o domain is anchored in the IMM and shapes a channel, allowing protons to escape from the IMS to MM along the concentration gradient. The proton-motive force propels rotation of the c-ring and central stalk of the complex, acting as a 'rotor' of the enzymatic machine. The F_1 domain forms a 'stator', binds ADP and inorganic phosphate (P_i), and the rotating stalk mechanically catalyzes ATP formation [71, 72]. Stoichiometry of the ATP synthesis is [1, 62]:

$$\text{ADP} + P_i + 3\text{-}4H^+ (\text{IMS}) \rightarrow \text{ATP} + 3\text{-}4H^+ (\text{MM})^7$$

Aside from the subunits, each respiratory complex involves a number of dedicated assembly factors that assist with the intricate complex assembly and maturation but are not part of the functional complex [24].

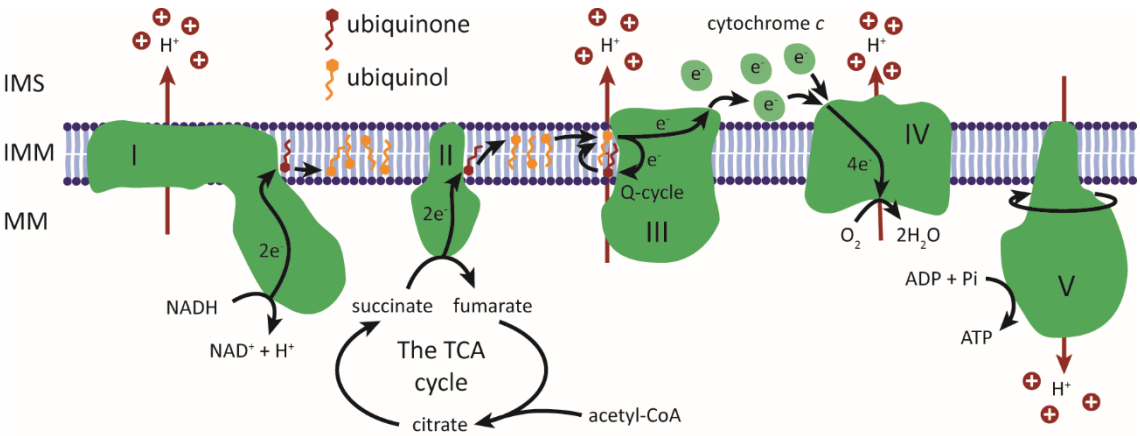

Introduction figure 2 – Simplified scheme of the OXPHOS machinery. The ETC comprises complexes I–IV, with complexes I and II contributing to ubiquinol pool, which is re-oxidized by complex III. Complex IV accepts electrons from cytochrome *c* and finishes the electron transfer by reducing O_2 molecule to H_2O. Complexes I, III and IV transfer protons across the IMM, complex V then uses potential energy of the proton gradient to synthesize ATP. Importantly, complex II is part of both the ETC and the TCA cycle.

[7] H^+/ATP ratio, the number of translocated protons needed for synthesis of one ATP molecule, differs between organisms, organelles (mitochondria and chloroplasts) as well as it may vary at different pH values [73, 74].

1.1.5.1. Supercomplexes

Invention of blue-native polyacrylamide gel electrophoresis revealed that OXPHOS complexes do not form as randomly distributed monomers but rather gather into supramolecular structures called supercomplexes[8] [76]. Mammalian mitochondria harbor predominantly supercomplexes containing complex I and two complexes III (I/III_2), two complexes III and one complex IV (III_2/IV), or the respirasome – complex I, two complexes III and complex IV ($I/III_2/IV$) [75]. Even a higher structure, the 'megacomplex' $I_2/III_2/IV_2$, was described [77]. Interestingly, while complex I is largely found in supercomplexes, more than 75% of complex IV is present as a monomer [75]. Nevertheless, the purpose of the supercomplexes and respirasome structures is not clear, some propose their role in stability of the individual complexes [78] or assisting in their assembly [79]; recent findings also suggest that formation of supercomplexes allows better ETC regulation [80]. In particular, supercomplex I/III_2 was found to play a role in controlling activity of complex I [81]. Noteworthy, complex V mostly forms dimers present at the IMM cristae edges, indicating its role in shaping the IMM cristae structure [82]. Some studies hypothesize that also complex II may assemble into higher structures [77, 83], with Kovářová and colleagues even reporting its association with complex V [84]. Notwithstanding the speculations, complex II is not widely considered as a part of any supercomplex formation; hence, it is considered the only respiratory complex that exists exclusively as a single unit [85].

1.2. Mitochondrial complex II

Outline of the TCA cycle in 1937 by Hans Krebs and other scientists was, undoubtedly, a milestone in biochemistry of mitochondrial metabolism [47]. However, almost three decades earlier in 1909, Swedish physician Torsten Thunberg described an enzyme with dehydrogenase activity that processes amber acid (succinate) in frog muscle tissue [86]. With emerging scientific techniques of the 20th century, the enzyme was identified as a four-subunit complex, containing several cofactors, anchored in the IMM [87, 88]. Catalyzing the dehydrogenation (oxidation) of succinate to fumarate, the enzyme was hence named succinate dehydrogenase (SDH, EC 1.3.5.1 [89]) or succinate-ubiquinone oxidoreductase (SQR), since the released electrons are transferred into the ubiquinone pool; and eventually mitochondrial respiratory complex II [90]. Therefore, complex II represents a crossroad between two essential processes – the ETC and the TCA cycle.

[8] Supercomplex discovery was initally considered as an artifact of the experimental procedure using a mild detergent; however, now the existence of supercomplexes is widely accepted [75].

1.2.1. Structure of complex II

Complex II (CII) consists of four structurally different subunits named succinate dehydrogenase subunit A, B, C and D (SDHA, SDHB, SDHC and SDHD, *Introduction figure 3A*). The whole heterotetrameric complex holds together mainly via hydrophobic interactions [91]. In assembled CII, two morphological parts can be recognized – a hydrophilic head and a hydrophobic tail. Hydrophilic head, comprising of SDHA and SDHB, is where enzymatic activity is accomplished. SDHC and SDHD then form the hydrophobic tail, anchoring the whole CII in the IMM [91, 92]. Notably, CII is a relatively conserved enzyme within evolution[9]. In particular, homologies of mammalian SDHA and SDHB subunits with *Escherichia coli* (*E. coli*) sdhA and sdhB are 51 and 50%, respectively; on the other hand, SDHC and SDHD share less than 20% homology with their prokaryotic counterparts [91].

SDHA is the largest of the CII proteins. Mammalian SDHA encompasses four subdomains – capping domain, helical domain, C-terminal domain and most notably, FAD-binding domain in the N-terminus. Therefore, SDHA is also called flavoprotein (Fp) due to the prosthetic group FAD. Crystal structure reveals that FAD is covalently bound to histidine residue $SDHA^{H99}$ and the cofactor is further coordinated by hydrogen bonds with number of other AA residues within the FAD-binding core comprising a ten-sheet β-barrel structure, three α-helices and a loop [91]. Interface of the capping domain and FAD-binding domain with covalently bound FAD then constitutes the active site of the whole enzyme [94]. FAD, which is derived from riboflavin, is thus an essential cofactor for SDHA and the whole CII function [92].

On mature SDHB protein, two distinct parts can be recognized – N-terminal domain, consisting of five β-sheets and one α-helix, and C-terminal domain with six α-helices. Both domains contain important prosthetic groups, Fe-S clusters, thus SDHB is referred to as iron-sulfur protein (Ip). Specifically, the N-terminal domain binds the [2Fe-2S] cluster, C-terminal domain contains [4Fe-4S] and [3Fe-4S] clusters [91]. The sulfur atoms of various cysteine residues of the SDHB polypeptide serve as ligands for coordinating the three Fe-S clusters. These prosthetic groups are carriers that promote movement of electrons from catalytic FAD of SDHA to ubiquinone. SDHB subunit further mediates a connection between SDHA and the hydrophobic part of CII composed of SDHC and SDHD [92].

[9] Bacteria have succinate:quinone oxidoreductase (SQR) with the same enzymatic function as the mitochondrial CII, and similar enzyme quinol:fumarate reductase (QFR) transferring electrons from quinol to fumarate during anaerobic respiration [93]

Subunits SDHC and SDHD form a membrane-spanning heterodimer. SDHC consists of five α-helices and SDHD compromises four α-helices. The N-terminal hydrophilic α-helix of SDHC points inside the MM and interacts with SDHB [91]. The core of the transmembrane anchor is formed by four helices, two from each subunit. While the rest of the helices surround the core, some of them present their charged AA residues outside the membrane, stabilizing the SDH complex in the phospholipid bilayer. The four-helix core then forms a cavity, where the heme *b* molecule is intercalated. The iron atom of the cofactor is coordinated by two histidine residues of the subunits, and heme propionate groups interact with charged amino acid residues. 'Stacking' of the interactions within four helices lead to further stabilization of the prosthetic group within the transmembrane anchor [91].

For the electron transport function of CII, interaction of its subunits with ubiquinone is essential. This occurs in one of two ubiquinone binding sites – the matrix-proximal Q_P and the matrix-distal Q_D. The Q_P site shows higher affinity for ubiquinone and constitutes of SDHC, SDHD and SDHB residues. In contrast, the Q_D site, which lies closer to the IMS, is composed of SDHD residues only and has significantly lower affinity for ubiquinone [92]. Q_P site is therefore the predominant ubiquinone-binding site within CII, essential for its SQR activity [63, 95].

1.2.2. Mechanism of the enzymatic activity of complex II

The main enzymatic activity of CII (*Introduction figure 3B*), conversion of succinate to fumarate, takes place within the catalytic site of the SDHA subunit, which is located at the interspace of the capping and FAD-binding domain. Succinate accesses the catalytic site and its molecule has to be aligned along the isoalloxazine ring of FAD group. Two reactions then occur – a hydride ion (H^-) transfer from succinate onto N5 of FAD, and a proton transfer from the substrate onto the catalytic arginine $SDHA^{R340}$ – yielding two electrons and two protons from the succinate molecule, therefore forming the double bond of fumarate [96]. Electrons are then tunneled through the SDHB subunit via three Fe-S clusters ([2Fe-2S], [4Fe-4S] and [3Fe-4S]). Fe-S cofactors wire the electrons along increasing redox potential to the ubiquinone-binding Q_P site where the AA residues of SDHB, SDHC and SDHD form a hydrophobic pocket. The molecule of ubiquinone accepts the two electrons passed from the [3Fe-4S] cluster and protons from the MM, being reduced to ubiquinol [95]. Nonetheless, the Fe-S cluster carries only one electron at a time, and reduction of ubiquinone by one electron would lead to radical semiquinone molecule, resulting in formation of ROS. To prevent this, semiquinone is stabilized within the Q_P site pocket by the aromatic ring of a conserved tyrosine residue. The function of the last cofactor of CII, heme *b*, is not well understood. The heme group apparently stabilizes the SDHC-SDHD anchor but, due to its

low redox potential, does not participate in electron transfer [63, 95]. Yankovskaya and colleagues point out to the potential role of heme *b* in ROS prevention. Heme *b* in the bacterial SQR enzyme serves as an electron sink, pulling the electrons down, away from the FAD molecule where electrons can react with oxygen and form ROS [95]. Cecchini and colleagues, on the other hand, suggest that the main role of heme *b* is not in succinate oxidation but in reverse action of CII, i. e. removing electrons from the reduced ubiquinol, whereby reducing fumarate to succinate [63]. This activity, indeed, occasionally occurs even in mammalian cells, for example in hypoxic tissue [97, 98].

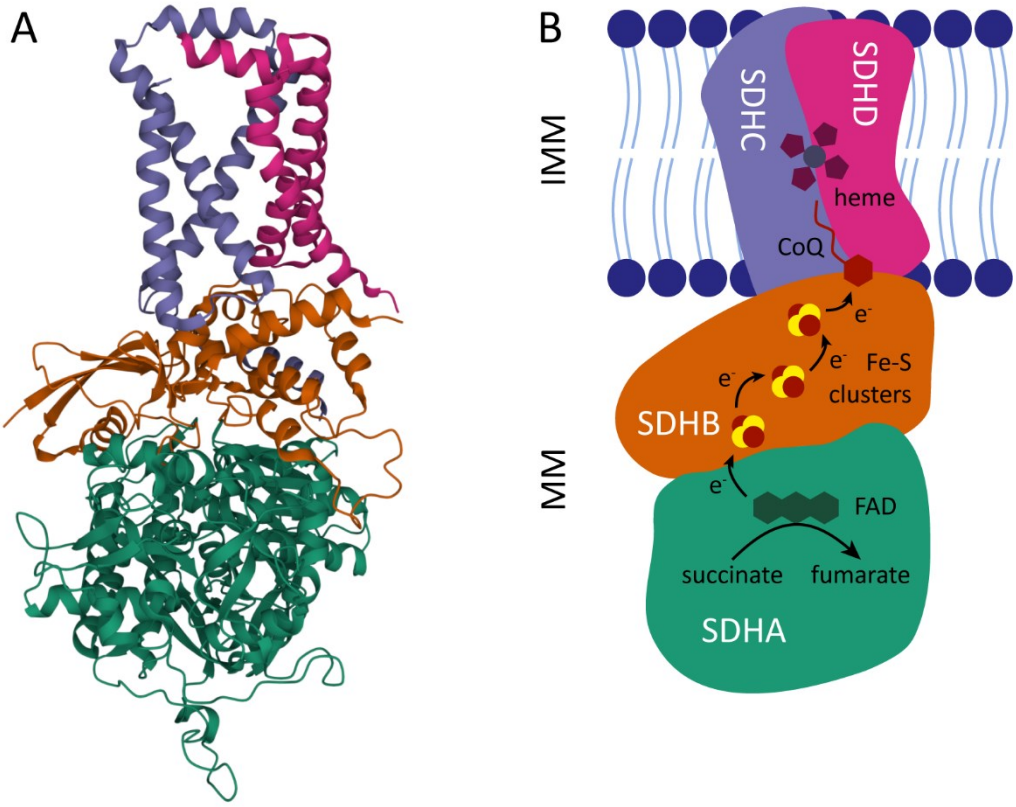

Introduction figure 3 – CII structure (A) and outline of its enzymatic activity (B). (A) CII crystal structure reveals four subunits SDHA-D. (B) The heterotetramer, anchored in the IMM, harbors covalently bound FAD, three Fe-S clusters and a heme group, and catalyzes succinate to fumarate interconversion (SDH activity) with electron transfer to ubiquinone (SQR activity). Adapted from [91, 99] and [100].

1.2.3. Complex II formation

All subunits of mitochondrial CII are encoded within the nuclear genome (*Introduction table 1*) [101]. The polypeptides are synthesized using the cellular proteosynthetic apparatus and translocated into mitochondria presumably via TOM and TIM complex [12, 102]. They are targeted into mitochondria by means of the MTS that constitutes several dozens of amino acids in the N-terminus. In the mitochondrion, MPP or Oct1 proteases then cleave the

targeting presequence [12], leaving the SDH polypeptides for further processing. Proper folding of the subunits requires substrate-non-specific mitochondrial chaperones, such as HSP60 [102]. Maturation of CII subunits and assembly of the whole complex requires dedicated assembly factors (see *Introduction figure 4*).

1.2.3.1. Assembly factors

Succinate dehydrogenase assembly factors 1-4 (SDHAF1-4, *Introduction table 1*) are four small MM proteins that assist with maturation of individual SDH subunits, mediate cofactor insertion, stabilize sub-complex intermediates and promote assembly of the whole complex, but are not part of the mature CII heterotetramer. SDHAF1-4 are also coded in the nucleus and transported into mitochondria in the same manner as CII subunits [92], except for SDHAF1, which has an MTS that is a part of the functional protein, therefore is not cleaved by MPP [101, 103].

SDHAF1 is the first reported SDH assembly factor [92]. Together with SDHAF3, it serves in processing the SDHB subunit. Both proteins share a unique LYR-motif of the amino acids L-Y-R (leucine-tyrosine-arginine) in the N-terminus, which is apparently involved in Fe-S clusters metabolism [104, 105]. SDHAF2 is the only SDH assembly factor with a described ortholog in prokaryotes, suggesting its conservation among all organisms [106]. SDHAF2 participates in SDHA maturation, together with the last discovered assembly factor SDHAF4 [92].

Human	Yeast	E. coli	AA length	Mw [kDa]	MTS	Chromosome
SDHA	SDH1	sdhA	664	72.7	1 – 42	5
SDHB	SDH2	sdhB	280	31.6	1 – 28	1
SDHC	SDH3	sdhC	169	18.6	1 – 29	1
SDHD	SDH4	sdhD	159	17.0	1 – 56	11
SDHAF1	SDH6	None*	115	12.8	Not cleaved**	19
SDHAF2	SDH5	sdhE	166	19.6	1 – 29	11
SDHAF3	SDH7	None*	125	14.7	1 – 30	7
SDHAF4	SDH8	None*	108	12.2	1 – 20	6

Introduction table 1 – Overview of succinate dehydrogenase subunits and assembly factors. Orthologs of SDHx proteins exist in yeast and *E. coli* with a different nomenclature. The table lists features of human CII-associated polypeptides (AA length, Mw in kDa, length of MTS in AA) and their genes (chromosome location). Mw – molecular weight, * – no ortholog has been found in *E. coli*, ** – SDHAF1 peptide has an MTS that is part of the functional protein. Data taken from [101].

1.2.3.2. SDHA maturation

The key prosthetic group of CII is FAD covalently bound within SDHA subunit, enabling the enzymatic function. Mitochondrial FAD synthase generates FAD pool in the MM, using dietary riboflavin (vitamin B_2) [107]. FAD binding (flavinylation) of SDHA is, however, not

autocatalytic and requires additional factors. First, a molecule bearing two carboxylic groups is needed, particularly succinate, fumarate or malate [94]. Second, the protein assembly factor SDHAF2 is required. The need for a dedicated flavinylation-mediating polypeptide evidently appears already in prokaryotes[10] [93, 109] and loss of SDHAF2 in eukaryotes leads to complete disappearance of SDHA flavinylation and SDH activity, while SDHA protein levels do not change [94, 110]. SDHAF2 binds to SDHA at the same place where SDHB, protecting the hydrophobic domain of the protein. SDHAF2 also helps SDHA to reach the mature, catalytic form by orienting the SDHA domains; the assembly factor therefore acts as a typical chaperone [93, 94, 109]. At this point, the dicarboxylic molecule incorporates into the SDHA during its maturation, forms several non-covalent bonds with amino acids residues, and helps to organize the active site. Finally, SDHAF2 forms, via its glycine residue $SDHAF2^{G78}$, hydrogen bond with the conserved FAD-binding histidine $SDHA^{H99}$, orienting the histidine residue in favorable position for the flavinylation reaction. Stability of the SDHA-SDHAF2 intermediate is considerably high [94], and when the ability of SDHAF2 to interact with SDHA is impaired, SDHAF2 is quickly degraded [111].

The last discovered SDH assembly factor, SDHAF4, also participates in SDHA maturation. SDHAF4 is a pan-eukaryotic protein, present from yeast to humans, with an evolutionarily conserved C-terminus [92, 112]. Loss of SDHAF4 results in 60 and 85% decrease in SDH activity in yeast and *Drosophila* cells, respectively; and leads to significant succinate accumulation. Interestingly, deletion of the *SDHAF4* gene ortholog in *Drosophila* manifests as classical mitochondrial dysfunction, characterized by neurodegeneration and short lifespan. Molecular level studies revealed that SDHAF4 exclusively binds already flavinylated SDHA; therefore, SDHA-SDHAF4 follows SDHA-SDHAF2 interaction. These findings suggest few possible explanations for SDHAF4 role within SDH assembly. SDHAF4 may serve as a chaperon for FAD-bound SDHA, stabilizing the subunit prior association with SDHB, since soluble SDHA with FAD cofactor may theoretically contribute to ROS generation. Indeed, SDHAF4-deficient cells show high sensitivity to oxidative stress, while overexpression of the *YAP1* gene, encoding a transcription factor capable of diminishing oxidative stress defects, restores cell growth. However, *YAP1* overexpression does not retrieve the SDH activity; hence, other mechanisms may be involved. Van Vranken and colleagues propose that SDHAF4 promotes SDHA-SDHB dimer formation [113]. Moreover, Belt and colleagues confirmed, using a plant model of SDHAF4 loss, the importance of the assembly factor in association of SDHA and SDHB [112]. Crystal structure studies of Sharma

[10] While eukaryotic SDHAF2 orthologs seem crucial for SDHA flavinylation and SDH function, *E. coli* lacking sdhE retains some SDH activity, therefore SDHAF2 ortholog only promotes SDHA flavinylation in bacteria [106]. Furthermore, certain bacteria completely lack any sdhE homolog, while having flavinalyted and functional SDH [108].

and colleagues revealed high stability of the SDHA-SDHAF2 intermediate, therefore SDHAF4 may serve in displacement of tightly bound SDHAF2 from SDHA, allowing formation of SDHA-SDHB [94]. In conclusion, SDHAF4 has been confirmed to serve in SDHA maturation; still, the exact role of the assembly factor remains to be fully elucidated.

1.2.3.3. SDHB maturation

The essential step in SDHB maturation is also prosthetic group insertion, which are Fe-S clusters. The ISC complex, mitochondrial highly conserved machinery, forms Fe-S clusters. Proteins such as cysteine desulfurase NFS1, the LYR-motif protein ISD11 and acyl carrier protein (ACP), with help of ferredoxin and frataxin, use free iron and sulfur atoms from cysteine to generate Fe-S clusters and bind the cofactors onto the ISCU scaffold protein [114]. ISCU then interacts with HSC20 and HSPA9. Nascent SDHB polypeptide was found to physically interact with HSC20 and HSPA9, forming an ISCU/HSC20/HSPA9/SDHB complex, which serves for Fe-S cluster cofactor insertion. Furthermore, assembly factor SDHAF1 promotes the cofactor insertion by interaction with both SDHB and HSC20. Non-stabilized Fe-S clusters are exceptionally sensitive to oxidative damage; thus, the additional role of SDHAF1, and likely also of the other SDHB assembly factor SDHAF3, may be to prevent such a detrimental event. SDHAF1 and SDHAF3 knockout models show decreased SDH activity, which is partially restored by adding of antioxidants or overexpression of *YAP1* [92, 103]. Since iron atoms within Fe-S clusters are the main targets for ROS, iron supplementation also partially ameliorates defects of SDHAF1/SDHAF3 knockout [92]. Taken together, the main function of SDHAF1 is to aid in Fe-S cluster insertion, and both SDHAF1 and SDHAF3 shield the SDHB subunit, and especially its Fe-S clusters, from ROS-mediated damage.

1.2.3.4. Holocomplex formation

Maturation of SDHA requires SDHAF2 and likely SDHAF4, and that of SDHB needs SDHAF1 and SDHAF3. Since SDHAF2 occupies the SDHB-binding site on SDHA, the assemble factor has to dissociate prior to SDHA-SDHB formation. As mentioned above, SDHAF4 may serve as a factor assisting in SDHAF2 removal [94]. Similarly, Sharma and colleagues suggest that SDHAF1 and SDHAF3 must be removed from SDHB because either of the factors occupies the site of SDHB that interacts with SDHA [102]. In contrast, Van Vranken and colleagues postulate that both SDHAF1 and SDHAF3 may also bind to SDHA-SDHB, protecting the dimer from ROS [92]. Even with lack of satisfying evidence, it is generally believed that the hydrophilic dimer SDHA-SDHB does form as an intermediate of SDH assembly [92, 102, 115]. Nevertheless, Grimm and colleagues claim that the SDHA-SDHB dimer rather dissociates from SDHC-SDHD upon drop of pH during apoptosis, participating in the programmed cell death process [116].

The mechanism of maturation of SDHC and SDHD and subsequent dimer formation is still unknown, compared to the relatively well-studied SDHA and SDHB maturation. Both anchor subunits are transported into the mitochondria but little is known about their insertion into the IMM. Further questions arise in the context of other potential assembly factors, for instance participating in insertion of heme *b* into the SDHC-SDHD dimer. In other OXPHOS complexes, a heme group is incorporated with assistance of dedicated assembly factors. However, neither heme *b* insertion mechanism nor even precise function of the cofactor is understood in case of CII [92]. The last step of the CII assembly is considered to be SDHA-SDHB and SDHC-SDHD dimers association into the complete heterotetramer. However, the mechanism of the whole complex assembly completion is not well studied either [92].

Protein docking studies, carried out by Hadrava Váňová and colleagues, brought a compelling hypothesis. Both subunits of the SUCL enzyme are predicted to interact with SDHA and SDHB. Specifically, SUCLG1 binds free SDHA, and SUCLG2 interacts with SDHB. This is further confirmed by the fact that *SUCLG2* deletion leads to SDHB decrease and, subsequently, results in CII destabilization and decrease of its activity [117].

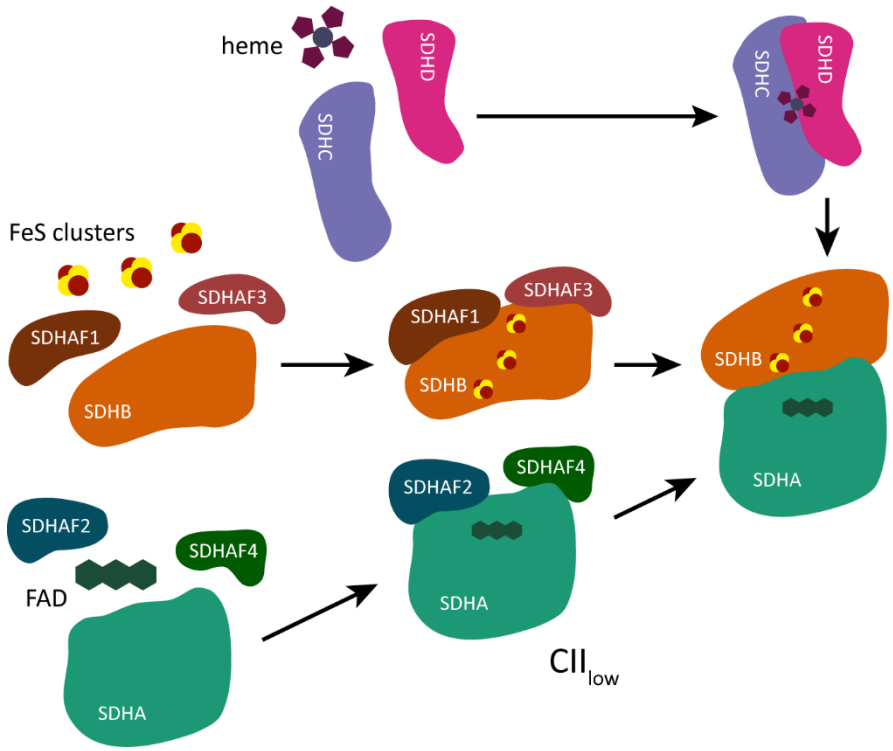

Introduction figure 4 – Complex II assembly. Maturation of subunit SDHA necessitates dedicated assembly factors SDHAF2, mediating FAD binding, and SDHAF4. SDHB subunit needs SDHAF1 for Fe-S clusters insertion and the assembly factor, together with SDHAF3, protects SDHB subunit from ROS-mediated damage. SDHA and SDHB presumably form a heterodimer that further associates with the SDHC-SDHD dimer with an intercalated heme molecule. Adapted from [100].

1.2.3.5. CII_{low} – an alternative assembly form of complex II

While *SDHx* mutation or any CII dysfunction, as well as the TCA cycle impairment or other mitochondrial disruption, lead to decrease in SDHB [117-119], SDHA level stays unchanged, making the *SDHA* a 'housekeeping' gene [120]. Rather than being degraded, SDHA is then present in the MM as a soluble intermediate of its maturation process. The sub-assembly was first observed in cells depleted of mtDNA in the study of Tan and colleagues in 2015 [121]. Since the subcomplex migrates faster on native gels than fully assembled CII, due to lower molecular weight (around 100 kDa compared to 140 kDa of mature CII), it was named CII_{low} in the study of Bezawork-Geleta and colleagues in 2018 (see *Introduction figure 5*). This alternatively assembled form of CII is present to some degree even in wild type, CII-functional cells, since it is an intermediate in normal CII assembly (as depicted in *Introduction figure 4)*. However, CII_{low} is significantly enriched in pathological states, which is also observed in case of *SDHx* mutated tumors in paraganglioma patients. Immunoprecipitation and mass spectrometry revealed that CII_{low} comprises SDHA, SDHAF2 and SDHAF4 [118]; still, it is not clear which of the the assembly subcomplexes prevails – SDHA-SDHAF2, SDHA-SDHAF4 or SDHA-SDHAF2-SDHAF4 [94, 118].

Overall, these findings raise a question if CII_{low} plays another role, besides being a pool for unbound SDHA, potentially in mitochondrial metabolism or signaling. The study of Bezawork-Geleta and colleagues demonstrates that, while significant shift in metabolism is mostly due to CII dysfunction, CII_{low} presence in SDHB knockout cells may attenuate pyrimidine *de novo* synthesis and subsequently affect cell cycle progression. In addition, the findings indicate that SDHB knockout leads to succinate accumulation; however, further SDHA depletion lowers the succinate level and rewires the metabolism. This suggests that CII_{low} may also somehow modulate the metabolism, acting as a sensor of bioenergetic stress. This may explain why *SDHA*-mutated tumors are relatively rare, compared to *SDHB*- or *SDHD*-defective ones (see the chapter *Paraganglioma syndromes*) [118]. It is important to mention that, according to the study of Maklashina and colleagues, an incompletely assembled form of CII, containing SDHA, lacks any enzymatic activity and does not even significantly contribute to ROS production. SDHA has to interact with SDHB, which results in open, catalytically active form of CII [96]. In summary, CII_{low} evidently plays a prominent role in metabolism of CII-deficient cancer cells; nonetheless, more studies are needed to elucidate its potential effect on mitochondrial metabolism and, generally, cancer progression.

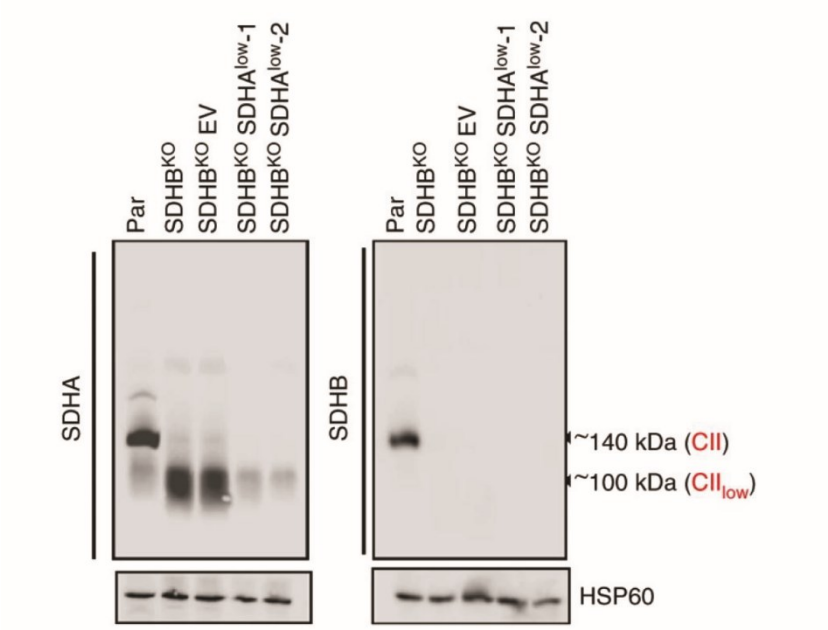

Introduction figure 5 – Determination of CII_{low} in SDHx-deficient cells using native gel electrophoresis. In $SDHB^{KO}$ cells, SDHA is accumulated within alternative assembly form CII_{low}, which diminishes upon SDHA silencing. SDHB staining reveals only assembled CII, confirming that CII_{low} comprises SDHA, not SDHB. Adapted from [118].

1.2.4. Regulation of complex II activity

Level of CII and its activity may be modulated on multiple levels. The chaperone TRAP1, a mitochondrial paralog of HSP90, seems to modulate activity of several OXPHOS enzymes, including SDH [122]. Studies confirmed that TRAP1 indeed associates with both SDHA [123] and SDHB [124], presumably promoting their folding. However, downregulation of TRAP1 leads to increased CII activity. Such ability of the chaperone to attenuate CII is thought to serve as a prevention of oxidative stress; on the other hand, subsequent accumulation of succinate caused by TRAP1 activity may promote tumor formation [123, 125].

CII is also regulated by covalent post-translational modifications. Four conserved lysine residues of the SDHA subunit undergo acetylation, which attenuates activity of the whole enzyme. Mitochondrial NAD^+-dependent deacetylase SIRT3 alters this SDHA modification, thus enhancing CII activity [126, 127]. Moreover, the tyrosine kinase Fgr was found to phosphorylate two tyrosine residues of SDHA [128], thereby increase complex II activity. Fgr kinase is ROS-activated; therefore, impaired complex I activity, leading to ROS production, enhances activity of complex II. Interestingly, this process is employed during T lymphocyte activation, which necessitates ROS-mediated signaling [129].

Finally, CII evidently requires physical interaction with some of the TCA cycle enzymes, since SUCL impairment leads to SDHB downregulation and attenuation of CII activity [117].

1.2.5. Formation of reactive oxygen species

The main source of mitochondrial ROS production is complex I and III [130]. However, CII was also found to contribute to ROS formation in several ways [95]. First, CII may directly generate ROS on FAD of the SDHA subunit by passing electrons from reduced FAD onto adjacent oxygen molecules, but only under physiological succinate concentration[11] [131]. ROS production is further alleviated by blocking of SDH ubiquinone-binding site by various molecules (see the chapter *Complex-II-targeted therapy*) or when complex III is inhibited. In contrast, inhibition of the succinate-binding site of SDHA prevents ROS formation. Furthermore, defects in CII structure or its assembly may also promote ROS generation [100, 132], as Grimm and colleagues suggest that under acidic environment of an early phase of apoptosis, SDHB-SDHA dimer disassociates from the membrane anchor of SDHC-SDHD and generates ROS via succinate oxidation [116].

Second, SDH generates considerable amount of ROS indirectly. Especially in case of succinate build-up, CII rapidly oxidizes excessive succinate, directing the electron flow onto complex I, from which the electrons leak and react with oxygen, forming large amounts of ROS [100, 133]. ROS generated via this mechanism, known as reverse electron transfer (RET), are important in both physiological [134] and pathophysiological processes, such as ischemia-reperfusion injury where succinate accumulates upon lack of oxygen in the tissue. Interestingly, succinate build-up during ischemia seems to be caused by reverse action of SDH, i. e. reduction of fumarate to succinate [97].

1.3. Physiological role of complex II and succinate

Besides its pivotal role in mitochondrial metabolism and bioenergetics, CII and especially succinate play an important part in physiological processes of signaling, homeostasis as well as immune system function.

1.3.1. Succinate signaling

Succinate may leave mitochondria via the dicarboxylate carrier (DIC) in the IMM and the voltage dependent anion channel (VDAC) of the OMM. Under physiological conditions, plasma membrane of the cell is impermeable for succinate. However, SLC-family transporters and other carriers may export succinate into the extracellular space [135]. The G-protein-coupled receptor 91 (GPR91), present on the cell surface, was found to serve as a succinate receptor, thus it was later named succinate receptor 1 (SUCNR1) [136]. Signaling

[11] High levels of succinate block access of oxygen to the FAD site, thereby in elevated succinate contentration, ROS production via CII does not occur [100, 131].

via this receptor involves inhibition of adenylate cyclase and cAMP synthesis; and also includes inositol phosphate formation, Ca^{2+} flux and ERK1/2 activation [136, 137].

Succinate attributes to muscle tissue homeostasis. Exercise leads to lowering of pH of muscle cells. A molecule of succinate, normally not able to cross the cell membrane, may be partially protonated at lower pH, forming monocarboxylate that can be excreted via monocarboxylate transporter 1 (MCT1) out of the cells. Succinate than binds to SUCNR1 on the surface of non-muscle cells (endothelial and stromal cells) of the muscle interstitium, promoting muscle remodeling, strengthening and perhaps modulating muscle innervation [138]. Considerable levels of SUCNR1 was found in the kidney, sensing elevated succinate in the blood, which results in hypertension via the angiotensin-renin system [137]. Succinate signaling via SUCNR1 is also employed in angiogenic process of the retina due to high abundance of succinate in hypoxia [139]. Temporary hypoxia, resulting in elevated succinate levels, is also the cause of ischemia-reperfusion injury that, besides detrimental ROS from RET (see the chapter *Formation of reactive oxygen species*) [97], may furthermore involve SUCNR1 signaling [136].

1.3.2. Protein succinylation

Among acetylation and other post-translational protein modifications, binding of a succinyl moiety to lysin residues (less frequently histidine or arginine) plays an important role in modulating activity of almost 800 proteins with more than 2,500 succinylation sites [140, 141]. Protein succinylation is predominantly abundant within mitochondrial proteins, since the main contributor to this process is succinyl-CoA. It is important to note that whereas succinyl-CoA performs lysin succinylation, fumarate may react with cysteine residues, forming succinyl-cysteine [142, 143]. On the other hand, succinate does not contribute to the succinylation process due to rather unreactive molecule [142]. The exact mechanism is not fully understood; the reaction may occur spontaneously or using a dedicated enzyme [144, 145]. Succinylation also occurs outside mitochondria, despite the non-permeability of the mitochondrial membrane for succinyl-CoA, also via an unknown process [144]. The level of succinylation of lysine residues is regulated by lysine deacetylases sirtuins, specifically SIRT5. Similar to acetylation, the succinylation is a widespread modification of histones [145], and succinylation also concerns the metabolic enzymes PDH and, interestingly, SDH itself, enhancing its function [140].

1.3.3. Complex II and succinate in immune system function

Succinate signaling is apparently, to some extent, exploited in hematopoietic cell proliferation and development, since hematopoietic progenitor cells express significant amounts of SUCNR1 [146]. Succinate further markedly contributes to pro-inflammatory

responses of various immune cell types; for instance, dendritic cells (DC) show high expression of SUCNR1. Extracellular succinate then serves as both a chemotactic molecule, promoting DC migration to lymph nodes, and an inflammatory mediator, promoting TNF-α secretion and specific T_H cell activation [147]. Also intracellular succinate participates in the immune system regulation. Immune cells are capable of shifting their metabolism under varying conditions, most notably attenuating OXPHOS and enhancing glycolysis upon activation. This shift may lead to succinate accumulation, stabilization of HIF-1 and establishment of pseudohypoxia (see the chapter *Pseudohypoxia*) [148]. HIF-1 is then a strong inducer of the pro-inflammatory T_H17 phenotype due to RORγT potentiation [149]. In addition, functional CII is essential in T cell activation and function [150]. Metabolic reprogramming is also a crucial component of macrophage activation. LPS stimulation re-wires metabolism to production of succinate and itaconate, a derivative of aconitate from the TCA cycle, which attenuates SDH function and leads to additional succinate build-up [151]. Subsequent HIF-1 stabilization, SUCNR1 signaling and enhanced protein succinylation all promote IL-1β secretion, thus contribute to a pro-inflammatory macrophage phenotype [148, 152]. On the contrary, macrophage IL-1β expression also requires high levels of ROS that are produced via succinate oxidation by SDH and RET (chapter *Formation of reactive oxygen species*) [134]. Therefore, not only accumulated succinate but also functional CII is necessary for the inflammatory macrophage phenotype.

1.4. Mitochondrial diseases linked to complex II

Inborn errors in enzymes participating in metabolism occur in 1 out of 2,500 births [153]. Mutations in the TCA cycle or OXPHOS enzymes-encoding genes, inherited either biparentally via chromosomes or maternally in case of mtDNA encoded genes, may allow postnatal development, but lead to mitochondrial dysfunction, usually manifesting as severe pathology. Mitochondrial diseases predominantly cause neuromuscular impairment and heart, liver or kidney malfunction because of high energy demand of the tissues [154, 155].

Deleterious mutations of *SDHx* were long thought to be incompatible with life. However, in 1995, an inherited CII defect was recognized as a rare cause of children encephalomyopathy [156]. Inborn dysfunction of CII is rather rare in humans, comprising only few percent of all ETC deficiency diagnoses [157]. Like other ETC dysfunctions, CII defects mostly clinically present as a neurodegenerative disorder. Vast majority of the patients have been found to harbor *SDHA* deleterious mutations, either homozygous or compound heterozygous, usually with autosomal recessive inheritance, often causing juvenile encephalopathy, known as Leigh syndrome [158, 159].

1.4.1. Leigh syndrome

The disease is an early-onset progressive neurodegenerative pathology with lesions forming within the central nervous system, manifesting as muscular hypotonia or spasms, ataxia and seizures [160]. Patients with Leigh disease often die during early childhood; however, some reach adulthood or develop the disease later in their life with similar symptoms as in the early-onset disease. The hereditary CII dysfunction may additionally cause optic atrophy, cardiomyopathy and leukoencephalopathy [158]. In addition to *SDHA* mutations, gene variants of *SDHB*, *SDHD* and *SDHAF1* were also described as a cause of a recessively inherited mitochondrial disease[12], presenting as infantile encephalopathy [162-165].

1.5. The role of complex II in cancer

Mutations or specific variants of mitochondrial enzymes vastly contribute to the carcinogenic process. Germline or somatic mutations in genes encoding both CII subunits and its dedicated assembly factors exhibit high significance in specific cancer types, such as neuroendocrine tumors pheochromocytoma and paraganglioma, gastrointestinal stromal tumors and renal cancer. Common feature of CII-dysfunction driven neoplasms is negative immunohistochemical staining for the SDHB subunit in all *SDHx* mutations [119].

1.5.1. Mechanisms of tumorigenesis

The mechanism of CII-mediated tumorigenesis is predominantly mediated via the oncometabolite succinate and the ensuing pseudohypoxia. However, emerging evidence points out to other potential molecular pathways.

1.5.1.1. Pseudohypoxia

α-Ketoglutarate-dependent dioxygenases attach a hydroxyl group onto target AA residues, using molecular oxygen and α-ketoglutarate as electron donor, producing succinate and CO_2 [51]. Importantly, the enzymes comprise HIF-α prolyl hydroxylases 1-3 (PHD1-3). Under normoxic conditions, PHD attaches two hydroxyl groups onto prolin residues of hypoxia inducible factor subunit alpha (HIF-α). PHDs require cofactors ascorbic acid and Fe^{2+}, and two aforementioned substrates, O_2 and α-ketoglutarate, hence 'sensing' oxygen level and nutrient availability[13], respectively. Protein of the Von Hippel-Lindau gene (pVHL), serving as an E3 ubiquitin ligase subunit, binds the hydroxylated HIF-α and targets the protein for

[12] Although not described in humans, other *SDHx* genes detrimental mutations might exert similar phenotype, considering that an experimental mouse model of SDHC defficiency manifests as Leigh-like syndrome [161].

[13] Besides the TCA cycle, α-ketoglutarate plays a role in AA metabolism (chapter *Catabolic pathways*).

degradation via the ubiquitin-proteasome pathway. Oxygen deprivation, hence, results in PHD attenuation and subsequent HIF-α accumulation, followed by its dimerization with HIF-β[14], forming the functional HIF transcription factor, the main orchestrator of hypoxic response characterized by enhanced glycolysis and neoangiogenesis [167].

Upon disrupted function of CII, succinate accumulate inside cells. High level of cytosolic succinate elicits similar effect as O_2 shortage even under normal oxygen concentration, referred to as pseudohypoxia. Succinate moves between mitochondria and cytosol using the above-mentioned transporters DIC and VDAC. Upon CII dysfunction, cytosolic succinate impedes decarboxylation of α-ketoglutarate by PHD, thus competitively inhibiting the enzyme and establishing pseudohypoxia via HIF-α stabilization. Active HIF heterodimer translocates into the nucleus and binds to the hypoxia-responsive element, which is a promotor of several genes. Specifically, those responsible for enhanced glycolysis (glucose transporter 1, GLUT1), cell proliferation (insulin-like growth factor 1, IGF1), angiogenesis (vascular endothelial growth factor A, VEGFA) or metastasis (lysyl oxidase, LOX) [168]. While HIF-1α mainly promotes the glycolytic response, HIF-2α rather supports cell proliferation [169]. Although some studies point to predominant role of HIF-1α in pseudohypoxia [167], identification of a stabilizing mutation of *HIF2A* gene in pheochromocytoma and paraganglioma tumors underlines the likely prevailing importance of HIF-2α [169, 170]. In addition, fumarate accumulation exhibits a similar effect as succinate by competitive inhibition of PHD [171], resulting in similar features of *FH*-mutated tumors as described for *SDHx*-mutated [172]. Noteworthy, Hadrava Váňová and colleagues report germline *SUCLG2* mutations in pheochromocytoma and paraganglioma patients that presumably result in SUCL impairment. This further impedes activity of CII and leads to succinate accumulation, thus promoting tumorigenesis [117].

1.5.1.2. Epigenetic modulation and DNA repair suppression

The group of α-ketoglutarate-dependent dioxygenases also includes epigenetic modulating enzymes, such as TET family 5-methyl cytosine (5-mC) hydroxylases and Jumonji (JMJ) histone demethylases[15]. Succinate directly inhibits TET enzymes and JMJ demethylases, attenuating DNA and histone demethylation, respectively. CII-deficient cells then accumulate methylation epigenetic changes, establishing a hypermethylator phenotype, mainly within CpG islands. This leads to epigenetic silencing of numeral genes, including various tumor suppressors [173]. Such epigenetic modulation may be, at least partially,

[14] The 'oxygen sensing' alpha subunit has three isotypes, HIF-1α, HIF-2α or HIF-3α, that heterodimerize with the HIF-1β or HIF-2β subunit [166].
[15] TET enzymes hydroxylate 5-methyl cytosine to 5-hydroxymethyl cytosine, which is removed by the base excision repair mechanism and replaced by cytosine. JMJ demethylases cleave methyl groups of lysines in histones [169].

responsible for high malignancy of *SDHB*-mutated tumors (discussed later in the chapter *Paraganglioma syndromes*) [169].

Succinate furthermore suppresses homologous recombination, the process of DNA double-strand break repair, thus leading to genetic instability that potentially also contributes to tumor progression [174].

1.5.1.3. Oxidative damage

One of other proposed mechanisms of how SDH contributes to the tumorigenic process is through ROS formation. While some studies suggest an indispensable role of ROS in tumorigenesis of *SDHx* mutation [132], specifically in the pseudohypoxia establishment upon CII dysfunction [175], the others disagree [176], so this point is still controversial.

CII defects, nevertheless, may increase cellular oxidative damage indirectly. Namely, *SDHB*-mutated tumors exhibit high expression of iron-transporting genes encoding the proteins transferrin (TF), transferrin receptor 2 (TFR2) or divalent metal transporter 1 (DMT1). This is caused by succinate-mediated pseudohypoxia and stabilization of mainly HIF-1α, which regulates expression of iron metabolism genes [177]. Elevated intracellular iron then contributes to ROS production via Fenton reaction ($Fe^{2+} + H_2O_2 \rightarrow Fe^{3+} + OH^- + HO^\bullet$ [178]), leading to redox imbalance and enhanced oxidative stress that may further contribute to the tumorigenic process.

1.5.1.4. Other contributions of high level of succinate

SUCL deficiency manifests as Leigh-like syndrome, evidently via accumulation of succinyl-CoA, causing pathological protein hyper-succinylation and metabolism alteration [144]. As Hadrava Váňová and colleagues describe, SUCL defects further result in succinate accumulation by attenuating CII activity [117]. Moreover, CII disruption itself may also lead to high level of succinyl-CoA, resulting in enhanced protein succinylation. Importantly, hyper-succinylation affects histone and non-histone nuclear proteins, resulting in chromatin opening, enhanced transcription and impaired DNA repair mechanisms [179]. Interestingly, accumulation of fumarate caused by gain-of-function mutation of *SDHA* (and hyperactive CII) in certain type of leukemia also leads to enhanced level of succinylation and pronounced pro-inflammatory course of the disease [143].

Succinate signaling may also play a part in the carcinogenic process. CII-defective cancer cells excrete excessive succinate via MCT1 into the extracellular space [138], binding it to SUCNR1 on the cell surface, thus mediating autocrine signaling. SUCNR1 upregulation was indeed found in SDHB-deficient cancer cells, along with its pro-proliferative downstream signaling cascade [180].

1.5.1.5. Immune evasion

Several components of the immune system maintain surveillance over cancer cells and, in most cases, effectively eliminate the potential danger. Namely cytotoxic ($CD8^+$) T lymphocytes, natural killer (NK) cells or NK-T cells play a crucial role in anti-tumor immune response [181]. Nevertheless, a tumor may develop environment capable of attenuating anti-cancer immune mechanisms, therefore escaping immune surveillance. This is especially the case for tumors in hypoxic and pseudohypoxic state. Low-oxygen environment or pseudohypoxia lead to stabilization of HIF-α in cancer cells, promoting secretion of chemokines attracting tumor-protective regulatory T cells [182]. Hypoxic tumor environment also directly supports regulatory T cells differentiation [183]. Tumor-associated macrophages (TAMs), mainly the M2-type polarized subset of macrophages, significantly promote tumor formation and aggressiveness [184]. Hypoxia apparently also lead to TAM generation and attraction since hypoxic tumors show high abundance of the tumor-promoting M2 macrophages [185], thereby, tumors with impaired CII activity show high TAM infiltration [186]. Tumor cells secrete excess succinate into the extracellular space where it can bind SUCRN1 on adjacent macrophages, further signaling via the PI3K/AKT/HIF-1α pathway, leading to TAM polarization. TAMs may subsequently promote cancer cell migration by IL-6 secretion [187].

Lactic acid and low pH, which are markedly abundant in hypoxic tumor environment due to enhanced glycolytic metabolism, are both capable of inhibiting cytotoxic T lymphocyte function and proliferation [188, 189]. Tumor cells with *VHL*-linked pseudohypoxia have even ability to defend themselves against NK cell cytotoxic granzyme B by enhancing autophagy [190]. Hypoxic environment also promotes secretion of a soluble form of CD137 by tumor cells. CD137 is also present on T lymphocytes and its binding of CD137L serves as a co-stimulatory signal for the T cell, thus CD137L binding by the secreted CD137 blocks T-cell-mediated anti-tumor responses [191]. Furthermore, hypoxic tumors show elevated expression of PD-L1 and PD-L2, ligands of the co-inhibitory programmed cell death (PD-1) receptor [192], as well as other T-cell attenuating ligand CTLA-4 [193], which the tumor cells apparently also exploit for immune evasion.

1.5.2. Pheochromocytoma and paraganglioma

Among CII-deficient neoplasms, the neuroendocrine tumors pheochromocytoma and paraganglioma (PCC and PGL) both have a privileged position in cancer research, since the first mitochondrial protein described as a tumor suppressor, SDHD, was reported for PGL [194]. PCC/PGL originate in paraganglia, small organs derived from embryonic neural crest, closely associated with the autonomous nervous system; paraganglia are, therefore,

sympathetic and parasympathetic. Sympathetic paraganglia are either small formations within the abdomen and chest (organ of Zuckerkandl at the bifurcation of the abdominal aorta) or, most importantly, constitute the medullar part of the adrenal gland. Paraganglia with sympathetic innervation harbor chromaffin cells[16] secreting catacholamines, i. e. adrenaline, noradrenaline and dopamine [169, 196]. Parasympathetic paraganglia occur mainly in the head, neck and chest, for example within carotid body; and serve as chemoreceptors, sensing oxygen level in the blood [197].

1.5.2.1. Clinical characterization

Majority of the literature as well as the World Health Organization define PCC (literally dusky-colored tumor[16]) as a tumor with its origin in chromaffin cells of the adrenal medulla, and paraganglioma (tumor of paraganglia) as its extra-adrenal counterpart[17] [199]. PCC and PGL are solid, highly vascularized tumors, distinguishable by positivity for chromogranin A and S100 by immunohistochemical staining [169, 199]. PCC was first described by physician Max Schottelius in the 19th century as a bilateral tumor of adrenal glands and the tumor is casually referred to as 'the great masquerader' because of the variety of symptoms that this tumor can cause [195]. Both adrenal PCCs and sympathetic PGLs found mostly in the abdomen or the chest cavity [200] secrete excessive amounts of catecholamines, which have numerous biological effects, clinically presenting as heart palpitations, headaches, sweating and furthermore as panic, anxiety and, most importantly, blood pressure changes. The symptoms may be persistent or occur in sudden attacks [201]. PCC/PGL are mostly benign tumors *per se*, around 10% of PCCs and 15–35% of PGLs are regarded as malignant[18] [203]. Nevertheless, high levels of catecholamines released by the tumor tissue may lead to lethal cardiovascular complications [199, 201]. In contrast, parasympathetic PGLs within head and neck mostly do not secrete catecholamines, the disease therefore being often asymptomatic [198].

1.5.2.2. Diagnosis and treatment

Upon consideration of the catecholamine-associated symptoms, further diagnosis includes biochemical evaluation of plasma and urinary catecholamine metabolites, metanephrines. Subsequently, imaging techniques including CT, MRI, and PET-CT using labeled molecules (such as the dopamine precursor L-DOPA) help with precise tumor localization; surgical

[16] Both chromaffin cells and pheochromocytoma got their names due to chromaffin reaction – staining the tissue with chromate-containing Müller's solution leads to oxidation of catecholamines and typical brown color [195].
[17] A lot of clinicians, however, virtually name all sympathetic paraganglia-derived tumors (catecholamine producing), even the extra-adrenal, as PCCs; and only the parasympathetic parangliomas as the true PGLs [197, 198].
[18] The World Health Organization defines malignant PCC/PGL by the presence of metastasis in other, non-chromaffin organs [202].

removal is then first-line treatment [199, 201]. Moreover, genetic screening, especially in case of family history of the tumors, has become an essential part of the diagnostic process of PCC/PGL [199]. Certain gene errors vastly contribute to malignancy of the disease, with PCCs forming metastases mostly in lymph nodes and bones; and PGLs disseminate into the liver. Metastases are then primarily surgically resected, and the patient may further undergo chemotherapy, the CVD-protocol consisting of cyclophosphamide, vincristine and dacarbazine [204]. Additional approach is radiotherapy with labeled carriers – noradrenaline analogue ^{131}I-MIBG or somatostatin receptor agonist ^{177}Lu-DOTATATE [199, 205]. Overall, 5-year survival of patients with metastatic PCC/PGL is between 34–74%. However, less than 40% of the metastatic tumors respond to the treatment [204, 206].

1.5.2.3. Incidence and genetic background

PCC/PGL are rather uncommon tumors with incidence of 0.6 cases per 100,000 people per year [199], with average diagnosis age around 40 years [206]. Interestingly, PCC/PGL show the highest degree of heritability among all other human neoplastic diseases [169], hence germline mutation screening may discover predisposition to the disease and help with its potential future management. Several heritable familial syndromes show high prevalence of PCC/PGL, including the Von Hippel-Lindau (VHL) syndrome, multiple endocrine neoplasia type 2 (MEN-2), neurofibromatosis type 1 (NF-1) syndrome and paraganglioma (PGL1-5) syndromes (listed in *Introduction table 2*).

The PCC/PGL susceptibility genes frequently encode proteins responsible for pseudohypoxia when mutated – *VHL, SDHx, HIF2A* (cluster I tumors). Rest of PCCs/PGLs than comprises tumors with errors in genes playing role predominantly in signaling cascades - *RET*, *NF1*, *MAX*, *TMEM127* (cluster II tumors) [198]. In conclusion, 35–50% of all PCC/PGL tumors are of familial origin, thus carry at least one germline mutation in over 20 susceptibility genes [169, 198, 206]. While vast majority of children and young age PCC/PGL cases have identified germline mutations, more tumors of sporadic origin arise with increasing age of diagnosis [199]. 25–30% of apparently sporadic tumors are associated with somatic mutations, mostly aforementioned susceptibility genes [206].

Affected gene	Syndrome	PCC/PGL	Other tumors
VHL	VHL	PCC > PGL	Hemangioblastoma, RCC, pancreatic tumor
RET	MEN-2	PCC	Medullary thyroid carcinoma, hyperparathyroidism
NF1	NF1	PCC > PGL	Neurofibroma, glioma, breast cancer
SDHA	PGL5	PGL	Rarely GIST, RCC, pituitary adenoma
SDHB	PGL4	PGL > PCC	Rarely GIST, RCC, pituitary adenoma
SDHC	PGL3	PGL	Rarely GIST, pituitary adenoma
SDHD	PGL1	PGL > PCC	Rarely GIST, RCC, pituitary adenoma
SDHAF2	PGL2	PGL	none
HIF2A	none	PGL > PCC	Polycythemia and somatostatinoma
MAX	none	PCC > PGL	none
TMEM127	none	PCC	Rarely RCC

Introduction table 2 – PCC/PGL associated gene mutations. Numerous heritable gene defects result in high incidence of PCC/PGL tumors. These are known as familial syndromes, since one gene mutation may manifest as more tumor types. Data taken from [169, 199, 201].

1.5.2.4. Paraganglioma syndromes

Inborn defects of CII contribute to 8–10% of hereditary PCC/PGL [207] and overall, 27% of all patients with advanced PCC/PGL have mutation in *SDHx*, with tumors predominantly of extra-adrenal origin [200, 206]. From the initially described *SDHD* mutation causing familial PGLs, other three SDH subunit and one assembly factor genes have been to date recognized as significant tumor suppressors, leading to the characterization of the five PGL syndromes [198].

In 2000, first germline deleterious mutations in the *SDHD* gene were found in several families with inherited head and neck PGLs [208], now there are 148 different gene variants listed that lead to PGL type 1 (PGL1) syndrome, causing almost exclusively head and neck PGLs. Although the carriers develop the disease in 75% under the age of 40, *SDHD*-mutated PCC/PGL are metastatic in less than 5% of the cases (as seen in *Introduction figure 6*) [198].

PGL2 syndrome, caused by an *SDHAF2* mutation, is considerably scarcer with only few pedigrees worldwide possessing the deleterious gene variants [209]. To this date, 5 deleterious mutations in only few dozens of patients have been identified, typically causing carotid body tumors [198].

The *SDHC* gene is responsible for the PGL3 syndrome with its 46 described disease-causing variants [198]. PGL3 shows high disease penetrance with most of the carriers developing tumors before 50 years of age, and again predominantly resulting in carotid body PGL. However, *SDHC*-associated tumors are almost always benign [210].

In contrast to PGL1-3 syndromes with mostly catecholamine non-producing head and neck PGLs, PGL4 syndrome, caused by one of 226 identified mutations in the *SDHB* gene, results in majority of cases in noradrenaline and dopamine producing PGLs located in the abdomen, rarely in adrenal PCC and other tumor types [198, 211]. *SDHB*-defective tumors have lower disease penetrance (less than 50% of the carriers develop tumors); nonetheless, they also pose very high risk of metastatic dissemination (as evident in *Introduction figure 6*). *SDHB*-linked PCC/PGL comprise 43% of all metastatic PCC/PGL, usually with poor prognosis and 5-year survival of 36% [199, 201, 212]. The exact mechanism behind such high malignancy of *SDHB*-mutated tumors, but not other *SDHx*-linked ones, has not been fully explained yet. The first notable hint is the loss of heterozygosity (LOH) of the *SDHB* gene within malignant tumors of most of the germline mutation carriers, fully preventing the CII function [213]. Some studies suggest that the malignant phenotype of *SDHB*-associated PCC/PGL may be due to enhanced epigenetic silencing of genes necessary for cellular differentiation [173] and for the process of epithelial-mesenchymal transition, explaining pronounced metastatic potential of the tumor cells [214].

From the initial link of *SDHA* mutations only to Leigh syndrome, overall 30 mutations have been described to cause the last of the PGL syndromes, PGL5. *SDHA* variants show very low incidence and only 10% of the carriers develop a tumor by the age of 70. However, *SDHA* mutations lead to both PCCs and PGLs, mostly catecholamine-producing, apparently with high metastatic rate of more than 20% (apparent in *Introduction figure 6*) [215], which further extends the view of only *SDHB* as the main malignancy risk in PCC/PGL.

Interestingly, while *SDHA*, *SDHB* and *SDHC* germline mutations show autosomal dominant inheritance [169], both *SDHD* and *SDHAF2* gene defects lead to the disease only when inherited from father, due to their nearby loci on chromosome 11 that undergo genomic imprinting [216, 217]. In summary, CII-associated genes play a major role in cancers of neuroendocrine origin PCC and PGL, with the most frequent incidence of *SDHB* and *SDHD* mutations. Especially *SDHB*-mutated tumors then significantly contribute to malignancy and lethality of PCC/PGL.

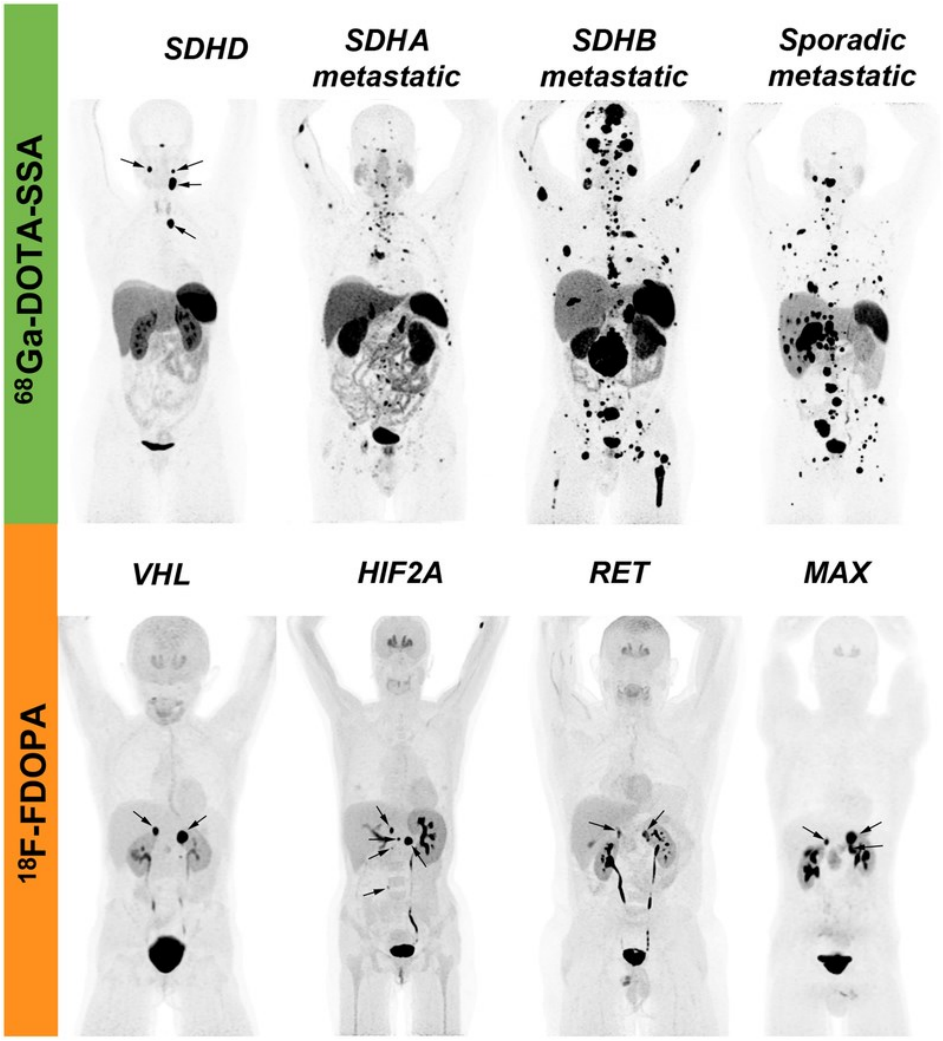

Introduction figure 6 – PET-CT image of patients with PCC/PGL-associated familial syndromes. The imaging was performed radioactively labeled somatostatin analogue (^{68}Ga-DOTA-SSA) and dopamine precursor analogue (^{18}F-DOPA). The PET-CT scans clearly show highly aggressive and metastatic potential of *SDHB*- and, to lower extent, *SDHA*-mutated PCC/PGLs. On the other hand, *SDHD*-mutated PGLs usually present as non-metastatic tumors. Mutations in other susceptibility genes *VHL*, *RET* and *MAX* predominantly manifest as adrenal PCC, as seen in the figure; additionally, *HIF2A* mutation causes rather PGL. Reprinted from [205].

1.5.3. Other tumors

Gastrointestinal stromal tumors (GIST) affect predominantly the stomach tissue. While majority of the tumors is driven by *KIT* or *PDGFRA* mutations, up to 7.5% of the apparently sporadic tumors comprise *SDHA*, *SDHB*, *SDHC* or *SDHD* mutations, mostly in pediatric patients [218]. Interestingly, epigenetic mutations of *SDHC*, caused by hypermethylation of the *SDHC* promotor without any alteration of the gene sequence, was also described in GIST and has similar presentation as deleterious *SDHx* mutation [219]. CII-deficient GISTs then express high level of IGF1R via the HIF-1 pathway, which may be responsible for *SDHx* mutated GIST tumorigenesis [220]. GISTs lacking the CII function show high recurrence and metastasis rate, and treatment options for the disease are very limited [221].

Renal cell carcinoma (RCC) was also found to carry mutations in all four SDH subunits [222], although with much lower incidence (less than 0.2% of renal tumors) [223]. Similarly, *SDHx* mutations rarely occur in 0.3% of pituitary adenomas [224]. It is worth noting that considerable number of patients with CII-dysfunctional neoplasms have synchronous incidence of more tumor types and report the disease in family history [223], pointing out to the attribution of the inherited germline *SDHx* mutations.

1.5.4. Ongoing research on tumor management

In case of advanced SDH-defect-driven tumors, therapy that is more specific is still needed since there is no truly curative treatment of the metastatic tumors, and current options are rather palliative.

1.5.4.5. Pharmacological intervention

Future interventions should consider genetic background of the tumor inasmuch as its mutation status mostly predicts tumor features that may be targeted by the therapy. Considerable portion of the advanced PCC/PGL of cluster I characteristic by pseudohypoxia, those with mutations in *SDHx*, *FH* and *VHL*. Since the detrimental effect of pseudohypoxia is caused mostly by HIF-2α [225], selective HIF-2α antagonists may potentially become a part of the future therapeutic regimen of the pseudohypoxic tumors. Phase II clinical trial of treatment with the HIF-2α inhibitor is currently ongoing for *VHL*-mutated RCC [206]. Additionally, PCC/PGL are typically vascularized tumors, and with pseudohypoxia further potentiating the angiogenic process, anti-angiogenic therapy comes into consideration. Therapy using anti-VEGFA monoclonal antibodies is currently approved for metastatic *SDHB*-mutated RCC [206] and could be potentially used also in metastatic PCC [226]. Another possible anti-angiogenic approach includes the use of small molecular VEGFR inhibitor sunitinib, which was also evaluated in phase II clinical trial of progressive PCC/PGL [227]. In addition, advanced GIST and RCC tumors seem to response to the VEGFR inhibitors as well [228, 229]. In case of SDH-deficient GIST, the patients may benefit from anti-IGF1R therapy since the receptor overexpression evidently drives tumor growth [230]. However, the treatment is accompanied by serious side effects, such as hyperglycemia and hyperinsulinemia [231].

Cluster I PCC/PGL also exhibit dependency on complex I function, NAD^+ pool and PARP-dependent DNA repair. PARP inhibitor olaparib, indeed, may show a therapeutic effect, particularly in *SDHB*-mutated tumors when combined with the conventional chemotherapeutic agent temozolomide [232]. Temozolomide alone shows high efficacy in *SDHB*-defective tumors. The drug acts by DNA methylation and also epigenetic silencing of the *MGMT* gene, encoding the enzyme repairing the methyl adducts on DNA [233].

The search for more efficient therapeutic approaches is subject of many studies. Interestingly, ascorbic acid in high doses shows promising effect on *SDHB*-defective tumors. Ascorbic acid treatment exploits elevated intracellular iron and ROS levels within *SDHB*-mutated cancer cell, generating additional oxidative damage that leads to apoptosis. Furthermore, ascorbic acid restores the activity of histone demethylases, remodeling the epigenome and reversing the detrimental hypermethylator phenotype [177].

1.5.4.6. Complex-II-targeted therapy

Some studies suggest CII as a potential target for anti-cancer therapy, especially in *SDHx* non-mutated tumors. CII inhibition leads to ROS generation with a detrimental effect on the cancer cell and, eventually, results in apoptosis [132, 234]. Indeed, a vitamin E analogue α-tocopheryl succinate (α-TOS), is a potential anti-cancer drug that exhibits its effect by associating with the ubiquinone-binding site of CII, promoting excessive ROS generation and killing the cancer cell. Even more intriguing anti-tumor effect was seen with a similar compound, MitoVES, which is a molecule of α-TOS linked to the charged triphenylphosphonium (TPP^+) group, specifically targeting the agent into mitochondria. MitoVES also inhibits Q_P site of CII and is more than 20-fold more efficient than α-TOS [235]. In addition, several other drugs inhibiting CII ubiquinone-binding site are possible candidates for cancer therapy [100, 235].

1.5.4.7. Immunotherapy

One of the first studied immunotherapies of PCC/PGL was interferon alpha-2b therapy, activating NK cells, that showed considerable benefit but also serious side effects [236]. Nowadays, a number of clinical trials focus on immune checkpoint inhibitors, examining several antibodies blocking PD-1, PD-L1 or CTLA-4 for the treatment of solid tumors, including progressive PCC/PGL [237]. Notably, pseudohypoxic tumors typically show increased expression of the immune-checkpoint-related proteins such as PD-L1 [193], which makes the immune-checkpoint-targeted therapy a promising way of management of pseudohypoxia-driven progressive tumors, including those with *SDHx* mutations [206].

1.6. Rationale for the research

PCC and PGL are rare, usually non-malignant diseases. However, when associated with a certain gene mutation, the tumor may become highly aggressive and potentially lethal. PCC/PGL frequently arise within familial paraganglioma syndromes caused by mutations in the genes encoding CII subunits SDHA-D or the SDHAF2 assembly factor. The tumor progresses mostly due to CII dysfunction, succinate accumulation and ensuing pseudohypoxia. Mutations of different *SDHx* genes, nonetheless, have a distinct clinical outcome, wherein mutations in *SDHB* gene are associated with the most aggressive disease course of PCC/PGL. There is no satisfactory explanation for this fact; moreover, neither truly curative therapy for the advanced metastatic disease exists to this date.

Bezawork-Geleta and colleagues showed that SDHB-deficient cells lack functional CII and accumulate alternative assembly form CII_{low}, comprising SDHA and its two dedicated assembly factors SDHAF2 and SDHAF4. They suggested that CII_{low} may have a signaling role, besides being a pool for unbound SDHA, modulating cell metabolism. Therefore, we focused on CII_{low} subspecies and its composition, considering the role of SDHAF2 and SDHAF4. In addition, we wanted to elucidate the purpose of SDHAF4 within CII maturation, since its exact role is not clear. For our study, we used human pheochromocytoma cell line for generation of stable knockout models of *SDHAF2* and *SDHAF4* genes, followed by re-expression of both genes; and we studied the cell models on several levels.

1.6.1. Human pheochromocytoma cell line

Neuroendocrine tumors PCC and PGL are a focus of many reserchers, especially in case of highly malignant tumors, such as those with *SDHB* mutations, despite relatively low prevalence of this type of cancer. The research of molecular mechanism leading to tumor progression and subsequent development of more specific therapy necessitates a suitable cell line. The first PCC cell line was introduced in rat model as early as in 1976, termed PC12 [238]. Later in 2000, a mouse PCC cell line MPC was developed using *NF-1* knockout mouse [239], and additional cell line was generated by injection of MPC cells in the mouse, subsequent harvest of the metastasis and isolation of the cells exhibiting high aggressivity and metastatic potential, which gave it a name of mouse tumor-tissue derived (MTT) cell line [240]. Human PCC cell line was first introduced in 1998, derived from a patient with PCC malignancy caused by the *RET* mutation; however, the line exerted limited cell lifespan and lacked the ability to form tumors in immunodeficient mice [241].

In 2013, Ghayee and colleagues introduced human progenitor-cell-derived line from pheochromocytoma tumor (hPheo1) [242]. In particular, neuroendocrine cells obtained from a benign tumor of a 38 years old female were transduced with the virus vector carrying the human telomerase reverse transcriptase (hTERT) gene, thus generating an immortalized cell line. Thereby, Ghayee and colleagues have finally established a stable human PCC cell line hPheo1, characterized by the PCC marker chromogranin A upon stimulation, but also very low secretion of catecholamines. hPheo1 cells appear to be dediferentiated, thus lacking catecholamine-producing enzymes; and pre-malignant cells, i. e. progenitor cells of the tumor. Moreover, the cells show loss of p16, further promoting their continued proliferation [242]. Taken together, the hPheo1 cell line makes a great candidate for the study of PCC/PGL susceptibilty genes and their impact on metabolism and eventual tumor progression, which is the subject of our study. The cell line was a kind gift from Professor Karel Pacák (Section of Medical Neuroendocrinology, *Eunice Kennedy Shriver* National Institute of Child Health and Human Development, National Institutes of Health, Bethesda, MD, USA).

2. Aims

This thesis focuses on the role of mitochondrial complex II (CII) in cancer cell biology, with the emphasis on its alternative assembly form. The study is pursued using human pheochromocytoma cell line hPheo1. The overall aim of the thesis comprises several sub-objectives:

- To generate stable knockout model of the *SDHAF2* gene, the *SDHAF4* gene and double knockout model of the *SDHAF2* and *SDHAF4* genes in hPheo1 cells
- To prepare model of re-expression of the *SDHAF2* and *SDHAF4* genes
- To examine the prepared hPheo1 clones on genomic and protein level, to determine CII assembly and functionality
- To estimate the effect of the gene knockout on whole-cell level by measuring cell proliferation rate and tumor formation in a xenograft mouse model
- To deduce the role of different forms of the alternative assembly form of CII in prepared cell clones
- To suggest a role of SDHAF4 in CII assembly and functionality

3. Materials and methods

3.1. Cell culture

The hPheo1 cells were cultivated at 37 °C under normoxic conditions and in 5% CO_2 atmosphere in a humidified incubator. The parental cell and subsequent KO clones were grown in the following medium (with final concentrations of the supplements in brackets):

RPMI-1640 Medium
10% FBS
Penicillin (100 U/ml) and streptomycin (100 µg/ml)
Glucose (4.25 g/l)
Sodium pyruvate (200 mg/l)
Uridine (50 mg/l)

An exception were in later prepared *SDHAF2*/*SDHAF4* dKO clones, which were cultivated in medium containing higher amount of glucose (6.5 g/l). Both reconstituted models, i. e. $SDHAF2^{rec}$ and $SDHAF4^{rec}$ cells, were continuously held under antibiotic selection of 2 µg/ml of puromycin.

The cells were cultivated in sterile polystyrene flasks, dishes and wells. When harvesting or passaging, the cells were washed by phosphate buffer saline (PBS), and trypsin/EDTA (0,25%/0,01%) solution was added, followed by 5 min incubation at 37 °C. The cells in culture were passaged 2-3 times a week, depending on the clone.

3.2. Preparation of knockout and reconstitution system

Genomic deletion of both *SDHAF2* and *SDHAF4* genes in hPheo1 cells was performed using the CRISPR/AsCpf1 (also known as CRISPR/AsCas12a) system [243]. The CRISPR/AsCpf1 system offers higher precision over the conventionally used Cas9 endonuclease, and allows to cleave more loci of the targeted gene at the same time thanks to self-cleaving sgRNA [244]. The re-expression of both proteins was accomplished using lentiviral transduction of the respective genes.

3.2.1. Design of crRNAs for *SDHAF2* and *SDHAF4* knockout

Relevant crRNAs for the CRISPR/AsCpf1 system were identified using the CRISPOR software [245]. The subsequent oligonucleotides were designed to contain overhang sequences 5'-AGAT and 3'-AAAA necessary for cloning. For *SDHAF2* KO, three different crRNAs were used, one targeting exon 2 of *SDHAF2* gene and the other two targeted introns before and after exon 2 (*Methodical figure 1A*). Exon 2 was selected because it encodes a highly conserved glycine $SDHAF2^{G78}$, which is crucial for SDHAF2 function [246].

For *SDHAF4* genetic KO, variant 6 was used containing three crRNAs and variant 7 with only one crRNA. *SDHAF4* KO variant 6 was therefore targeted again inside exon 2 of the gene, before and after the exon; variant 7 only inside exon 2 of *SDHAF4* (*Methodical figure 1B*). Exon 2 of the *SDHAF4* gene was targeted since it represents the largest exon, covering almost half of the protein-coding region [112].

SDHAF2 gene targeted crRNAs:

1) 5'-GTCATGAGGAAATTACACTGCTG-3'

2) 5'-GGAATCTGTTGGGCTGTCACCTC-3'

3) 5'-CTACTGGGCCACAGGTACTGGGT-3'

Designed oligonucleotides:

5'-AGATGTCATGAGGAAATTACACTGCTGAATTTCTACTCTTGTAGATGGAATCTGTTG-GGCTGTCACCTCAATTTCTACTCTTGTAGATCTACTGGGCCACAGGTACTGGGT-3'

3'-AAAAACCCAGTACCTGTGGCCCAGTAGATCTACAAGAGTAGAAATTGAGGTGA-CAGCCCAACAGATTCCATCTACAAGAGTAGAAATTCAGCAGTGTAATTTCCTCATGAC-5'

SDHAF4 gene targeted crRNAs of variant 6:

1) 5'-TACATTCACATTTCTCAAAGTTC-3'

2) 5'-CTCAGAGAATGACACAGAAGGGG-3'

3) 5'-TTAAGAAATCTACATGTATCGAT-3'

Designed oligonucleotides of variant 6:

5'-AGATTACATTCACATTTCTCAAAGTTCAATTTCTACTCTTGTAGATCTCAGAGAATGA-CACAGAAGGGGAATTTCTACTCTTGTAGATTTAAGAAATCTACATGTATCGAT-3'

3'-AAAAATCGATACATGTAGATTTCTTAAATCTACAAGAGTAGAAATTCCCCTTCTGTGT-CATTCTCTGAGATCTACAAGAGTAGAAATTGAACTTTGAGAAATGTGAATGTA-5'

SDHAF4 gene targeted crRNA of variant 7:

2) 5'-CTCAGAGAATGACACAGAAGGGG-3'

Designed oligonucleotides of variant 7:

5'-AGATCTCAGAGAATGACACAGAAGGGG-3'

3'-AAAACCCCTTCTGTGTCATTCTCTGAG-5'

Methodical figure 1 – Designed crRNAs targeting SDHAF2 (A) and SDHAF4 (B) genes. The sequences were determined using the CRISPOR software. Targeting sequences of the designed crRNAs are depicted as red boxes, with exon 2 as a blue box. For both systems, crRNA-1 and -3 were designed to target introns before and after exon 2, with crRNA-2 targeting exon 2.

3.2.2. Generation of CRISPR/AsCpf1 system

Expression plasmid 55 pX AsCpf1-Venus-NLS, which was a kind gift from Dr. Björn Schuster (Institute of Molecular Genetics, Czech Academy of Sciences), was used for the CRISPR/AsCpf1 system generation. First, 5 µg of the empty vector was digested using 3 µl of FastDigest BpiI endonuclease with 3 µl FastAP, 6 µl FastDigest Green Buffer (10×) in total 60 µl of reaction. The reaction was carried out in thermal cycler MasterCycler, at 30 °C for 30 min followed by 60 °C for 20 min. The digested product was resolved using 1% agarose gel electrophoresis with TAE and GelRed® Nucleic Acid Gel Stain at constant voltage of 90 V; the cleaved portion of the plasmid was visualized using UV-light visualizer MiniBIS Pro, cut out of the gel and purified using NucleoSpin® Gel and PCR Clean-up kit.

Lyophilized oligonucleotides were dissolved in ddH_2O to 100 µM concentration and then diluted 100×. 1 µl of each diluted oligonucleotide was mixed with 0.5 µl of T4 polynucleotide kinase, and 1 µl of 10× T4 DNA ligase buffer, and 6.5 µl of ddH_2O was added. The reaction of phosphorylation and annealing of the oligonucleotides was performed in thermal cycler at 37 °C for 30 min followed by 5 min of 95 °C with gradual decrease of the temperature to 25 °C. The reaction product was then diluted 1:200 and used in the next step.

The phosphorylated and annealed oligonucleotides were then ligated into the previously digested empty 55 pX AsCpf1-Venus-NLS plasmid. 50 ng of the cleaved plasmid was mixed with 1 µl of the diluted oligonucleotide mixture, 1 µl of T4 DNA ligase and 1 µl of 10× T4 DNA ligase buffer into 10 µl of total volume of the reaction mixture that was incubated for 30 min at room temperature (RT). 5 µl of the reaction mixture was then added to *Escherichia coli* strain Endura™ Competent Cells. Transformation of the bacteria was accomplished by heat-shock, i. e. 30 min incubation on ice followed by 45 sec in 42 °C bath and then for 1 min on ice. Pre-heated SOC medium was added to the bacteria, which were incubated for 1 h at 37 °C, spread over ampicillin-containing agar plate and incubated overnight.

For confirmation of successful insertion of the plasmid of our interest, colony PCR was performed on the colonies grown on the agar plate, even though 55 pX AsCpf1-Venus-NLS plasmid encodes ampicillin resistance. The selected colonies were carefully collected by a sterile pipette tip and further smeared over a fresh ampicillin-selective agar plate. The tip was concurrently washed in a PCR reaction mixture, containing 7.5 µl of DreamTaq™ Green PCR Master Mix (2×), 0.75 µl of DMSO, 0.15 µl of 10% Tween-20, 6.6 µl of ddH_2O and 3 µl of mixture of PXPR and crRNA-specific primers (*Methodical table 1*). The point is that the PXPR primer anneals with the plasmid itself, while the crRNA-specific primer binds to the borderline of the plasmid and the inserted oligonucleotides (specifically their 3'-AAAA overhang); therefore, PCR reaction occurs only in plasmids with correct inserts. The

samples were run in a thermal cycler at 95 °C for 3 min, then 35 cycles of PCR (94 °C for 30 s, 55 °C for 30 s, 72 °C for 70 s) and 4 min of 72 °C. The PCR products were resolved on a 2% agarose TAE gel with GelRed® at 90 V, and positive clones were selected using UV light visualization (data not shown). Next day, the selected confirmed bacterial clones were scraped off the second agar plate, pre-incubated in the LB medium and transferred into 100 ml of LB with 200 µg/ml ampicillin in an Erlenmeyer flask. The bacteria were cultivated by overnight, shaking at 37 °C. Finally, the plasmid was isolated from the grown bacterial culture using NucleoBond® Xtra Midi kit according to the manufacturer's instructions.

Tris-acetic acid-EDTA (TAE) buffer 50× concentrated:

Tris (2 M)
EDTA (50 mM)
Acetic acid (1 M)

SOC medium:

KCl (2.5 mM)
$MgCl_2$ (10 mM)
$MgSO_4$ (10 mM)
Glucose (20 mM)

The reagents dissolved in 50 ml of dH_2O and added to the LB medium

To further confirm oligonucleotide insertion and to eliminate the risk of potential mutations originated in bacteria, the isolated plasmids were sequenced. 0.5 µg of the plasmid was mixed with 0.5 µl of stock 100 µM mixture of PXPR and crRNA-specific primers (*Methodical table 1*) and diluted to 10 µl in a sterile Eppendorf tube. The sample was marked with a barcode sticker and sent to Eurofins Genomics Company for Sanger sequencing. The results were then analyzed using SeqMan Pro 15 software (DNASTAR Lasergene).

PXPR (forward)	5'-GGACTATCATATGCTTACCGTAACTTGAAAG-3'
crRNA insert (reverse)	5'-AAAAGCACCGACTCGGTGCC-3'

Methodical table 1 – Plasmid sequences for colony PCR confirmation of oligonucleotide insertion.

3.2.3. hPheo1 cells transfection

Either hPheo1 parental cells (for *SDHAF2* and *SDHAF4* KO), or later SDHAF2^{KO7} (for SDHAF2/SDHAF4^{dKO2}) and SDHAF4^{KO36} (for SDHAF4/SDHAF2^{dKO8}) were seeded into a 6-well plate at the density of 1-3×10^5 per well. Next day, the standard hPheo1 growth medium was changed to serum-free Opti-MEM™ medium specific for transfection. Lipofectamine™ 3000 was then used to transfect 2 µg of the isolated plasmid, encoding specific CRISPR/AsCpf1, per one well of the cells, according to the manufacturer's instructions. The cells were incubated with the transfection reagent for 6 h and then the medium was changed to the standard hPheo1 growth medium without penicillin/streptomycin. After 24–48 h, the

cells were trypsinized and resuspended with the serum-free hPheo1 growth medium. The cells positive for the fluorescent Venus protein (which is also encoded within the 55 pX AsCpf1-Venus-NLS plasmid) were single-cell-sorted into a 96-well plate in the Imaging Methods Core Facility in BIOCEV, Vestec.

3.2.4. Knockout confirmation

After 2–3 weeks of cultivation, several clones of the desired KO were obtained, and the clones were examined on several levels. For the CRISPR/AsCpf1 system targeting three gene loci at once, the expected outcome was to cut off the whole sequence of the gene; therefore, this could be visualized as a shift on PCR-electrophoresis. However, CRISPR/AsCpf1 with only one crRNA (*SDHAF4* KO variant 7) could be examined only by sequencing, since the system was thought to generate rather point sequence alterations. Furthermore, *SDHAF2* KO could be confirmed using SDS-PAGE/WB, which was not feasible in *SDHAF4* KO (see the chapter *SDS-PAGE/WB analysis*).

Both SDHAF2^{KO7} and SDHAF2^{KO9} clones were obtained as one single-cell clone first. The *SDHAF2* KO in this clone was confirmed using PCR-electrophoresis and SDS-PAGE/WB (data not shown). The clone, however, started to recover CII activity, presumably due to somewhat heterogeneous clone population. The cells were therefore single cell-sorted once again, generating stable SDHAF2^{KO7} and SDHAF2^{KO9}. The KO phenotype of both clones is further confirmed in this thesis.

SDHAF4^{KO81} was generated using *SDHAF4* KO variant 6 system. DNA from the clones was harvested using genomic the DNA isolation buffer, incubated at 55 °C for 30 min and denatured at 95 °C for 5 min. 1 µl of the DNA lysate was mixed with 5 µl DreamTaq™ Green PCR Master Mix (2×) with 1 µl of forward and reverse genomic primer 1 µM mixture (*Methodical table 2*) into 10 µl of the reaction mixture. The PCR was performed in a thermal cycler according following protocol: 98 °C for 2 min, 95 °C for 12 min, then 35 cycles (98 °C for 2 s, 63 °C for 30 s, 72 °C for 1 min) and finally 72 °C for 5 min. The PCR product was then resolved in the 2% agarose TAE gel with GelRed® at voltage of 90 V and visualized using UV light, with apparent shift of the SDHAF4^{KO81} band (*Methodical figure 2A*).

SDHAF4^{KO36} was obtained via *SDHAF4* KO variant 7 system. Genomic DNA of high purity was isolated using the Wizard® SV Genomic DNA Purification System, according to the manufacturer's instructions. DNA concentration was measured using NanoDrop and 1 µl of the eluted DNA was added to PCR reaction (as described in the previous paragraph, but with clear DreamTaq™ PCR Master Mix). 0.4 µg of PCR product was mixed with 0.5 µl of each of 100 µM stock genomic primers and ddH_2O was added to the total of 10 µl. The samples were sent to Eurofins Genomics Company for Sanger sequencing and the data was evaluated in

SeqMan Pro 15 software, confirming the gene alteration in SDHAF4^{KO36} cells (*Methodical figure 2B*). Later, SDHAF4^{KO81} was also sequenced, additionally confirming the missing gene sequence (*Methodical figure 2A*).

SDHAF2/SDHAF4^{dKO2} cells were generated using one crRNA *SDHAF4* KO variant 7 system, the clone was hence also confirmed by sequencing (*Methodical figure 2C*). SDHAF4/SDHAF2^{dKO8} status was confirmed mainly on PCR-electrophoresis (*Methodical figure 2D*) and the subsequent SDS-PAGE/WB.

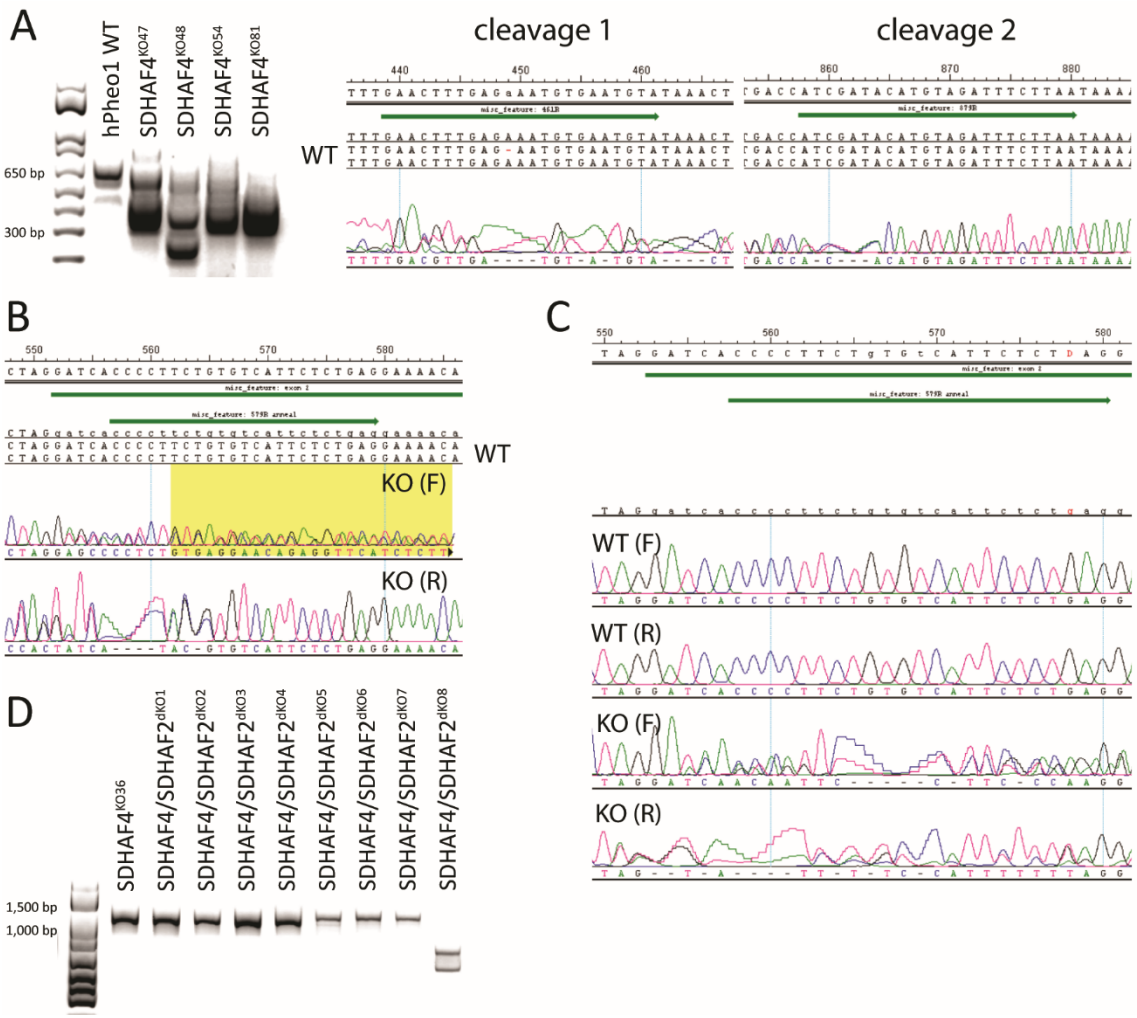

Methodical figure 2 – Confirmation of SDHAF4 KO (A, B), SDHAF2/SDHAF4 dKO (C) and SDHAF4/SDHAF2 dKO (D). (A) SDHAF4^{KO81} was confirmed using PCR with genomic SDHAF4 primers, where the product is shifted on a gel without any product in wild-type (WT) allele height (left) and by Sanger sequencing of the *SDHAF4* gene (right). The sequencing shows, compared to the WT *SDHAF4* sequence, two cleavages (crRNA-2 and crRNA-3 from the chapter *Design of crRNAs for SDHAF2 and SDHAF4 knockout*) in the gene with missing sequence in between. (B) SDHAF4^{KO36} clone was validated by sequencing, showing deletions in both alleles of the *SDHAF4* gene. (C) SDHAF2/SDHAF4^{dKO2} was also confirmed using sequencing data, showing two upper sequences of the *SDHAF4* gene of SDHAF2^{KO7} cells, lower two sequences show the same gene of SDHAF2/SDHAF4^{dKO2}, containing deletions. (D) SDHAF4/SDHAF2^{dKO8} was confirmed by PCR of *SDHAF2* gene and the only dKO8 exhibits clear shift of the reaction product without a trace of the WT allele.

Genomic SDHAF2 (forward)	5‘-TTTCAGGGGGATAGGGTCCG-3‘
Genomic SDHAF2 (reverse)	5‘-AATTACCCGGGTGTGGTGAC-3‘
Genomic SDHAF4 (forward)	5‘-CCAGGAAGGGAAATGGCTGGA-3‘
Genomic SDHAF4 (reverse)	5‘-CTTTTCGTTGAGTTATTGGAGTCCT-3‘

Methodical table 2 – Genomic primers for PCR and sequencing confirmation of the KO.

Genomic DNA isolation buffer:

EDTA (250mM) pH 8-9
SDS (1%)
Proteinase K (1 mg/ml)

3.2.5. SDHAF2 and SDHAF4 re-expression

For reconstitution of the knocked-out proteins, cDNA encoding human *SDHAF2* and *SDHAF4* genes (sequences available online), which was kindly provided by Dr. Jared Rutter (Department of Biochemistry and HHMI, University of Utah), was sub-cloned into pCDH-CMV-MCS-EF1-Puro vector. *SDHAF2* gene was used in its WT form; however, a sequence encoding Flag-tag (*Methodical table 3*) was added to the C-terminus of SDHAF4 for better detection of the re-expressed protein. First, PCR was performed with specific cloning primers (*Methodical table 3*), generating overhang sequences that will later ligate with the pCDH-CMV-MCS-EF1-Puro plasmid, digested with two different restriction endonucleases. For the reaction, iProof High-Fidelity DNA Polymerase was used. The resulting PCR product and pCDH-CMV-MCS-EF1-Puro plasmid were cleaved by the restriction FastDigest enzymes XbaI and BamHI. 1 µl of each enzyme was added to 1 µg of DNA and 2 µl of FastDigest Green Buffer (10×) in 20 µl of the reaction mixture. The reaction was carried out in a thermal cycler at 37 °C for 5 min followed by 10 min at 80 °C. The product was resolved using 1% agarose TAE gel with GelRed®, the cleaved products were cut out and cleaned using the NucleoSpin® Gel and PCR Clean-up kit. Concentrations of the digested plasmids and inserts were measured using NanoDrop. Plasmid/insert were mixed at the molecular ratio 1/5, respectively, into the ligation reaction carried out by T4 DNA ligase. For ligation 10 µg of the insert and 50 µg of the plasmid was mixed with 1 µl of T4 ligation buffer (10×) and 1 µl of T4 DNA ligase. The reaction was performed in a thermal cycler at 25 °C for 30 min.

Ligation reaction (5 µl) was then used to transform One Shot™ Stbl3™ Chemically Competent *E. Coli* and the plasmids were isolated identically to the procedure used for *Generation of CRISPR/AsCpf1 system* described above. The final constructs were also sequenced, confirming the insertion of non-altered wild-type (WT) *SDHAF2* or *SDHAF4* DNA. The constructs were then transfected into HEK293 cells using calcium-phosphate transfection together with the lentivirus packaging plasmids psPAX2 and pMD2.G. The medium containing the desired lentiviral particles was collected 48 h post infection and the

viral particles were precipitated using the PEG-it™ Virus Precipitation Solution, according to the manufacturer's instructions. Finally, the cells were transduced with the lentiviral particles at the multiplicity of infection (MOI) of 10. SDHAF2^{KO7} cells were transduced with viruses carrying *SDHAF2* WT gene, SDHAF4^{KO36} cells were transduced with *SDHAF4* Flag-tagged gene. Since the pCDH-CMV-MCS-EF1-Puro plasmid also encodes puromycin selection, the reconstituted cells were kept at 2 μg/ml of puromycin.

Flag-tag sequence	5'-GACTACAAAGACGATGACGACAAG-3'
SDHAF2 cloning primer (forward)	5'-TAAGCATCTAGACCACCATGGCGGTGTCTACAGTGTTCTC-3'
SDHAF2 cloning primer (reverse)	5'-TGCTTAGGATCCTCAACGTGGCTTTTCAAAGAGGTAC-3'
SDHAF4 cloning primer (forward)	5'-TAAGCATCTAGACCACCATGACCCCATCGAGGCTTCC-3'
SDHAF4 cloning primer (reverse)	5'-TGCTTAGGATCCTTAAAAATCAATACAGCGTCCTTTTCGTTC-3'

Methodical table 3 – Flag-tag sequence used in re-expression of SDHAF4, and SDHAF2- and SDHAF4-specific cloning primers.

3.3. Protein-analyzing methods

3.3.1. Sodium dodecyl sulfate – polyacrylamide gel electrophoresis (SDS-PAGE)

For purpose of the sodium dodecyl sulfate – polyacrylamide gel electrophoresis (SDS-PAGE), selected clones of hPheo1 cells were cultivated in 100 mm plates, washed with ice-cold PBS and scraped in small volume of the PBS into an Eppendorf tube. The cells were centrifuged at 300*g* for 5 min at 4 °C and resuspended in 100 μl of radio-immunoprecipitation assay (RIPA) buffer. The samples were then vortexed vigorously and kept on ice for 30 min, while shaking. Subsequently, the tubes were centrifuged at 10,000*g* for 10 min at 4 °C and the supernatant, representing the whole cell lysate, was acquired. Protein concentration of the samples was determined using the Pierce™ BCA Protein Assay Kit, according to the manufacturer's instructions. The samples were mixed with 4× concentrated SDS-PAGE loading buffer.

For the electrophoresis, gels were prepared, using 1.5 mm wide Mini-PROTEAN® glass plates, combs and a stand. After the gel plates assembly, 12% resolving gel was poured, covered with a layer of isopropyl alcohol and let to polymerize for approximately 30 min. Then, 4% resolving gel was poured and a 10-well comb was inserted into the gel. After complete hardening, the gels were placed in the Mini-PROTEAN® Tetra Vertical Electrophoresis Cell filled with SDS-PAGE running buffer. 50-100 μg of protein of each sample mixed with SDS-PAGE loading buffer was placed into the wells, together with 5 μl of the Precision Plus Protein™ marker.

Electrophoresis was run initially at 80 V until the samples reached the resolving gel, then voltage was increased to 100-120 V and the samples were run to the bottom of the gel. Subsequently, western blotting (WB) was performed according the protocol in Western blotting (WB) and protein detection.

RIPA buffer:

NaCl (150 mM)
Tris (50 mM)
NP-40 (1%)
SDS (0.1%)
EDTA (1 mM)
Sodium deoxycholate (0.5%)
dH_20 added to 200 ml

12% resolving acrylamide gel:

1.5 M Tris-HCl, pH 8.8 (375 mM)
Sodium dodecyl sulfate (0.1%)
Acrylamide/bis-acrylamide (12%)
Tetramethyl ethylenediamine (TEMED; 0.05%)
Ammonium persulfate (APS; 0.05%)

4% focusing acrylamide gel:

0.5 M Tris-HCl, pH 6.8 (125 mM)
Sodium dodecyl sulfate (0.1%)
Acrylamide/bis-acrylamide (4%)
Tetramethyl ethylenediamine (TEMED; 0.06%)
Ammonium persulfate (APS; 0.06%)

SDS-PAGE loading buffer:

Tris-HCl (250 mM)
Glycerol (40%)
Sodium dodecyl sulfate (8%)
Dithithreitol (20%)
Bromphenol blue (0.02%)

SDS-PAGE running buffer 10× concentrated:

Tris (250 mM)
Glycine (1.92 M)
Sodium dodecyl sulfate (34.7 mM)
dH_2O added to 1l, diluted with dH_2O for SDS-PAGE running buffer

3.3.2. Isolation of mitochondria

For the following experiments, mitochondria were isolated as previously published [247]. In our case, the cells were cultivated on 5–10 150 mm dishes, washed with ice-cold PBS and scraped. The cells were centrifuged for 8–10 min at 500*g*, 4 °C and the pellet was resuspended in 5 ml of sucrose-Tris-EDTA (STE) buffer. The cells were then homogenized

using a Balch homogenizer. The suspension was drawn up into a 1 ml syringe and passed three times through 8 μm-wide opening of the homogenizer. The homogenate was centrifuged for 5 min at 800*g* and 4 °C, the supernatant was then centrifuged for 5 min at 3,000*g*, 4 °C. The supernatant was collected and finally centrifuged for 15 min at 10,000*g* and 4 °C, using a fixed-angle rotor. The supernatant was aspirated and the mitochondrial fraction was present as the pellet after the last centrifugation. The samples were stored in -80 °C.

STE buffer:

Sucrose (250 mM)
Tris (10 mM)
0.5 M EDTA (1 mM)
dH_20 added to 100 ml, pH adjusted to 7.6

3.3.3. Native blue gel electrophoresis (NBGE)

The method of blue-native polyacrylamide gel electrophoresis (BN-PAGE) or native blue gel electrophoresis (NBGE) differs from SDS-PAGE in non-reducing and non-denaturing environment, allowing to observe whole protein complexes and supercomplexes [76]. The key point is the use of mild detergent digitonin, which is able to isolate the complexes from membranes without breaking the non-covalent intra-molecular bonds, thus preserving the complexes in their native state. The complexes are then covered with charged molecules of the Coomassie blue stain, mediating their migration along the gradient gel. The method was performed according to the published protocol [248].

First, protein complexes were isolated from the mitochondrial fraction. The mitochondrial pellet was resuspended in 100–150 μl of STE buffer supplemented with the protease inhibitor mix M diluted 1:100. Protein mass was determined using the Pierce™ BCA Protein Assay Kit. The mitochondrial isolate was centrifuged at 10,000*g* for 10 min at 4 °C, the supernatant was discarded and the pellet was resuspended in the NBGE extraction buffer in ratio 35 μl of the extraction buffer per 100 μg of protein. Digitonin (dissolved in dH_2O to 20% w/v) was then added at 8 μg of digitonin per 1 μg of protein. The sample was then vigorously vortexed, kept on ice for 15 min, while shaking and centrifuged at 23,000*g* for 15 min at 4 °C. The supernatant was collected and concentration of the solubilized protein was determined using the BCA Protein Assay Kit.

The sample was mixed with the NBGE loading buffer, at 0.015 μl of the loading buffer per 1 μg of the protein, and immediately loaded onto the precast NativePAGE Novex Bis-Tris 4–16% gradient gel. For CII subunits and SDHAF2 detection, 10 μg of the sample was loaded into the well; and for SDHAF4 detection, 30 μg of sample was used.

The gels were assembled into a Mini Gel Tank. The tank was filled with NBGE blue cathode buffer and anode buffer, and the electrophoresis was run at 4 °C for 60 min at constant voltage of 35 V. Afterwards, the NBGE blue cathode buffer was aspirated and the chamber filled with NBGE clear cathode buffer instead, and electrophoresis was then set to 25 V and run overnight at 4 °C.

NBGE extraction buffer:

Aminocaproic acid (1.5 M)
Bis-Tris (50 mM)
0,5 M EDTA (2 mM)
dH_2O added to 100 mL, pH adjusted to 7

NBGE loading buffer:

Aminocaproic acid (0.75 M)
Bis-Tris (50 mM)
0.5 M EDTA (0.5 mM)
dH_2O added to 10 ml, pH adjusted to 7
Coomassie Brilliant Blue G 250 added to 5% w/v, and glycerol added to final concentration of 12%

NBGE cathode buffer 10× concentrated:

Bis-Tris (100 mM)
Tricine (500 mM)
dH_2O added to 1l, pH adjusted to 7

For NBGE clear cathode buffer, the 10x concentrated cathode buffer was diluted with dH_20. For NBGE blue cathode buffer, 0.2 g of Coomassie blue was added to 1 l of the clear cathode buffer, dissolved and filtered.

NBGE anode buffer 10× concentrated:

Bis-Tris (500 mM)
dH_2O added to 0.5 l, pH adjusted 7, diluted with dH_2O for NBGE anode buffer

3.3.4. Western blotting (WB) and protein detection

After both SDS-PAGE and NBGE run, WB was performed. Gels from SDS-PAGE were washed in the SDS-PAGE/transfer buffer and assembled with soaked nitrocellulose membranes with 0.45 µm pores and blotting papers and cloths into a Mini-PROTEAN® Tetra Vertical Electrophoresis Cell with Blotting Module. The SDS-PAGE/WB was run for 1 h at 100 V at 4 °C.

Gels after NBGE were incubated for 10 min in the NBGE/transfer buffer supplemented with 0.1% SDS in order to denature the protein complexes prior to the transfer. For this method, polyvinylidene difluoride (PVDF) membrane with 0.2 µm pores was used. The membranes were activated by soaking in 100% methanol for 10 min, washed with dH_2O and then soaked

in the NBGE/transfer buffer. The gels and activated membranes were assembled into a blotting sandwich of the Mini Gel Tank with Blot Module. The NBGE/WB was run for 2 h at 30 V at 4 °C. The membranes were destained with 100% methanol after the run.

At this point, membranes after both SDS-PAGE/WB and NBGE/WB were washed in Tris buffer saline/Tween (TBS/Tween). The membranes were blocked in 5% w/v skimmed milk in TBS/Tween for 1 h. Finally, the membranes were incubated overnight with the primary antibodies (listed in the chapter *Antibodies*) in 2% skimmed milk supplemented with 0.1% sodium azide. The next day, the membranes were washed in TBS/Tween, stained for 1 h with the respective HRP-conjugated secondary antibodies and again washed with TBS/Tween. The proteins of interest were then detected as chemiluminiscence signal with HRP substrates Radiance ECL or Radiance Plus using the Azure 600 Imaging system.

TBS/Tween:

10× PBS (1 l)
Tris (20 mM)
Tween 20 (0.05%)
dH_2O added to 10 l

3.3.5. High resolution clear native gel electrophoresis (hrCNE)

The method of high-resolution clear native gel electrophoresis (hrCNE) is similar to NBGE. However, the hrCNE method does not include the Coomassie blue stain that would interfere with the enzymatic reaction of interest. The protein complexes are therefore resolved only using their intrinsic charge, instead of charge of the Coomassie molecules, which unfortunately leads to protein aggregation and lower resolution [249]. The method was also performed as described in the literature [248].

Sample preparation for hrCNE is equal to NBGE (see *Native blue gel electrophoresis*). The sample was mixed with the hrCNE loading buffer (50% glycerol, 0.1% Ponceau; 10× concentrated) and loaded onto 4–16% NativePAGE Novex Bis-Tris gel within the same Mini Gel Tank apparatus connected to the power supply. Instead of the cathode buffer, the hrCNE-3 buffer was used, while the anode buffer was the same as for NBGE. Electrophoresis was run at the same constant voltage, first at 35 V for 1 h, then overnight at 25 V, without change of the cathode buffer.

hrCNE-3 buffer:

Sodium deoxycholate monohydrate (0.05%)
Dodecylmaltoside (0.01%)
NBGE clear cathode buffer added to 500 ml

3.4. Assays to measure complex II activity

3.4.1. Succinate dehydrogenase (SDH) activity assay

The hrCNE serves in resolving protein complexes in their native, functional state and the method does not use any color, therefore a colorimetric assay estimating the SDH enzymatic activity was performed after hrCNE. The assay buffer contains succinate as the SDH substrate, phenazine methosulfate (PMS) as the electron carrier, transferring the electrons onto nitro tetrazolium blue (NTB) molecules, turning the color from yellow to dark blue upon reduction. Furthermore, reduced NTB forms non-soluble crystals, which are captured inside the structure of the gel. The gel, after hrCNE run, was incubated in the SDH activity buffer for 20–40 min.

SDH activity assay buffer:

25 mg NTB
8 µl of 250 mM PMS in DMSO (1.5 mg in 20 µl)
200 µl sodium succinate dissolved in dH_2O (1 M, pH 7)
10 ml of 5 mM Tris-HCl (pH 7.4)

3.4.2. Succinate-ubiquinone oxidoreductase (SQR) activity assay

For the purpose of the succinate-ubiquinone oxidoreductase (SQR) activity assay, the cells were grown in 6-well plates, each clone in two replicates. The cells were washed with ice-cold PBS, scraped in PBS and centrifuged at 300*g* for 5 min at 4 °C. The pellet was then resuspended in hypotonic 25 mM potassium phosphate (K_2HPO_4) buffer. The Eppendorf tubes were then alternately placed onto dry ice and in 42 °C bath, overall tree times, assuring sufficient cell lysis. Protein concentration of the lysates was determined using the BCA Protein Assay Kit. 25 mg of the protein sample was loaded per one well of a 96-well plate and 50 µl of 100 mM K_2HPO_4 buffer and dH_2O to 147 µl was added. Each sample was loaded in four replicates – two containing 2 µl of 1 M malonate (as a negative control), two with 2 µl 25 mM K_2HPO_4 buffer. 49.5 µl of the SQR activity assay buffer was added to each well, and the plate was inserted for 5 min pre-incubation into Tecan Infinite M200 instrument pre-heated to 37 °C. Afterwards, 2 µl of 10 mM decylubiquinone was added to each well and the plate was placed back into the spectrophotometer for the measurement of absorbance at 600 nm every minute for 30 minutes.

SQR activity assay buffer:

Sodium succinate (20 mM)
Antimycin A (2 µM)
Rotenone (5 µM)
Sodium cyanide (10 mM)
Bovine serum albumin (50 mg/ml)
2,6-dichlorphenol indophenol (DCPIP; 0.015% w/v)

Linear portion (10–20 min) of the curve was then evaluated, using regression analysis in GraphPad PRISM software. Mean slopes of the malonate-inhibited reactions were subtracted from the mean uninhibited SQR reactions, and individual values for hPheo1 *SDHAFx* KO clones were evaluated as relative values to hPheo1 parental cells used in the respective measurement.

3.4.3. Routine and complex-II-mediated respiration

Cells were cultivated in 100 mm dishes, trypsinized, centrifuged at 300*g* for 5 min at RT, and washed with warm PBS. After second centrifugation, the cell pellet was resuspended in warm MiR05 medium specifically formulated for mitochondrial metabolism assays. The cell suspension, containing approximately 2 million cells, was transferred into a chamber of Oxygraph-2k instrument, measuring oxygen concentration. The cells were counted using the Bürker chamber. The measuring chamber of the Oxygraph-2k instrument was closed and oxygen consumption rate was measured. Afterwards, following chemicals were added into the chamber (with stock concentrations in brackets):

1 µl digitonin (8 mM)
1 µl rotenone (1 mM)
20 µl succinate (1 M)
30 µl ADP (500 mM)
5 µl cytochrome *c* (4 mM)
10 µl malonate (2 M)
1 µl antimycin A (5 mM)

Digitonin mediates cell membrane permeabilization, necessary for all other chemicals to reach mitochondria. Rotenone inhibits complex I, thus suppressing potential background. Succinate allows CII-specific respiration, and ADP dissipates built proton gradient by promoting the ATP synthase function. Cytochrome *c* serves as a control for intact OMM, since it does not cross the membrane; its addition does not change the oxygen consumption. Malonate selectively inhibits CII and antimycin A suppresses complex III – thus lowering overall mitochondrial respiration.

The recorded data was evaluated using DatLab software (Oroboros) as oxygen consumption rates. The value after antimycin A addition was subtracted from all other values. Routine respiration was considered as oxygen consumption before addition of digitonin, for specific

CII-mediated respiration, the value after malonate addition was subtracted from the value after cytochrome *c* addition.

MiR05 medium:

EGTA 0.5 mM
$MgCl_2$ 3 mM
K-lactobionate 60 mM
taurine 20 mM
KH_2PO_4 10 mM
sucrose 110 mM
1 g/l essentially fatty acid-free BSA
HEPES 20 mM (pH 7.1)

3.5. Growth characterization

3.5.1. Proliferation assay

The hPheo1 *SDHx* KO cells were trypsinized and number of the cells was assessed using an automated cell counter. The cells were then seeded into 96-well plate at two densities; 1,500 and 3,000 cells per well, in three replicates. Basic cultivating medium was added to 200 µl. The Incucyte® Live-Cell Analysis System was then used for the experiment, capturing cell density of each well every 2 h during a 144-h experiment.

Acquired data were analyzed using GraphPad PRISM for both experiments. Proliferation assay basic data obtained from two experiments on the IncuCyte® instrument were depicted as XY graphs in *Figure 6A* and *B*. Quantification of the results was carried out as follows: first, only exponential part of each growth curve was selected. This was done for initial seeding density of 1,500 cells over 0–72 h; for 3,000 cells over 0–48 h. The data were then transformed via $Y=Log_2(Y)$, where Y values are individual measurements, thus converting exponential function to linear function, which was subsequently analyzed using linear regression. Each slope was plotted on the bar graph on *Figure 6C*. Moreover exponential parts of the growth curves were analyzed via non-linear regression, evaluating of doubling time values is shown in *Figure 6D*.

3.5.2. Experimental model for tumor growth

Growth of selected hPheo1 *SDHx* KO clones was examined in the NSG/SGM3 immunodeficient mice. The mouse strain is based on NOD.*scid.Il2Rγc*^{null} ('NSG'), therefore lacking any mature T and B lymphocytes, or functional NK cells. Thus, the remaining system constitutes only functional neutrophils and monocytes [250]. Experimental animals were housed in The Animal Facility Module of the Czech Center for Phenogenomics (CCP), part of the BIOCEV research center.

The hPheo1 KO clones were harvested using a trypsin/EDTA solution, centrifuged at 300*g* for 5 min at RT, and resuspended in warm PBS. The cells were counted using a Bürker chamber, and specific volume of the suspension was taken, spun down at 300*g* for 5 min at RT and resuspended to 2×10^6 million cells per 100 µl of suspension. The cells were then grafted subcutaneously on the right flank of mice, 2×10^6 cells per one animal. Growth of the tumors was then measured each week over four months, using calipers for measurement of two dimensions of the tumor. Tumor volume was estimated using the following formula, where length is the larger dimension of the tumor:

$$\text{Tumor volume} = \text{length} \times \text{width}^2 / 2$$

Mice were sacrificed when tumor volume exceeded 1,000 mm^3. From tumor growth data, XY graph was compiled in *Figure 7A*. For better quantification, the area under curve was taken for each mouse, the means were then compared in *Figure 7B*.

3.6. Data analysis and statistics

Statistical analysis was carried out using GraphPad PRISM software (GraphPad Software). For analysis of all bar graphs, one-way or two-way ANOVA was used, followed by Tukey's multiple comparisons test. The graphs were plotted as mean values ± SD (or SEM in *Figure 7*). Significant differences between individual groups are marked with the (*) or (°) symbols. Number of the symbols represent following P values:

(*) $P \leq 0.05$

(**) $P \leq 0.01$

(***) $P \leq 0.001$

(****) $P \leq 0.0001$

For SQR activity assay, linear regression analysis in GraphPad PRISM was used to estimate differences of reaction kinetics. Proliferation kinetics were evaluated in GraphPad PRISM using transformation function Y=Log2(Y), followed by linear regression analysis, and by means of non-linear regression estimating doubling time. Tumor growth experiment was analyzed in GraphPad PRISM via Area under curve function.

3.7. List of materials and instruments

3.7.1. Chemicals

Chemical	Manufacturer	Chemical	Manufacturer
2,6-dichlorphenol indophenol	Fluka	NaCl	Sigma
Acrylamide/bis-acrylamide	Bio-Rad	Nitro tetrazolium blue	Sigma
Agarose	Nippon Genetics	NP-40	Sigma
Aminocaproic acid	Sigma	Penicillin	Sigma
Ammonium persulfate	Sigma	Phenazine methosulfate	Sigma
Antimycin A	Sigma	Ponceau	Fluka
Bis-Tris	Sigma	Protease inhibitor mix M	Serva
Bromphenol blue	Sigma	Proteinase K	Sigma
Coomassie Brilliant Blue G 250	Fluka	Puromycin	InvivoGen
Decylubiquinone	Sigma	Rotenone	Sigma
Digitonin	SERVA	RPMI-1640 Medium	Sigma
Dithithreitol	Promega	Skimmed milk	SERVA
DMSO	Sigma	Sodium azide	Sigma
Dodecylmaltoside	Sigma	Sodium cyanide	Sigma
EDTA	Sigma	Sodium deoxycholate monohydrate	Sigma
EGTA	Sigma	Sodium dodecyl sulfate	GE Healthcare
Esentially fatty-acid free BSA	Sigma	Sodium pyruvate	Sigma
Fetal bovine serum	Sigma	Sodium succinate	Sigma
GelRed® Nucleic Acid Gel Stain	Biotium	Streptomycin	Sigma
Glucose	Roth	Sucrose	Penta
Glycerol	Penta	Taurin	Sigma
Glycine	Penta	Tetramethyl ethylenediamine	GE Healthcare
HEPES	Sigma	Tricine	Sigma
Isopropyl alcohol	Penta	Tris	Penta
KH_2PO_4	Sigma	Tris-HCl	Penta
K-lactobionate	Sigma	Trypan Blue	Bio-Rad
LB medium	BIOCEV	Trypsin	Sigma
Malonate	Fluka	Tween 20	Sigma
Methanol	Penta	Uridine	Sigma
$MgCl_2$	Sigma		

3.7.2. Kits and markers

Product	Manufacturer	Catalog #
1 Kb Plus DNA Ladder	Invitrogen™	10787026
Pierce™ BCA Protein Assay Kit	Thermo Scientific™	23225
Precision Plus Protein™ All Blue Prestained Protein Standards	Bio-Rad	1610373
Radiance ECL	Azure Biosystems	AC2204
Radiance Plus	Azure Biosystems	AC2103
Wizard® SV Genomic DNA Purification System	Promega	A2361

3.7.3. Enzymes and reagents for cloning and transfection

Product	Manufacturer	Catalog #
DreamTaq™ Green PCR Master Mix (2X)	Thermo Scientific™	K1081
DreamTaq™ PCR Master Mix (2X)	Thermo Scientific™	K1071
Endura™ Competent Cells	Lucigen	60240-1
FastAP Thermosensitive Alkaline Phosphatase	Thermo Scientific™	EF0651
FastDigest BamHI	Thermo Scientific™	FD0054
FastDigest BpiI	Thermo Scientific™	FD1014
FastDigest Green Buffer (10X)	Thermo Scientific™	B72
FastDigest XbaI	Thermo Scientific™	FD0684
iProof High-Fidelity DNA Polymerase	Bio-Rad	1725301
Lipofectamine™ 3000	Invitrogen™	L3000015
NucleoBond Xtra Midi kit for transfection-grade plasmid DNA	MACHEREY-NAGEL	740410,1
NucleoSpin® Gel and PCR Clean-up	MACHEREY-NAGEL	740609,5
One Shot™ Stbl3™ Chemically Competent E. Coli	Invitrogen™	C737303
Opti-MEM™	Gibco™	31985062
pCDH-CMV-MCS-EF1-Puro	System Biosciences	CD510B-1
PEG-it™ Virus Precipitation Solution	System Biosciences	LV810A-1
pMD2.G plasmid	Addgene	12259
psPAX2 plasmid	Addgene	12260
T4 DNA ligase	Thermo Scientific™	15224017
T4 DNA ligase buffer	Thermo Scientific™	B69
T4 Polynucleotide Kinase	Thermo Scientific™	EK0031

3.7.4. Antibodies

Antibody	Manufacturer	Catalog #	Specifications	Dilution
SDHA (2E3GC12FB2AE2)	Abcam	ab14715	Mouse monoclonal	1:1,000
SDHB (21A11AE7)	Abcam	ab14714	Mouse monoclonal	1:1,000
SDH5/SDHAF2 (D1S8D)	Cell Signaling Technology	45849	Rabbit monoclonal	1:1,000
SDHAF4	Novus Biologicals	NBP1-86324	Rabbit polyclonal	1:500
GAPDH (D16H11) XP®	Cell Signaling Technology	5174	Rabbit monoclonal	1:1,000
HSP60 (D6F1) XP®	Cell Signaling Technology	12165	Rabbit monoclonal	1:1,000
Anti-mouse IgG-HRP	Invitrogen	31439	Goat	1:10,000
Anti-rabbit IgG-HRP	MERCK/Sigma	AP132P	Goat	1:10,000

3.7.5. Machines, instruments and accessories

Product	Manufacturer
0.2 µm-PVDF membrane	Bio-Rad
0.45 µm-nitrocellulose membrane	Bio-Rad
Agar plates	BIOCEV
Azure 600 Imaging system	Azure Biosystems
Balch homogenizer	Isobiotec
Blotting module for Mini-PROTEAN®	Bio-Rad
Bürker counting chamber	Hecht Assistent
Cell culture flasks and dishes	Sarstedt or Thermo Scientific™ Nunc™
Centrifuge 5415R	Eppendorf
Centrifuge 5804R	Eppendorf
Centrifuge MiniSpin Plus	Eppendorf
Counting slides for TC20™	Bio-Rad
Flow box SafeFAST Classic 218 A	Schoeller
Incubator Sanyo CO2	Schoeller
Incucyte® Live-Cell Analysis System	Sartorius
Infinite M200 plate reader	Tecan
MasterCycler PRO S PCR Thermal Cycler	Eppendorf
Mini Gel Tank with blotting module	Invitrogen™
MiniBIS PRO	DNR Bio Imaging Systems
Mini-PROTEAN® gel assembly	Bio-Rad
Mini-PROTEAN® Tetra Vertical Electrophoresis Cell	Bio-Rad
MP-3AP Power supply	Major Science
NanoDrop ND-2000	Thermo Scientific™
NativePAGE Novex Bis-Tris gel	Invitrogen™
Oxygraph-2k instrument	Oroboros
PowerPac™ Power Supply	Bio-Rad
TC20™ Automated Cell Counter	Bio-Rad
Water bath TW20	Julabo GmbH

4. Results

4.1. Protein analysis of hPheo1 knockout cells

First, analysis of the protein levels was performed in stable hPheo1 knockout (KO) and double knockout (dKO) cell lines. Two clones of each *SDHAF2* KO and *SDHAF4* KO cells with reconstituted SDHAF2 and SDHAF4, and *SDHAF2*/*SDHAF4* with *SDHAF4*/*SDHAF2* dKO were used. The analysis was done using two methods, SDS-PAGE followed by WB using whole-cell lysates, providing denaturing conditions for analyzing individual peptides; and NBGE with WB using lysates of the isolated mitochondrial fraction, allowing to observe protein complexes in their native state due to non-denaturing conditions.

4.1.1. SDS-PAGE/WB analysis

Protein analysis using SDS-PAGE/WB was used to determine changes in protein levels. The primary antibody was used against SDHA, SDHB, SDHAF2 and SDHAF4, and GAPDH was used as a loading control. The representative image is in *Figure 1A*. None of the analyzed hPheo1 KO clones show a pronounced change in the SDHA protein level. On the other hand, SDHB is almost missing in *SDHAF2* KO and *SDHAF2*/*SDHAF4* dKO cells, and the protein is strongly decreased in *SDHAF4* KO cells, with evident SDHB restoration in the individual cell lines with re-expressed proteins. The SDHAF2 protein is completely missing in *SDHAF2* KO and *SDHAF2*/*SDHAF4* dKO, further confirming the genetic KO (in addition to the validation in *Knockout confirmation*). Interestingly, the SDHAF2 protein level is upregulated in *SDHAF4* KO cells. Unfortunately, we were not able to stain SDHAF4 protein in hPheo1 parental cells; nonetheless, the protein is apparent in SDHAF4^{rec} cells, presumably due to its overexpression.

Subsequently, densitometric analysis was performed, based on three or more independent SDS-PAGE/WB experiments of the KO clones. The results are shown in *Figure 1B*. Although SDHA levels slightly vary in the lines, their differences are not significant. SDHB is significantly downregulated in all hPheo1 KO clones with increase toward levels found for parental cells upon reconstitution of the respective proteins. *SDHAF2* KO and both dKO lack the SDHAF2 protein. The SDHAF4 KO cells show higher levels of the SDHAF2 protein compared to parental cells, although not significant.

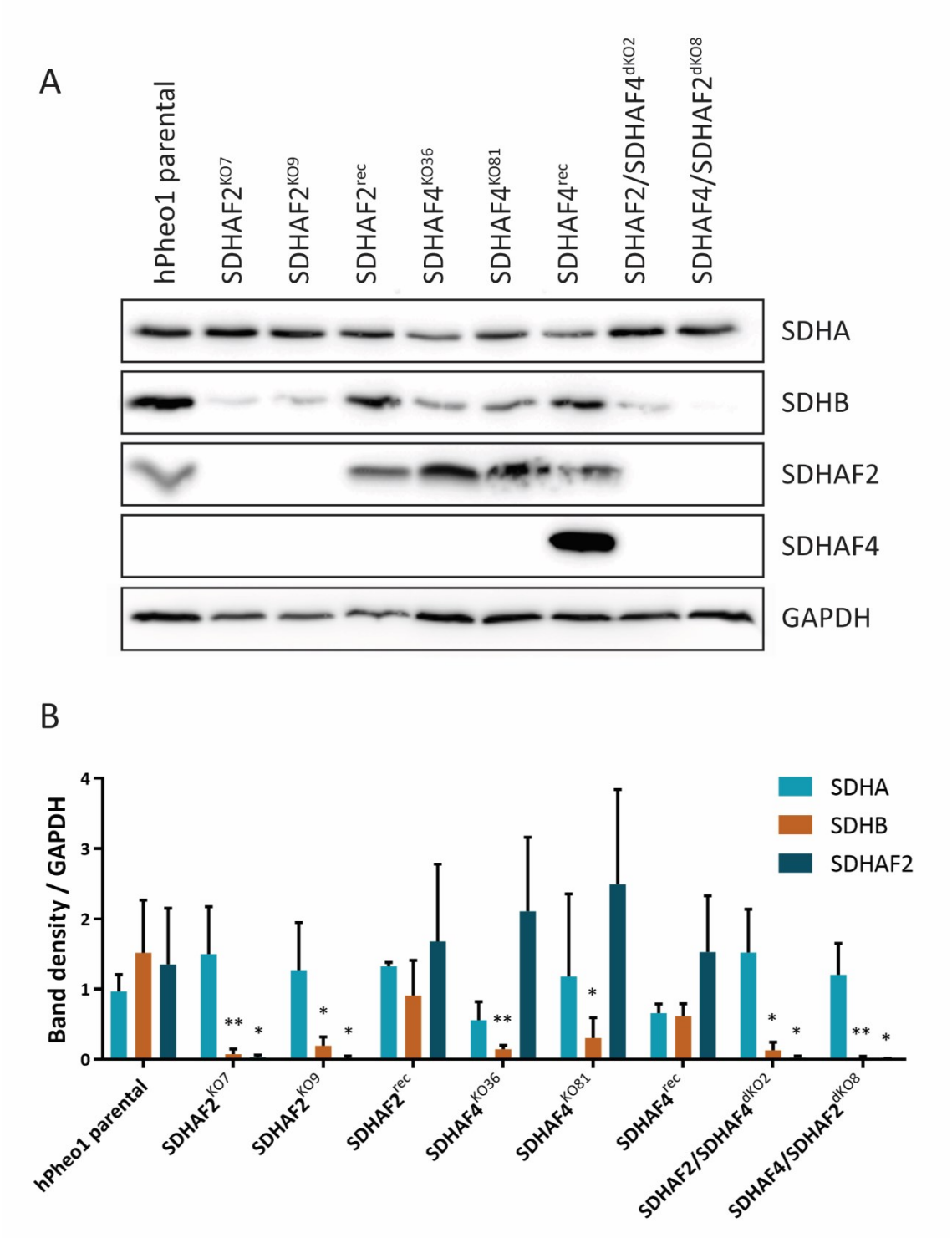

Figure 1 – Representative image of SDS-PAGE/WB of hPheo1 KO cells (A) and densitometric analysis (B). (A) SDS-PAGE/WB analysis reveals stable levels of the SDHA protein and decreasing level of the SDHB protein in hPheo1 KO cells. The SDHAF2 protein is absent in *SDHAF2* KO and *SDHAF2*/*SDHAF4* dKO cells and is upregulated in *SDHAF4* KO cells. The SDHAF4 protein is stained only in SDHAF4^{rec} cells. GAPDH was used as a loading control. (B) Densitometric analysis of SDS-PAGE/WB experiments of hPheo1 KO cells. The values are expressed as respective mean band densities, divided by density of GAPDH band, serving as a loading control. The (*) symbol represents significant differences between mean band densities of hPheo1 parental and the respective KO line. Statistical analysis was performed using two-way ANOVA with Tukey's multiple comparisons test. (*) P value ≤ 0.05, (**) P value ≤ 0.01. Data are shown as means ± SD (n ≥ 3).

4.1.2. NBGE/WB analysis

In order to analyze protein-protein interactions of CII subunits and assembly factors within the mature complex or its assembly intermediates, NBGE was performed followed by WB, using mitochondrial-fraction lysates with a mild detergent digitonin. The blots were stained with anti-SDHA, SDHB, SDHAF2 and SDHAF4 antibodies, with anti-HSP60 serving as a mitochondrial loading control.

SDHA staining reveals distribution of the protein between fully assembled CII and alternative assembly form referred to as CII_{low} (as seen in *Figure 2*). In hPheo1 parental cells, vast majority of the SDHA protein is within mature CII; however, some of it is present also as two distinct bands of CII_{low}. SDHB, on the other hand, is present only within one band of the same high as SDHA, in fully assembled CII in hPheo1 parental cells. SDHAF2 is present only within the lower band of the CII_{low} subspecies.

In *SDHAF2* KO cells (*Figure 2A*), CII is almost absent and SDHA is present within one band of CII_{low}. The SDHB protein staining is not visible and SDHAF2 protein is completely absent.

In *SDHAF4* KO cells (*Figure 2B*), level of CII is decreased and CII_{low} is elevated. SDHB staining is almost not visible. The band of the SDHAF2 protein is markedly enriched in *SDHAF4* KO cells. Staining for SDHAF4 was successfully performed only in *SDHAF4* KO group. $SDHAF4^{rec}$ cells show high amount of the SDHAF4 protein, thus resulting in smear-like pattern. Nonetheless, SDHAF4 was also detected in hPheo1 parental cells, with the band height similar to the upper CII_{low} band on SDHA staining.

The *SDHAF2*/*SDHAF4* dKO cells (*Figure 2C*) lack both SDHAF2 and SDHB, similar to SDHAF2 KO cells. The fully assembled CII is also nearly absent and SDHA shows as one band of CII_{low}. In both *SDHAF2* and *SDHAF4* cells, fully assembled CII returns upon protein re-expression, detected by SDHA and SDHB staining.

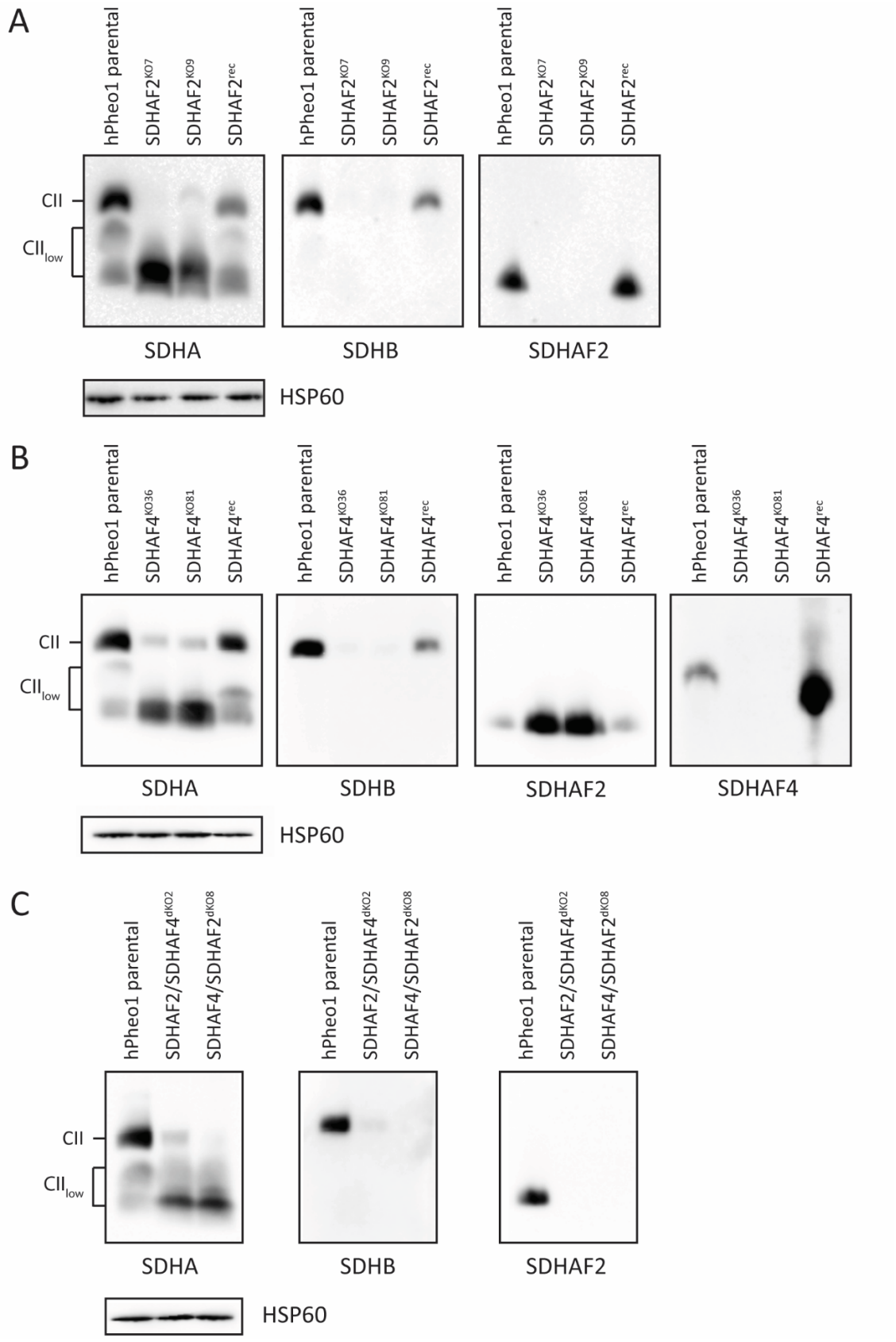

Figure 2 – NBGE/WB analysis of CII assembly states in hPheo1 KO cells. Staining for SDHA reveals at least three different CII assembly forms in hPheo1 parental cells, i. e. fully assembled CII and two CII_{low} subspecies. While SDHB is present only in fully assembled CII, SDHAF2 staining corresponds with the lower band of CII_{low}. All *SDHAFx* KO cells show significant CII disassembly and CII_{low} accumulation, which is restored upon protein re-expression. HSP60 was used as a mitochondrial loading control.

4.2. Complex II functionality

Next, we focused on assessing whether CII is functional in cells with KO of *SDHAF2* and/or *SDHAF4*. Previous results show that SDHB is almost missing in *SDHAF2* KO and *SDHAF2*/*SDHAF4* dKO cells, and the protein is downregulated upon *SDHAF4* KO, strongly indicating impairment of CII function.

4.2.1. SDH activity assay

For purpose of estimating enzymatic SDH activity, high resolution clear native electrophoresis (hrCNE) was performed, using the same extraction method as for NBGE, with digitonin solubilization of the mitochondrial fraction. The difference is in clear gel running conditions, allowing us to observe colorimetric reaction of succinate oxidation catalyzed by functional SDH upon addition of the reaction buffer.

Results of hrCNE followed by SDH activity buffer incubation, shown in *Figure 3*, represent the reaction occurring in hPheo1 parental cells as a clear band, located at comparable height as fully assembled CII band on NBGE/WB (data not shown). In *SDHAF2* KO and both *SDHAF2*/*SDHAF4* dKO clones, no sign of the reaction is present, whereas the SDHAF2^{rec} sample exhibits SDH activity. Both *SDHAF4* KO clones show a marked drop in SDH activity, seemingly around 25 % of hPheo1 parental SDH activity, with complete restoration upon SDHAF4 reconstitution.

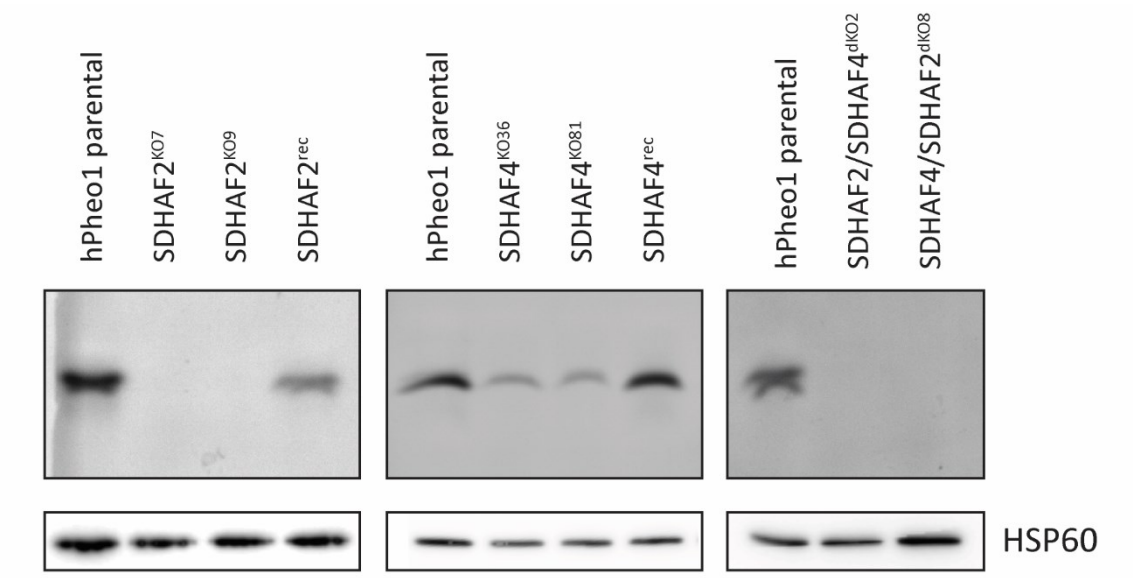

Figure 3 – SDH enzymatic activity after hrCNE. Functional, fully assembled CII performs SDH activity, occurring as a dark band. The assay clearly shows lack of SDH activity in *SDHAF2* KO and *SDHAF2*/*SDHAF4* dKO cells; while in SDHAF4^{KO} cells, SDH activity is attenuated. Re-expression of the proteins restores SDH activity. HSP60 stained from NBGE/WB, using identical samples, was used as a loading control.

4.2.2. SQR activity assay

SDH activity assay after hrCNE is a useful tool for determination of loss of SDH activity. For complete quantification of the decrease of the enzymatic activity, succinate-ubiquinone oxidoreductase (SQR) activity assay was used. The assay uses ubiquinone analogue for electron transfer, instead of the non-specific electron carrier PMS in the SDH activity assay, which provides information about the flow of electrons from SDHA's FAD to CoQ within the ubiquinone-binding site comprising of AA residues of the SDHB, SDHC and SDHD subunits.

The summarized results depicted in *Figure 4* show individual SQR activity mean values, relative to hPheo1 parental values. All *SDHAF2* KO and *SDHAF2*/*SDHAF4* dKO clones completely lack measurable SQR activity[19]. SDHAF2^{rec} cells show SQR activity restoration to the extent of 75 % of the parental cell activity. *SDHAF4* KO leads to attenuation of the SQR activity to 30 and 38 % (in SDHAF4^{KO36} and SDHAF4^{KO81}, respectively) of the parental cell SQR activity. Reconstitution of SDHAF4 then results to over 80 % of the parental cell enzymatic activity.

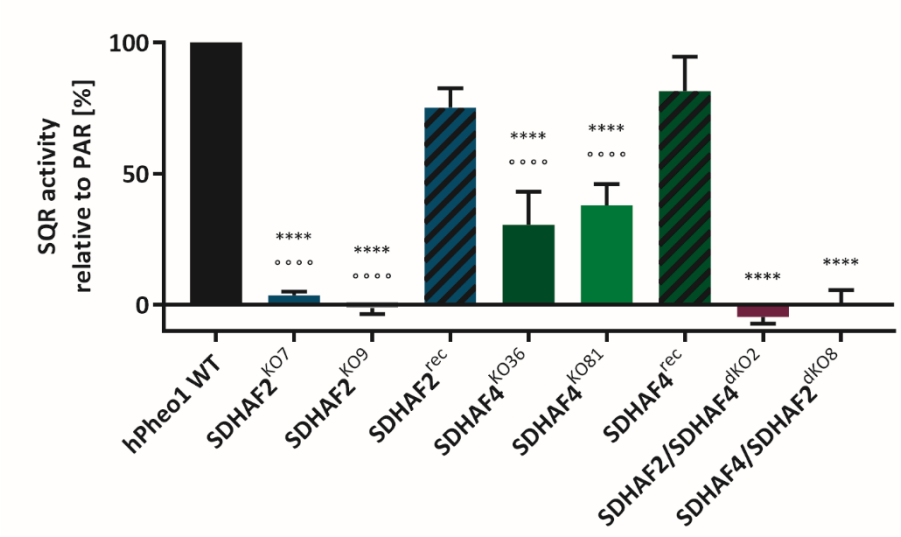

Figure 4 – SQR enzymatic activity assay of hPheo1 KO clones. The SQR activity was measured as discoloration of the reaction mixture in time as the result of reduction of DCPIP dye. Linear parts of the reactions (10–20 min) were analyzed using linear regression. Slope values of the reaction kinetics of each KO clone were compared to hPheo1 parental cell reaction. The mean relative values are plotted. The (*) symbol represents significant difference between respective clones and hPheo1 parental cells, (°) represents significant difference between the KO and the clone with reconstituted protein. For the statistical analysis, one-way ANOVA followed by Tukey's multiple comparisons test was used. (****/° ° ° °) P value ≤ 0.0001. Data are shown as means ± SD (n ≥ 3).

[19] The values of few % of the activity, both in positive and negative scale, are likely an artifact of the method, rather than some residual enzymatic activity, since the signal is very close to the 'noise'.

4.2.3. Evaluation of mitochondrial respiration

To observe CII function in the context of whole OXPHOS machinery, we measured routine and CII-dependent respiration of parental hPheo1 cells and the KO clones using Oxygraph-2k instrument. After permeabilization of the cells and addition of rotenone, succinate, ADP and cytochrome *c*; O_2 consumption rate was evaluated as seen in *Figure 5A*. *SDHAF2* KO and *SDHAF2*/*SDHAF4* dKO cells lack CII-dependent respiration that returns upon SDHAF2 reconstitution. *SDHAF4* KO clones have CII-dependent respiration significantly decreased to approximately 15 % of the hPheo1 parental cell respiration. SDHAF4^{rec} cells then exhibit recovery of CII-mediated respiration to almost 80 % of the parental cell level.

Additionally, routine respiration was measured before digitonin permeabilization and addition of any substrates (*Figure 5B*). *SDHAF4* KO cells exhibit moderate, although significant decrease of routine respiration. Nonetheless, in case of two *SDHAF2* KO clones, only SDHAF2^{KO9} cells have respiration level similar to hPheo1 parental cells, while the other, SDHAF2^{KO7} cells, show considerably decreased routine respiration. Moreover, both dKO clones of *SDHAF2*/*SDHAF4* almost lack routine oxygen consumption.

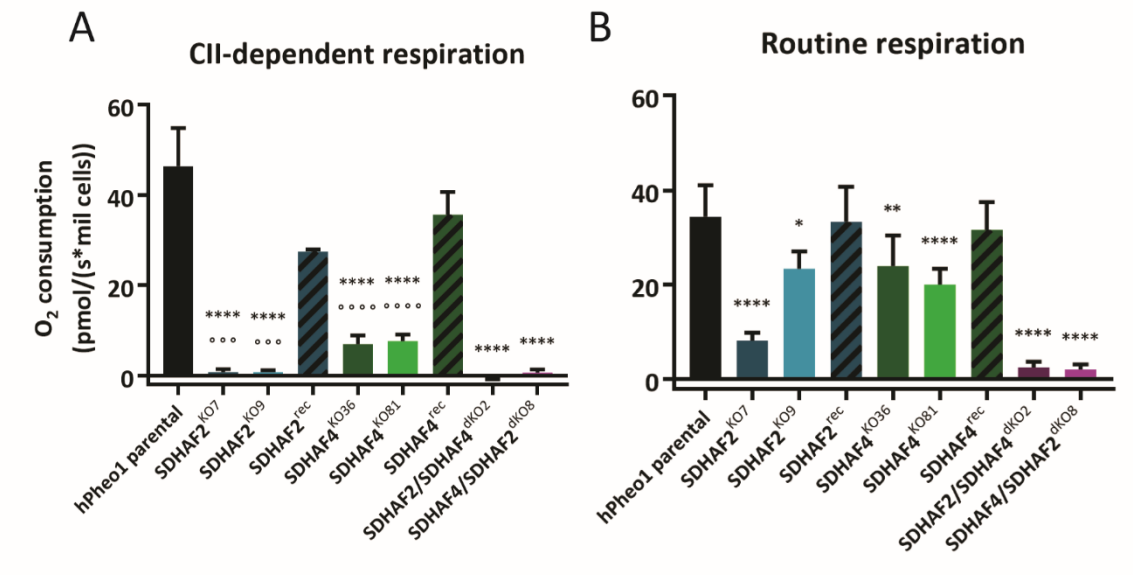

Figure 5 – CII-specific respiration upon addition of succinate (A) and routine respiration of intact cells (B). The respiration was evaluated as O_2 consumption rate (pmol/(s*mil cells)) using Oxygraph-2k instrument. (A) CII-dependent respiration expresses O_2 consumption rate after cell permeabilization, addition of rotenone, succinate, ADP and cytochrome *c*, with subtracted value after malonate addition. (B) Routine respiration was measured before the permeabilization and addition of the inhibitors and substrates. The (*) symbol represents significant difference between respective clones and hPheo1 parental cells, (°) represents significant difference between the KO and the clone with reconstituted protein. Statistical analysis was performed as one-way ANOVA followed by Tukey's multiple comparisons. (*) $P \leq 0.05$; (**) $P \leq 0.01$ (****/°°°°); (° ° °) $P \leq 0.001$; $P \leq 0.0001$. Data are shown as means ± SD ($n \geq 2$).

4.3. Growth characterization of the knockout cells

To define the effect of *SDHAF2* or/and *SDHAF4* KO on the cellular level, not only on the CII functionality or mitochondrial respiration, we examined the individual clones for the rate of proliferation *in vitro* and, eventually, determined their ability to form tumors in a mouse model. For the following studies, we also included hPheo1 *SDHB* KO as model of cells with all SDHA in CII_{low}, which was used in the study of Bezawork-Geleta and colleagues [118]. hPheo1 $SDHB^{KO}$ cells were prepared as described earlier [180].

4.3.1. Cell proliferation *in vitro*

All examined hPheo1 KO clones were seeded in 96-well plates at two densities – 1,500 and 3,000 cells per well. The cell density of each well was recorded every 2 h during the 144-h course of the experiment.

The growth curves in *Figure 6A* and *B* clearly show very distinct proliferation rates between the individual hPheo1 *SDHAFx* KO clones. The cells were seeded in two different initial densities, both showing similar results. *SDHAF2* KO clones exert highly decreased proliferation, comparable to $SDHB^{KO}$, and interestingly, re-expression of SDHAF2 returns growth rate to almost parental cell level. *SDHAF4* KO clones exhibit moderately retarded growth, with partial recovery upon the protein reconstitution. Both clones of *SDHAF2*/*SDHAF4* dKO show quite different growth pattern – the cells grow considerably fast at the beginning, however, the proliferation decelerates after 72 or 48 hours (in 1,500 or 3,000 cells seeded, respectively) and after plateau phase, the confluence even decreases.

To better quantify the differences between growth rates of individual clones, only exponential parts of the growth curves were taken into consideration, transformed to linear functions, and slopes of the individual clones were compared, as seen in *Figure 6C*. The exponential portions of the growth curves were also used to calculate doubling times of the clones, the results are shown in *Figure 6D*. Both analyses show that besides hPheo1 WT cells, also both re-expressed models exhibit considerable fast proliferation with doubling time around 20 hours. *SDHAF2* KO then grow more than twice slower, together with $SDHB^{KO}$ with more than 50 % decrease in growth rate. Both *SDHAF4* KO clones show growth rates also significantly decreased, although the cells grow considerably faster than *SDHAF2* KO cells. In contrast to the growth curves, where both *SDHAF2*/*SDHAF4* dKO were unable to reach confluence, both dKO exhibit considerably fast growth comparable to hPheo1 WT, especially in case of $SDHAF4/SDHAF2^{dKO8}$.

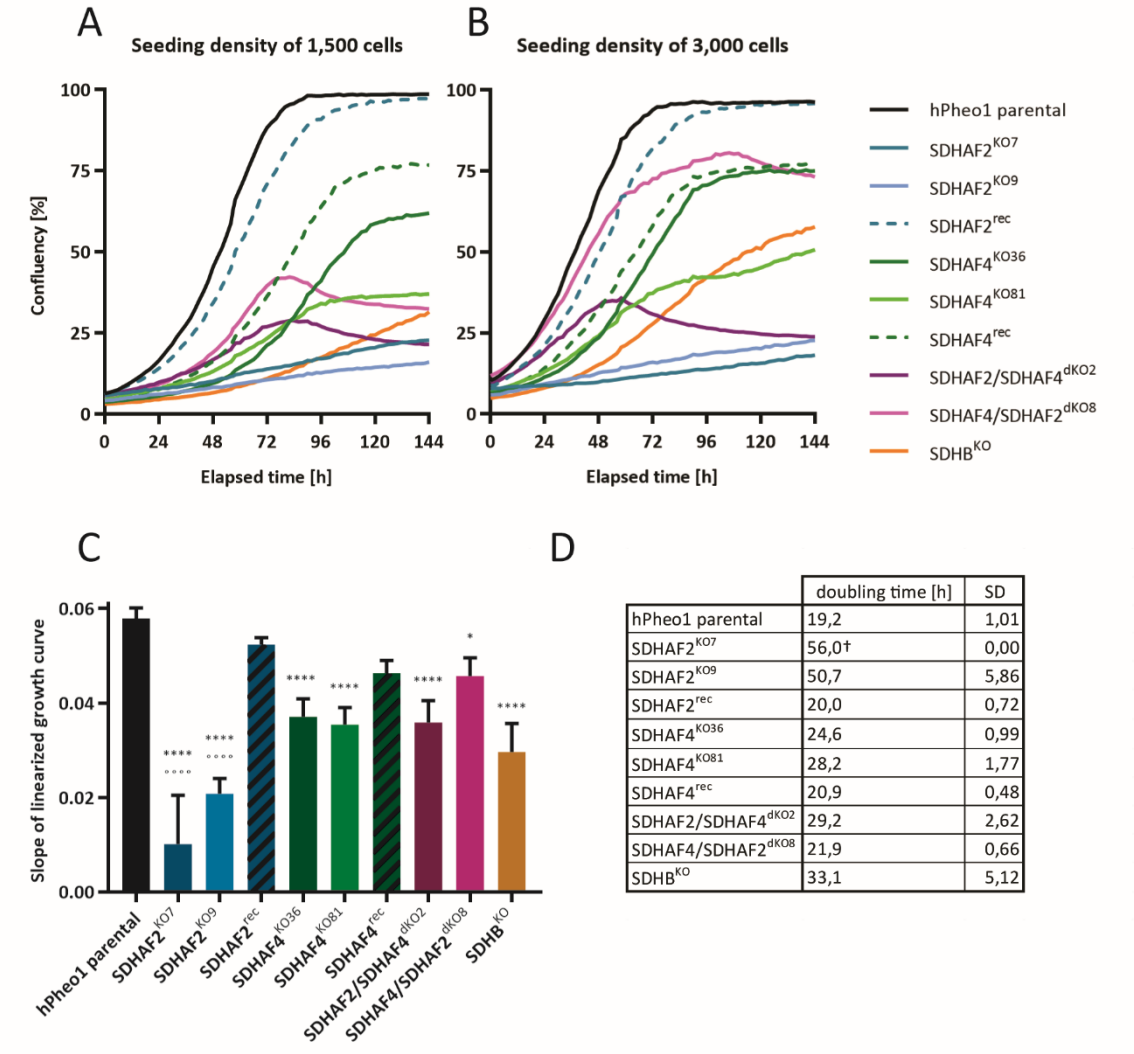

	doubling time [h]	SD
hPheo1 parental	19,2	1,01
SDHAF2^{KO7}	56,0†	0,00
SDHAF2^{KO9}	50,7	5,86
SDHAF2^{rec}	20,0	0,72
SDHAF4^{KO36}	24,6	0,99
SDHAF4^{KO81}	28,2	1,77
SDHAF4^{rec}	20,9	0,48
SDHAF2/SDHAF4^{dKO2}	29,2	2,62
SDHAF4/SDHAF2^{dKO8}	21,9	0,66
SDHB^{KO}	33,1	5,12

Figure 6 – Proliferation of hPheo1 SDHx KO clones. 1,500 (A) or 3,000 (B) cells were seeded into 96-well plates and cell density was recorded every 2 h over 144-h experiment. (C) Exponential portions of each curve, i. e. over 0–72 h at 1,500; and 0–48 h at 3,000 seeding density, were linearized and analyzed using linear regression. Slope values of the regression lines were compared. The bars depict means ± SD (n = 4). (D) Doubling time for each hPheo1 clone was also calculated from the exponential part of the growth curves. The (*) sign marks significant difference between a respective clone and hPheo1 WT, (°) between *SDHAF2* KO and SDHAF2^{rec}. For the statistical analysis, one-way ANOVA followed by Tukey's multiple comparisons test was used. (*) $P \leq 0.05$; (****/°°°°) $P \leq 0.0001$. The (†) symbol represents only one measurement of doubling time for SDHAF2^{KO7}, therefore SD = 0.

4.3.2. Tumor growth in a mouse model

Finally, the selected KO clones were evaluated for their ability to form tumors in a mouse model. 2×10^6 cells were injected subcutaneously into NSG/SGM3 immunodeficient mice, and tumor growth was followed over the course of four months. As shown in *Figure 7A*, first measurable tumors appeared around one month after grafting the cells. Some two months post grafting, tumors derived from SDHB^{KO} and SDHAF2^{KO7} cells started to differ from those of hPheo1 parental cells or other KO clones. The mice bearing SDHB^{KO}- and SDHAF2^{KO7}-derived tumors had to be sacrificed after three months because the mean tumor volume exceeded 1,000 mm^3 in most cases. In the meantime, tumors of hPheo1 parental,

SDHAF4^{KO36} and SDHAF4/SDHAF2^{dKO8} cell origin grew considerably slower. While parental-cell-derived tumors appeared at similar time as SDHB^{KO}- and SDHAF2^{KO7}-cell-derived tumors but showed a lag in the growth rate. Tumors of SDHAF4^{KO36} and SDHAF4/SDHAF2^{dKO8} cell origin appeared mostly after three months post grafting. SDHAF4^{KO36}-cell-derived tumors were examined in two independent experiment, with very similar result.

For the quantification of different growth kinetics of the tumor models, area under curve (AUC) was estimated for each experimental animal. We decided to use this approach since the tumor growth kinetics do not allow direct growth evaluation and the individual experiments did not match in the day of measurement. The results comparing mean AUC values are shown in *Figure 7B*. Indeed, both SDHB^{KO}- and SDHAF2^{KO7}-derived tumors exhibit significantly enhanced growth rate compared to parental tumors, whereas tumors of SDHAF4^{KO36} and SDHAF4/SDHAF2^{dKO8} origin do not show a significant difference, with AUC rather reduced.

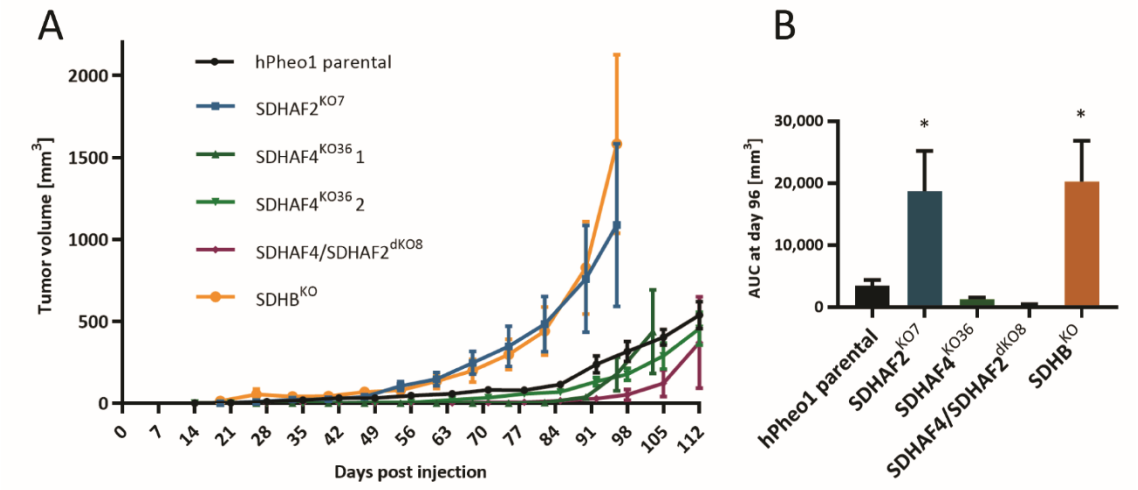

Figure 7 – Tumor growth of selected hPheo1 SDHx KO cells. (A) The hPheo1 cells were grafted into NSG/SGM3 mice and tumor growth was measured once a week over four months. Data are shown as mean tumor volume ± SEM (n ≥ 5). (B) For comparison of tumor growth rate kinetics, area under curve (AUC) for each mice was computed in the interval 0–96 days, since mice bearing SDHAF2^{KO7}- and SDHB^{KO}-cell-derived tumors were sacrificed at the day 96. The statistical analysis was done using one-way ANOVA followed by Tukey's multiple comparisons test. The (*) sign represents significant difference between a respective clone and hPheo1 parental cell-derived tumors, (*) $P \leq 0.05$. Each bar represents mean AUC ± SEM (n ≥ 5).

5. Discussion

This thesis was pursued under the supervision of Professor Jiří Neužil, the Head of the Laboratory of Molecular Therapy on the Institute of Biotechnology of the Czech Academy of Sciences. This group has long been focusing on cancer research with particular interest in mitochondrial metabolism, with potential translation into clinical practice. Recently, Neužil and Ralph proposed the term 'mitocans', used for anti-cancer drugs targeting mitochondria [251]. Outcome of such therapy, aiming at mitochondria of cancer cells, is demonstrated by successful Phase 1/1b clinical trial of a mitochondrially-targeted tamoxifen (MitoTam), a drug developed by the Laboratory of Molecular Therapy. MitoTam shows benefit for cancer patients, especially those with renal tumors; therefore, Phase 2 trial is being planned. Anti-cancer drug MitoTam, moreover, has additional effects, such as elimination of senescent cells, which may be exploited in the treatment of age-related diseases, e. g. type 2 diabetes [252].

As far as in 2001, Neužil and colleagues studied anti-cancer properties of a vitamin E analogue α-tocopheryl succinate (α-TOS) [253-255]. The target of this agent was described later. Molecular modelling and biochemical data revealed that α-TOS selectively blocks the proximal ubiquinone-binding site of CII, whereby promoting ROS generation, resulting in apoptosis [256, 257] (see chapter *Complex-II-targeted therapy*). This finding raised interest of the Molecular Therapy group in CII in context of cancer therapy. Considering that CII defects due to *SDHx* mutations play a dominant role in carcinogenesis, particularly of PCC/PGL tumors, the group conducted research using the triple-negative breast cancer MDA-MB-231 cell and, later, the unique hPheo1 cell line. Considerable effort then resulted in preparation of KO models of genes encoding all four SDH subunits. First in 2015, Neužil and colleagues observed that mtDNA depletion results in accumulation of an unassembled form of CII containing SDHA [121]. Later in 2018, they identified that the subcomplex contains also two SDH assembly factors, SDHAF2 and SDHAF4, and named the subspecies as CII_{low} as it migrates on native gels below fully assembled CII. In the study, the authors claim that CII_{low} is a physiological substep of CII assembly; however, the species may accumulate in pathological state upon CII impairment. Indeed, this study documented high level of CII_{low} in tumors with mutations in SDHB. The study further shows that, besides being pool of unbound SDHA, CII_{low} participates in bioenergetics stress signaling, affecting the cellular metabolism.

In order to study role of CII_{low} in cancer cells, we generated *SDHAF2* and *SDHAF4* KO models in hPheo1 cells using the CRISPR/AsCpf1 system. Our stable hPheo1 clones with KO of *SDHAF2*, *SDHAF4*, and both assembly factors, with cells re-expressing the respective

proteins, were evaluated on several levels. The used methods are ordered by gradually increasing complexity, i. e. first individual proteins and then their association into higher structures is evaluated, then functionality of the present complex II species is studied and finally, impact of the gene KO on cell growth abilities is being assed. We therefore focused on the role of the two assembly factors in CII properties.

5.1. Protein analysis

5.1.1. Level of SDHx proteins in *SDHAFx* KO cells

We evaluated the effect of the *SDHAF2* and/or *SDHAF4* genomic KO on the other components of CII. For fully functional CII, mature subunits SDHA, SDHB, SDHC and SDHD must assemble into a heterotetrameric holocomplex with assistance of four dedicated assembly factors SDHAF1-4. Since both SDHAF2 and SDHAF4 serve in maturation of SDHA, it raises a question whether SDHA level changes upon *SDHAF2* and/or *SDHAF4* KO. Our data of SDS-PAGE/WB (*Figure 1A*) and subsequent densitometry analysis (*Figure 1B*) clearly show that neither *SDHAF2* KO nor *SDHAF4* KO nor dKO of both genes influences level of the SDHA protein in hPheo1 cells. This is in agreement with the notion that *SDHA* gene is stably expressed, even upon removal of other SDH subunits [118], and therefore serves as a 'housekeeping' gene [120].

In contrast, SDHB subunit is severely downregulated in all examined hPheo1 KO clones, the most significantly within *SDHAF2* KO and *SDHAF2*/*SDHAF4* dKO cells. SDHB level is restored in SDHAF2^{rec} and SDHAF4^{rec} cells, supporting the idea that SDHB decrease (and presumably CII malfunctioning) is, indeed, caused by *SDHAF2* and *SDHAF4* KO. We hereby confirm the previous finding that SDHB level is strictly regulated because the protein amount vastly decreases upon any CII impairment [118, 119], or even upon other mitochondrial disruptions [118]. The study of Hadrava Váňová and colleagues proposes that SDHB physically interacts with SUCLG2, a subunit of SUCL enzyme, showing that *SUCLG2* KO decreases SDHB level [117]. This finding suggests that the SDHB protein requires interactions with other CII subunits and with the SUCLG2 protein. Unbound SDHB may be an intrinsically unstable protein, rapidly degraded by mitochondrial LON protease [258], in contrast with the SDHA protein, which is apparently highly stable in unbound state. This fact is well known to the extent that negative staining for SDHB has become a standard in characterization of SDH dysfunctional PCC/PGL tumors [119]. The reason for the tight protein level regulation is, however, unclear. It is known that Fe-S clusters are highly sensitive to ROS-mediated damage. Unbound SDHB associates with assembly factors SDHAF1 and SDHAF3, which are thought to prevent the detrimental effect of oxygen [92]. Thus, it is possible that unprotected SDHB is degraded due to surface exposure of one of the

SDHB Fe-S clusters. Notably, iron is considered a limiting nutrient and is necessary for several essential enzymes; therefore, it is highly convenient for cells to preserve this element [259]. On the other hand, in pathological state of CII dysfunction and succinate accumulation in cancer cells, intracellular iron level increases [177] and it is apparently essential for tumor cell survival and progression [260]. Moreover, Grimm and colleauges showed that SDHA-SDHB dimer, possibly present only under non-physiological conditions, is able to mediate succinate to fumarate conversion with production of ROS [116]. Considering the finding of Maklashina and colleagues, claiming that only SDHA bound with SDHB exhibits the enzymatic activity, SDHB attenuation may also serve to prevent ROS production by unassembled CII [96].

Our data also show completely absent SDHAF2 protein in *SDHAF2* KO and *SDHAF2*/*SDHAF4* dKO cells, which confirms our successful approach in generating a genetic KO. It is noteworthy that SDHAF2 protein levels increases in *SDHAF4* KO cells. A possible fate of the abundant SDHAF2 protein is discussed in detail below with other NBGE/WB results.

The SDHAF4 protein was detectable only in SDHAF4^{rec} cells. This points out to the distinct expression levels between hPheo1 parental cells and our reconstituted model. The *SDHAF2* and *SDHAF4* re-expression was performed using the pCDH-CMV-MCS-EF1-Puro vector, containing the cytomegalovirus (CMV) promotor, which is considerably strong when used for transgene expression [261]. In context of our data, this shows that physiological levels of the SDHAF4 protein are rather low. When used for reconstitution of *SDHAF2* gene, the protein levels are comparable to the parental cells, suggesting that SDHAF2 is present in much higher amount than SDHAF4 protein under physiological states.

5.1.2. Complex II assembly evaluation

Next, NBGE followed by WB was performed on mitochondrial fraction lysates, detecting the same proteins of interest (only with HSP60 as a loading control, GAPDH is not present in mitochondria). We used the mild detergent digitonin that preserves weak non-covalent interactions between proteins, which then co-migrate along concentration gradient of a native gel, being resolved mainly according to molecular mass of the complexes[20]. The proteins are in next step partially denatured during the process of WB and detected by antibodies, allowing us to estimate interaction partners of the proteins of our interest.

As described in the chapter *Complex II formation*, functional CII is present as a heterotetramer of subunits SDHA-D and several cofactors are needed for enzymatic activity

[20] The protein complexes are separated by both their hydrodynamic size and shape, thus two complexes with exactly same molecular weight might migrate differently due to their diverse shape [262].

of the complex, namely FAD group bound within the succinate-binding site of SDHA, three Fe-S clusters in the subunit SDHB and heme *b* group between SDHC and SDHD. Few transitional states of CII assembly may occur within mitochondria. Both SDHAF2 and SDHAF4 directly interact with SDHA during its maturation; hence, three assembly intermediate subcomplexes may exist: SDHA-SDHAF2, SDHA-SDHAF2-SDHAF4 and SDHA-SDHAF4. In a similar manner, SDHB maturation requires SDHAF1 and SDHAF3, therefore, SDHB may theoretically occur in several transient forms as well. Lastly, SDHA-SDHB dimer formation may precede the SDH tetramer formation [92] as existence of this dimer was reported, albeit in non-physiological situation [116].

In the next part, we will first discuss hPheo1 parental cells, characterized by fully assembled CII. SDHA-stained WB of all experimental groups unequivocally show presence of at least three different SDHA-containing species in mitochondria of hPheo1 parental cells (*Figure 2*). Therefore, we confirm that the subspecies CII_{low}, identified in our recent study [118], indeed is a physiological substep of CII assembly, and is present in cells with fully functional CII. The upper SDHA band, marked as CII in the figure, is complete CII composed of all four subunits, which should be approximately 140 kDa in size. Staining for SDHB reveals a band at the same position as the upper band of SDHA, thus supporting the notion that the band represents mature CII. Two lower bands then may be the individual maturation steps of SDHA. SDHA-SDHAF2 and SDHA-SDHAF4 subspecies should be around 90 kDa in size and trimer of SDHA-SDHAF2-SDHAF4 is about 105 kDa in size. Nonetheless, staining for SDHAF2 shows only one band in hPheo1 parental cells, at height corresponding to the lower band of CII_{low}. Hence, the lower CII_{low} band definitely comprises the SDHA and SDHAF2 proteins. SDHAF4 staining was performed only on experimental group containing *SDHAF4* KO and re-expressed cells (*Figure 2B*); still, showing a thought-provoking result. At this time, we were able to detect the SDHAF4 protein in hPheo1 parental cells. Height of the band corresponds to the upper band of the CII_{low} subspecies identified by SDHA staining[21]. Nevertheless, the SDHA-SDHAF4 dimer would be definitely smaller than SDHA-SDHAF2 or SDHA-SDHAF2-SDHAF4 trimer, therefore SDHA-SDHAF4 should not migrate much slower than the SDHAF2-containing subspecies. The explanation may be that either SDHA associates with more than one SDHAF4 proteins at once, or the subcomplex SDHA-SDHAF4 interacts with yet another protein. Taken together, mitochondria of parental hPheo1 cells contain three different subcomplexes containing SDHA, i. e. fully assembled CII,

[21] It is important to note that 30 μg of sample was loaded for SDHAF4 staining, compared to 10 μg for other proteins detection. Therefore, height of the SDHAF4 band might not be comparable to those in SDHA staining.

SDHA-SDHAF2 dimer and SDHA most likely associated with SDHAF4 and possibly with some other proteins.

Although SDHB was found to physically interact with its both assembly factors SDHAF1 and SDHAF3, we detected only one band positive for SDHB staining. The band, corresponding to the SDHA band by its height, most probably represents SDHB within the SDHA-D holocomplex. Absence of any other band with the SDHB protein indicates that the maturation process of SDHB is rather fast; therefore, minimum of the SDHB protein is present in non-assembled form. This is in contrast with SDHA, where considerable portion of the protein is in the precursor form of CII_{low}. Similarly, the SDHA-SDHB dimer, which should also migrate faster than CII, has never been either detected. This is on the contrary to the concept of SDHA-SDHB dimer as an intermediate of CII assembly, suggesting that the substep either does not occur at all and SDHA binds concurrently SDHB and SDHC-SDHD, or that SDHA-SDHB dimer does exists only for a negligible period of time, presumably to prevent potential ROS formation [116].

It is apparent from NBGE/WB data that assembly state of CII in all examined *SDHAFx* KO cells is completely different than in parental cells. First and foremost, all hPheo1 KO clones show significantly decreased amount of fully assembled CII. In *SDHAF2* KO (*Figure 2A*) and *SDHAF2*/*SDHAF4* dKO cells (*Figure 2C*), CII is almost absent, and in *SDHAF4* KO cells (*Figure 2B*), less than 10% of assembled CII is present compared to parental cells. This is further confirmed by the SDHB protein staining, which is missing upon *SDHAF2* KO and disappearing in *SDHAF4* KO cells, thus in agreement with the results from SDS-PAGE/WB analysis. Considering the SDS-PAGE/WB data, SDHA staining revealed unaffected levels of the protein in *SDHAFx* KO cells. With NBGE/WB analysis, we show that SDHA is 'stored' within the CII_{low} subspecies in all studied KO clones. Mass spectrometry analysis by Bezawork-Geleta and colleagues uncovered composition of the CII alternative assembly form, comprising SDHA, SDHAF2 and SDHAF4, with a potential signaling function. We therefore purport that CII_{low} does occur in cells lacking SDHAF2 or SDHAF4 and, most interestingly, the CII_{low} subspecies is also present when both assembly factors are missing.

In *SDHAF2* KO cells, the CII_{low} subspecies contains definitely SDHA; however, the subcomplex should not contain SDHAF4. Van Vranken and colleagues claim that SDHAF4 binds only covalently flavinylated SDHA [113] and several studies have shown that SDHAF2 is necessary for FAD binding [94]. Therefore, CII_{low} of *SDHAF2* KO cells should comprise only the SDHA protein. In case of *SDHAF4* KO cells, we conclude from both SDHA and SDHAF2 staining that the CII_{low} subassembly undoubtedly comprises an SDHA-SDHAF2 species. This also explains the upregulation of SDHAF2, which then associates with unassembled SDHA into a stable, long-lived CII_{low} form. Finally, in *SDHAF2*/*SDHAF4* dKO cells, SDHA is also

present, presumably occurring as a monomer, similarly to *SDHAF2* KO cells as described above.

Upon re-expression of the respective proteins, CII assembly restores, according to both SDHA and SDHB staining. Lastly, SDHAF4 reconstitution is rather intriguing. Staining for SDHAF4 results in a smear, indicating over-expression of the protein. However, SDHA-stained blot shows different CII_{low} distribution compared to parental cells. In $SDHAF4^{rec}$ cells, the lower CII_{low} band seems the same as in parental cells (the SDHA-SDHAF2 dimer), on the other hand, the upper band of CII_{low} shifts down. This alteration may indicate that in SDHAF4 over-expressing cells, the surplus of the SDHAF4 protein leads to accumulation of some non-physiological subassembly step, comprising SDHA and perhaps the accumulated SDHAF4. It is important to note, that SDHA-SDHAF4 dimer alone would not be higher than SDHA-SDHAF2 dimer. If we consider that the upper CII_{low} band in parental cells with WT SDHAF4 expression comprises SDHA, SDHAF4 and presumably some other protein, resulting in higher mass; SDHAF4 over-expression then disrupts such complex formation and results in lower-molecular-mass subcomplex.

5.2. Complex II functionality

NBGE/WB analysis revealed that in *SDHAF4* KO cells, some portion of assembled CII remains; and even in cells lacking SDHAF2, it appears that a minute amount of CII is still present, particularly in $SDHAF2^{KO9}$ and $SDHAF2/SDHAF4^{dKO2}$. To test if any CII activity remains in our *SDHAFx* KO clones, we assessed SDH activity in a clear native gels, allowing to determine which of SDH assembly forms possess the enzymatic activity. Furthermore, we evaluated SQR activity using whole-cell lysates, and CII-specific mitochondrial respiration of permeabilized cells.

For SDH activity assay, protein complexes of mitochondrial lysates were separated using hrCNE, similarly to the NBGE method without the use of the dye. For visualization of SDH activity, the gel was incubated in the reaction buffer containing succinate, PMS and the dye NTB. Succinate is being oxidized by functional SDH, generating electrons that are carried via PMS onto an the NTB molecule, resulting in color change. The small molecule of PMS is proposed to extract electrons directly from [3Fe–4S] cluster of SDHB [263]; hence, PMS does not occupy the SDH ubiquinone-binding site. Thus, the SDH activity assay evaluates the enzymatic activity of conversion of succinate to fumarate. On the contrary, SQR activity assay uses a ubiquinone analogue as electron carrier, decylubiquinone, which does enter the ubiquinone-binding site of CII, acquires electrons and subsequently reduces a molecule of DCPIP dye. Therefore, the SQR activity represents the activity of electron transfer from FAD to ubiquinone.

Next, in order to examine CII function in native conditions of intact mitochondria, CII-specific mitochondrial respiration was evaluated. In native state, CII is intrinsically regulated on multiple levels. Several post translationally modifying enzymes sculpt the CII activity [126, 128], which can also be due to certain mitochondrial metabolites acting as CII inhibitors, e. g. oxaloacetate and itaconate [51]. Moreover, CII is part of the OXPHOS machinery, therefore contributes to the pool of ubiquinol, which is then a substrate of respiratory complex III. Hence, functional downstream complexes of OXPHOS are also necessary for optimal CII activity [100].

According to the study of Maklashina and colleagues, SDHA without bound SDHB, i. e. SDHA also within CII_{low} subspecies, does not exhibit enzymatic activity [96]. Data from hrCNE followed by SDH activity assay (*Figure 3*) show one band of SDH activity in hPheo1 parental cells, therefore confirming that only fully assembled CII is catalytically active.

All three methods clearly show that *SDHAF2* KO, in both single KO and *SDHAF2*/*SDHAF4* dKO cases, results in non-functional CII, notwithstanding the small amount of assembled CII in the cells. This finding in in agreement with the previous studies, claiming that SDHAF2 is an indispensable factor for CII functionality in eukaryotic cells [94, 110]. A recent study of Sharma and colleagues elucidated the exact mechanism of SDHAF2 function, confirming that the assembly factor assists SDHA subunit in binding of the FAD cofactor, which is necessary for CII function [94]. We further confirm the role of SDHAF2 by re-expressing SDHAF2 protein, thereby restoring CII activity to almost parental level.

In contrast, SDH activity after hrCNE reveals that *SDHAF4* KO cells retain some CII activity, which occurs in assembled CII band, thus agreeing with Maklashina and colleagues that unassembled SDHA (within CII_{low}, which is abundant in *SDHAF4* KO cells) lacks enzymatic activity. Quantification of the functional CII then shows 35% and 15% of the parental levels in case of SQR activity and CII respiration, respectively. This is similar finding to the study of Van Vranken and colleagues, where they observed that SDHAF4-deficient yeast cells retain around 50% of CII activity. Therefore, SDHAF4 is definitely involved in CII assembly and it is needed for its full activity, since CII enzymatic activity and specific respiration are significantly decreased upon *SDHAF4* KO, and the cells regain CII activity comparable to parental cells with SDHAF4 reconstitution. However, unlike SDHAF2, SDHAF4 in not an absolute requirement for CII function.

In addition, evaluation of routine respiration of the individual *SDHAFx* KO clones is also very intriguing. These assays revealed that KO of *SDHAF4* gene in hPheo1 cells leads to moderate decrease in mitochondrial respiration. Nevertheless, in $SDHAF2^{KO7}$ cells, overall respiration is severely attenuated, in contrast to $SDHAF2^{KO9}$ cells, which show rather unchanged routine

respiration level. This might be an artifact of the genetic manipulation rather than result of the *SDHAF2* KO itself. Even more interesting, however, is almost zero routine respiration of both *SDHAF2*/*SDHAF4* dKO clones. The 'missing' respiration is presumably due to OXPHOS attenuation, since the O_2-consuming mitochondrial component is complex IV. This correlates with an observation that both *SDHAF2*/*SDHAF4* dKO clones are highly glycolytic in cell culture (discussed in *Growth characterization*) and, therefore, had to be kept in high-glucose medium. The question is whether the OXPHOS-deficient phenotype is truly due to the double genetic KO status, maybe with contribution of CII_{low} containing only the SDHA subunit. Nonetheless, we concluded that the same CII_{low} species is present in *SDHAF2* KO cells, due to ability of SDHAF4 to bind only flavinylated SDHA; but only $SDHAF2^{KO7}$ exhibits possible impairment of OXPHOS machinery, according to also decreased routine respiration.

5.3. Growth characterization

According to the study of Bezawork-Geleta and colleagues, the CII_{low} species in *SDHB* KO cells exhibits a signaling function, affecting cellular metabolism [118]. Therefore, we examined our stable *SDHAFx* KO models also for their proliferation rate *in vitro* and their ability to form tumors.

Analysis of proliferation rate of the cells revealed significant differences in proliferation rates among all studied KO clones. The cells were seeded at the densities of 1,500 and 3,000 cells per well, in identical growth medium (*Figure 6A and B*). Growth curves show the highest growth rate for hPheo1 parental cells, together with $SDHAF2^{rec}$ and $SDHAF4^{rec}$ cells. In contrast, *SDHAF4* KO cells clearly show moderately attenuated growth and, furthermore, *SDHAF2* KO cells proliferate slowly, similar to *SDHB* KO cells. *SDHAF2*/*SDHAF4* dKO cells then manifest quite distinct growth pattern; the cells proliferate considerably fast at the beginning; however, they stop proliferating after some time and then the cells start to go into demise. The most probable explanation is that glucose is a limiting factor for the growth of these cells, which may further support the idea that these cells lack OXPHOS and, thus, rely predominantly on glycolysis. Consumption of glucose would result in impaired growth with ensuing cell death.

For quantification and comparison of proliferation rates in *Figure 6C*, we used only exponential parts of the growth curves, i. e. 0–72 and 0–48 h (for the 1,500 and 3,000 seeding density, respectively). Computation of doubling-time values and logarithmization of the exponential curves, followed by regression analysis, confirms significantly decreased proliferation of *SDHAF4* KO and *SDHB* KO cells, and the most reduced growth rate for *SDHAF2* KO cells. Proliferation rate was reversed for both KO phenotypes following re-

expression of the respective proteins, leading to growth rates similar to parental cells. Based on this, it is obvious that proliferation rates of the KO clones correlate, at least partially, with CII functionality, since *SDHAF4* KO cells exhibit only decreased CII activity, which is virtually absent in *SDHAF2* KO cells. Further, *SDHAF2*/*SDHAF4* dKO clones show growth rate rather comparable to *SDHAF4* single KO cells, and even faster found for SDHAF4/SDHAF2^{dKO8} cells. As previous experiments confirmed that neither of the *SDHAF2*/*SDHAF4* dKO clones retains CII activity, this then raises a question why dKO exhibit enhanced growth rate relative to single *SDHAF2* KO cells. Bezawork-Geleta and colleagues showed that CII_{low} presence may be responsible for metabolic alteration, e. g. pyrimidine synthesis attenuation; however, both *SDHAF2* single KO and *SDHAF2*/*SDHAF4* double KO cells reveal similar levels of CII_{low}, consisting of only SDHA. Therefore we deduce that the enhanced growth rate of *SDHAF2*/*SDHAF4* dKO cells *in vitro* is due to the highly glycolytic metabolism, which is often utilized to maintain fast proliferation, as seen both in cancer cells and activated immune cells [40, 41].

Last, selected *SDHx* KO clones were injected subcutaneously as a xenograft model in immunocompromised NSG-SGM3 mice that lack the overall adaptive immune system and vast majority of innate immunity. In general, all grafted hPheo1 cells take rather long time, around one to two months, to start forming tumors. When small tumors appear, the growth kinetics than significantly diverges between hPheo1 parental and both SDHB- and SDHAF2-deficient tumors. While tumors of parental origin grow moderately, SDHB^{KO} and SDHAF2^{KO7} tumors exhibit relatively accelerated growth. On the contrary, tumors derived from SDHAF4^{KO36} cells, assessed in two independent experiments, and particularly SDHAF4/SDHAF2^{dKO8} tumors feature rather long lag-phase of about three months. Still, majority of the SDHAF4-lacking tumors occurred after such low delay and then grew in an exponential manner.

Taken together, the findings from the *in vitro* proliferation assays and tumor growth study show quite different results. Growth rates of *SDHB*, *SDHAF2* and, to lower extent, *SDHAF4* KO cells is significantly reduced, presumably due to impairment of CII activity. *SDHAF2*/*SDHAF4* dKO cells, with non-functional CII and with highly glycolytic phenotype, however, manifest faster proliferation rates. Tumor growth rate findings are then completely different, SDHB^{KO}- and SDHAF2^{KO7}-derived tumors grow the fastest, when compared to parental hPheo1 cell-derived tumors and two other KO tumors. This is in agreement with clinical cases of *SDHB*-mutated tumors, presenting as a highly aggressive metastatic disease [212], and few cases of *SDHAF2* germline mutations causing PGL [209]. Non-functional CII results in accumulation of succinate and, as discussed in the chapter *Mechanisms of tumorigenesis*, high level of succinate is principally responsible for tumor

progression due to the pseudohypoxic and hypermethylator phenotype, among other possible reasons. Tumors originating from SDHAF4^{KO36} cells, however, show growth kinetics more similar to parental hPheo1 cell-derived tumors. This may be explained by lower succinate levels. Since *SDHAF4* KO cells retain some CII enzymatic activity, succinate build-up may not be sufficient for cancer progression. Notwithstanding this, the explanation does not apply in case of double KO of *SDHAF2* and *SDHAF4*, where active CII is also absent; still, the tumors form with a long delay. Several pieces of evidence point out that overall OXPHOS is impaired in SDHAF4/SDHAF2^{dKO8} cells, however, OXPHOS seems attenuated also in SDHAF2^{KO7} according to routine respiration measurement. This hence leaves the growth pattern of the tumors somewhat unexplained and points to the possibility that there are additional molecular effects due to the absence of both assembly factors.

5.4. Impact of CII_{low} assembly form in KO clones

Bezawork-Geleta and colleagues used the *SDHB* KO MDA-MB-231 cells in their studies [118]. Therefore, our hPheo1 *SDHB* KO model should contain the same CII_{low} subspecies, comprising SDHA, SDHAF2 and SDAHF4. In our study, we show that cells lacking SDHAF2, SDHAF4, or both assembly factors comprise CII_{low}, however, likely of different composition. Our NBGE/WB data show that in *SDHAF4* KO clones, CII_{low} contains the SDHA-SDHAF2 dimer. Consistent with findings of Van Vranken and colleagues, *SDHAF2* KO cells should contain only SDHA within CII_{low}, as in case of *SDHAF2*/*SDHAF4* dKO. Therefore, three distinct forms of CII_{low} theoretically exist in the studied KO models. We found that all *SDHx* KO clones feature significant growth retardation *in vitro*, most pronounced in *SDHB* KO and *SDHAF2* KO cells. *SDHAF2*/*SDHAF4* dKO cells exhibit a highly glycolytic phenotype, which is to some degree present also in SDHAF2^{KO7} cells. This may suggest that CII_{low} containing only SDHA modulates the glycolytic shift, unlike CII_{low} comprising the SDHA-SDHAF2 and SDHA-SDHAF2-SDHAF4 subspecies; however, SDHAF2^{KO9} cells do not manifest OXPHOS attenuation as shown for SDHAF2^{KO7} cells, indicating a possible effect of clonality.

Data from tumor growth are even more complicated. While SDHAF2^{KO7} cells and SDHB^{KO} cells form tumors in an 'accelerated manner', consistent with high tumorigenic potential of *SDHB* and *SDHAF2* mutations in humans, SDHAF4^{KO36} cells show growth kinetics similar to parental cells. Interestingly, SDHAF2/SDHAF4^{dKO8} tumors then show the slowest tumor progression. We cannot therefore conclude that the tumor growth features are due to the CII_{low} assembly state, since SDHAF2^{KO7}- and SDHAF4/SDHAF2^{dKO8}-cell-derived tumors should both have only SDHA present in CII_{low}; still, the respective tumors grow with rather different kinetics. An alternative explanation may be that the SDHAF4 protein plays a thus far unknown role beyond the CII assembly. While an impact of its gene KO is not that

apparent in *in vitro* studies, *SDHAF4* KO cells grow moderately and *SDHAF2*/*SDHAF4* dKO cells are quite fast proliferating, although being of glycolytic phenotype; the *SDHAF4* gene KO may affect the cells under considerably more complex conditions of mouse *in vivo* model.

5.5. The enigmatic role of SDHAF4

All SDH subunits are considered tumor suppressors as germline mutations in all four *SDHx* genes have been identified as causative in certain cancer types. In addition, few *SDHAF2* mutations were identified in cases of carotid body PGL. Besides cancer, inherited CII defect also result in neurodegenerative diseases such as Leigh syndrome. *SDHA*, *SDHB*, *SDHD* and, interestingly, *SDHAF1* mutations have been reported as a cause of numerous encephalopathy cases. To this date, 55 different somatic *SDHAF4* gene mutations in 197 tumor cases, other than PCC/PGL, have been listed in the Catalogue of Somatic Mutations in Cancer (COSMIC) database, with some of the gene variants potentially pathogenic [264]. The Cancer Genome Atlas (TCGA) database of National Cancer Institute then lists 46 somatic mutations of the *SDHAF4* gene in 50 cancer cases, also with several variants of deleterious impact on the protein function [265]. Moreover, the study of Kudryavtseva and colleagues found two PGL patients with an *SDHAF4* somatic mutation of unknown pathogenicity; however, together with additional mutations in other genes [266]. Therefore, recent data do not confirm *SDHAF4* mutations as a causative factor in cancer formation, with no germline mutations found to this date. The identified *SDHAF4* gene variants are, hence, rather 'passenger' mutations than drivers of tumor formation. Van Vranken and colleagues observed that *SDHAF4* deletion in the *Drosophila* model manifests as typical mitochondrial disease with neuronal and muscular impairment, suggesting that defect of SDHAF4 may also give rise to neurodegenerative diseases [113], still, with no such described clinical case in humans. Taken together, no disease-causing mutations in the *SDHAF4* gene have been identified in humans, in neither cancer nor neurodegenerative disorder patients. Our observation of significantly delayed tumor formation using SDHAF4-lacking cells may be in agreement with the fact that SDHAF4 has not been identified as a susceptibility gene in PCC/PGL, unlike genes encoding the SDHA-D subunits and SDHAF2 assemby factor, thus proposing that *SDHAF4* deleterious mutations may not contribute to the carcinogenic process.

The study of Van Vranken and colleagues, performed mostly on a yeast model, suggests that SDHAF4 promotes SDHA and SDHB association and acts as an SDHA chaperone, preventing ROS formation due to the potentially exposed FAD cofactor [113]. However, this is in contrary to the finding of Maklashina and colleagues that SDHA alone, without bound SDHB subunit, is not catalytically active and generates only negligible amounts of ROS [96]. Van

Vranken and colleagues, indeed, show that growth impairment of SDHAF4-deficient cells is caused by elevated ROS level and increased ROS sensitivity, since the cell growth was restored upon over-expression of oxidative-stress-ameliorating genes *YAP1* and *SOD2* [113]. Considering that SDHAF4 is a conserved protein from yeast to human, this could explain the significant growth retardation of hPheo1 SDHAF4-lacking tumors. Van Vranken and colleagues also show that *SDHAF4* KO in cultured cells, either yeast or mammalian, has milder phenotype (around 50% decrease of CII activity) than whole organism KO of the gene in *Drosophila*, wherein individual cells almost completely lose functional CII. This may explain the discrepancy between slightly reduced proliferation rate of hPheo1 *SDHAF4* KO cells *in vitro* and considerably slower tumor formation *in vivo*. However, the mechanism of elevated ROS level and sensitivity upon *SDHAF4* KO needs to be further elucidated. Theoretically, SDHAF4 may play a role in ROS prevention/removal, beside the already mentioned prevention of SDHA-mediated ROS generation. SDHAF4 may also participate in some other oxidative-stress-preventing processes, via yet unidentified interactions.

The exact role of SDHAF4 in eukaryotic CII assembly is, however, not fully understood either. Two studies claim that SDHAF4 mediates SDHA-SDHB dimer formation, as SDHAF4 binds to SDHA only after its flavinylation, therefore SDHA-SDHAF4 interaction occurs after formation of the SDHA-SDHAF2 dimer [112, 113]. In 2018, Sharma and colleagues suggested that SDHAF4 serves in SDHAF2 dissociation from flavinylated SDHA [93]. Later study further supported this model by claiming that the SDHA-SDHAF2 dimer is stable and not likely to dissociate without an additional factor [94]. At this time, our laboratory has established a collaboration with the group of Professor Tina Iverson (senior author on papers by Sharma and colleagues) from Vanderbilt University, Nashville, TN, USA; and a team lead by Professor Gary Cecchini (senior author on papers by Maklashina and colleagues) from University of California, San Francisco, CA, USA. Both teams specialize in structural biology, and our collaboration will result in a joint publication in near future. This work will further elucidate the role of SDHAF2 and SDHAF4 in CII assembly, and, importantly, our data are consistent and in agreement with findings of the Cecchini team using reconstituted systems based on recombinant proteins, and the team of Iverson, who is focusing on crystallization-based studies. Therefore, it is with great pleasure that results generated in the course of this Master's degree project will be utilized in this collaboration and will be included in the above mentioned planned joint paper, i. e. will be utilized beyond this Master's degree thesis.

6. Conclusions

Germline mutations of the genes encoding subunits and assembly factors of mitochondrial complex II are a major cause of the hereditary forms of the tumors pheochromocytoma and paraganglioma. In this thesis, we studied the role of mitochondrial complex II in cancer cell biology, using the unique human pheochromocytoma cell line hPheo1. Recent studies have shown that inborn defects of complex II, resulting in tumor formation, lead to accumulation of alternative assembly form of complex II; referred to as CII_{low}. This sub-assembly comprises the SDHA subunit and two assembly factors SDHAF2 and SDHAF4, and may potentially exert a signaling function. The main aim of the thesis, therefore, was to evaluate the role of the two assembly factors in the CII_{low} subspecies. Furthermore, we focused on the SDHAF4 protein, whose role within complex II assembly needs to be fully elucidated.

We have successfully generated KO model of the *SDHAF2* and *SDHAF4* genes in hPheo1 cell line. Using various approaches, we studied the prepared models on several levels, i. e. individual proteins and their assembly, the functionality of respiratory complex II, and proliferation rate of the cells and their ability to form tumors. The conclusions we reached in this study can be summarized in the following points:

- Both assembly factors SDHAF2 and SDHAF4 participate in the maturation process of complex II.
- The SDHAF2 protein is essential for functionality of complex II, promoting FAD-binding in the SDHA subunit, which is required for the enzymatic activity of complex II. Although a small amount of complex II may assemble without SDHAF2, the enzyme lacks both SDH and SQR activity.
- The SDHAF4 protein promotes complex II assembly, albeit is not absolutely required for maturation and function of the complex. Loss of SDHAF4 protein results in significant decrease of the fully assembled complex II level, thereby reducing SDH and SQR activity, and complex-II-specific respiration.
- Steady-state-level of the SDHAF4 protein is apparently very low, as seen as the difference between the protein level in hPheo1 parental cell and upon the protein reconstitution; unlike SDHAF2 reconstitution, which results to parental-like protein level. In CII assembly, only little of the SDHAF4 protein is therefore needed, compared to the SDHAF2 protein.
- Upon *SDHAF2* or *SDHAF4* genetic KO, alternative assembly form CII_{low} accumulates in the cells, present as one subcomplex.
- The CII_{low} sub-assembly represents the SDHA-SDHAF2 dimer in *SDHAF4* KO cells, and presumably only SDHA in both *SDHAF2* KO and *SDHAF2*/*SDHAF4* dKO cells.

- Genetic KO of *SDHAF4* results in moderately reduced proliferation rate, *SDHAF2* KO leads to highly decreased proliferation. Double KO of the *SDHAF2* and *SDHAF4* genes leads to altered metabolism, characterized by enhanced glycolysis and proliferation rate.
- Tumors derived from *SDHB* KO and *SDHAF2* KO cells show enhanced growth rates relative to parental cells, which corresponds to clinical practice, where *SDHB*-mutated PCC/PGLs represent highly aggressive tumors of PGL4 syndrome. Moreover, *SDHAF2* mutations have been identified as causative in PGL2 syndrome.
- The *SDHAF4* KO- and *SDHAF4*/*SDHAF2* dKO-derived tumors, however, feature significantly delayed tumor formation, comparable to hPheo1 parental cells. This observation may correlate with the fact that no disease-causing *SDHAF4* mutations have been identified to this date in PCC/PGL.
- Unfortunately, we cannot conclude whether the CII_{low} form participates in the metabolic shift and the cell characteristics. Considering that *SDHAF2* KO cells and SDHAF2/SDHAF4 dKO cells share the same CII_{low} subspecies, they differ greatly in both rate of proliferation and tumor growth.
- The discrepancy between proliferation rate and tumor growth of *SDHAF4* KO cells and *SDHAF2*/*SDHAF4* dKO cells suggests the contribution of the SDHAF4 protein. These findings may point to some other yet unidentified role of the SDHAF4 assembly factor, possibly beyond complex II maturation and functionality.

The results published in this Master's thesis will be utilized in future joint publication in the collaboration with the groups of Professor Tina Iverson and Professor Gary Cecchini.

Published research articles

Hadrava Vanova, K., **M. Kraus**, J. Neuzil and J. Rohlena (2020). "Mitochondrial complex II and reactive oxygen species in disease and therapy." Redox Rep **25**(1): 26-32. [100]

Vanova, K. H., Y. Pang, L. Krobova, **M. Kraus**, Z. Nahacka, S. Boukalova, S. Pack, R. Zobalova, J. Zhu, T. Huynh, I. Jochmanova, O. Uher, S. Hubackova, S. Dvorakova, T. Garrett, H. Ghayee, B. Schuster, P. Knapp, Z. Frysak, I. Hartmann, N. Nilubol, J. Cerny, D. Taieb, J. Rohlena, J. Neuzil, C. Z. Yang and K. Pacak (2021). "Novel Germline SUCLG2 Mutations in Patients With Pheochromocytoma and Paraganglioma." Journal of the Endocrine Society **5**(Supplement_1): A168-A169. [117]

References

1. Scheffler, I.E., *Mitochondria*. 2nd ed. 2008, Hoboken, N.J.: Wiley-Liss. xviii, 462 pages, 12 unnumbered pages of plates.
2. Karnkowska, A., et al., *A Eukaryote without a Mitochondrial Organelle.* Curr Biol, 2016. **26**(10): p. 1274-84.
3. Martin, W. and M. Muller, *The hydrogen hypothesis for the first eukaryote.* Nature, 1998. **392**(6671): p. 37-41.
4. Gray, M.W., G. Burger, and B.F. Lang, *Mitochondrial evolution.* Science, 1999. **283**(5407): p. 1476-81.
5. Zhang, D., et al., *Mitochondria in oocyte aging: current understanding.* Facts Views Vis Obgyn, 2017. **9**(1): p. 29-38.
6. Friedman, J.R. and J. Nunnari, *Mitochondrial form and function.* Nature, 2014. **505**(7483): p. 335-43.
7. Kuhlbrandt, W., *Structure and function of mitochondrial membrane protein complexes.* BMC Biol, 2015. **13**: p. 89.
8. Yen, K., et al., *The emerging role of the mitochondrial-derived peptide humanin in stress resistance.* J Mol Endocrinol, 2013. **50**(1): p. R11-9.
9. Lee, C., et al., *The mitochondrial-derived peptide MOTS-c promotes metabolic homeostasis and reduces obesity and insulin resistance.* Cell Metab, 2015. **21**(3): p. 443-54.
10. Temperley, R.J., et al., *Human mitochondrial mRNAs--like members of all families, similar but different.* Biochim Biophys Acta, 2010. **1797**(6-7): p. 1081-5.
11. Al Rawi, S., et al., *Postfertilization autophagy of sperm organelles prevents paternal mitochondrial DNA transmission.* Science, 2011. **334**(6059): p. 1144-7.
12. Pfanner, N., B. Warscheid, and N. Wiedemann, *Mitochondrial proteins: from biogenesis to functional networks.* Nat Rev Mol Cell Biol, 2019.
13. Herzig, S. and R.J. Shaw, *AMPK: guardian of metabolism and mitochondrial homeostasis.* Nat Rev Mol Cell Biol, 2018. **19**(2): p. 121-135.
14. Fransson, S., A. Ruusala, and P. Aspenstrom, *The atypical Rho GTPases Miro-1 and Miro-2 have essential roles in mitochondrial trafficking.* Biochem Biophys Res Commun, 2006. **344**(2): p. 500-10.
15. Forrest, M.D., *Why cancer cells have a more hyperpolarised mitochondrial membrane potential and emergent prospects for therapy.* bioRxiv, 2015: p. 025197.
16. Zorova, L.D., et al., *Mitochondrial membrane potential.* Anal Biochem, 2018. **552**: p. 50-59.
17. Youle, R.J. and D.P. Narendra, *Mechanisms of mitophagy.* Nat Rev Mol Cell Biol, 2011. **12**(1): p. 9-14.
18. Falkenberg, M., N.G. Larsson, and C.M. Gustafsson, *DNA replication and transcription in mammalian mitochondria.* Annu Rev Biochem, 2007. **76**: p. 679-99.
19. Osawa, S., et al., *Recent evidence for evolution of the genetic code.* Microbiol Rev, 1992. **56**(1): p. 229-64.
20. Wiedemann, N. and N. Pfanner, *Mitochondrial Machineries for Protein Import and Assembly.* Annu Rev Biochem, 2017. **86**: p. 685-714.
21. Vogtle, F.N., et al., *Mitochondrial protein turnover: role of the precursor intermediate peptidase Oct1 in protein stabilization.* Mol Biol Cell, 2011. **22**(13): p. 2135-43.
22. Cheng, M.Y., et al., *Mitochondrial heat-shock protein hsp60 is essential for assembly of proteins imported into yeast mitochondria.* Nature, 1989. **337**(6208): p. 620-5.

23. Kang, P.J., et al., *Requirement for hsp70 in the mitochondrial matrix for translocation and folding of precursor proteins.* Nature, 1990. **348**(6297): p. 137-43.
24. Signes, A. and E. Fernandez-Vizarra, *Assembly of mammalian oxidative phosphorylation complexes I-V and supercomplexes.* Essays Biochem, 2018. **62**(3): p. 255-270.
25. Tovar, J., et al., *Mitochondrial remnant organelles of Giardia function in iron-sulphur protein maturation.* Nature, 2003. **426**(6963): p. 172-6.
26. Sutak, R., et al., *Mitochondrial-type assembly of FeS centers in the hydrogenosomes of the amitochondriate eukaryote Trichomonas vaginalis.* Proc Natl Acad Sci U S A, 2004. **101**(28): p. 10368-73.
27. Lill, R. and G. Kispal, *Maturation of cellular Fe-S proteins: an essential function of mitochondria.* Trends Biochem Sci, 2000. **25**(8): p. 352-6.
28. Rouault, T.A., *Mammalian iron-sulphur proteins: novel insights into biogenesis and function.* Nat Rev Mol Cell Biol, 2015. **16**(1): p. 45-55.
29. Hamza, I. and H.A. Dailey, *One ring to rule them all: trafficking of heme and heme synthesis intermediates in the metazoans.* Biochim Biophys Acta, 2012. **1823**(9): p. 1617-32.
30. Bajzikova, M., et al., *Reactivation of Dihydroorotate Dehydrogenase-Driven Pyrimidine Biosynthesis Restores Tumor Growth of Respiration-Deficient Cancer Cells.* Cell Metab, 2019. **29**(2): p. 399-416 e10.
31. Spinelli, J.B. and M.C. Haigis, *The multifaceted contributions of mitochondria to cellular metabolism.* Nat Cell Biol, 2018. **20**(7): p. 745-754.
32. Tatsuta, T., M. Scharwey, and T. Langer, *Mitochondrial lipid trafficking.* Trends Cell Biol, 2014. **24**(1): p. 44-52.
33. Chipuk, J.E., L. Bouchier-Hayes, and D.R. Green, *Mitochondrial outer membrane permeabilization during apoptosis: the innocent bystander scenario.* Cell Death Differ, 2006. **13**(8): p. 1396-402.
34. Chandel, N.S., et al., *Mitochondrial reactive oxygen species trigger hypoxia-induced transcription.* Proc Natl Acad Sci U S A, 1998. **95**(20): p. 11715-20.
35. Weinberg, F., et al., *Mitochondrial metabolism and ROS generation are essential for Kras-mediated tumorigenicity.* Proc Natl Acad Sci U S A, 2010. **107**(19): p. 8788-93.
36. West, A.P., et al., *TLR signalling augments macrophage bactericidal activity through mitochondrial ROS.* Nature, 2011. **472**(7344): p. 476-80.
37. Sena, L.A., et al., *Mitochondria are required for antigen-specific T cell activation through reactive oxygen species signaling.* Immunity, 2013. **38**(2): p. 225-36.
38. Voet, D. and J.G. Voet, *Biochemistry, 4th Edition*. 2010: W. Ross MacDonald School Resource Services Library.
39. Herzig, S., et al., *Identification and functional expression of the mitochondrial pyruvate carrier.* Science, 2012. **337**(6090): p. 93-6.
40. Schell, J.C., et al., *A role for the mitochondrial pyruvate carrier as a repressor of the Warburg effect and colon cancer cell growth.* Mol Cell, 2014. **56**(3): p. 400-13.
41. Frauwirth, K.A., et al., *The CD28 signaling pathway regulates glucose metabolism.* Immunity, 2002. **16**(6): p. 769-77.
42. Patel, M.S., et al., *The pyruvate dehydrogenase complexes: structure-based function and regulation.* J Biol Chem, 2014. **289**(24): p. 16615-23.
43. Sellers, K., et al., *Pyruvate carboxylase is critical for non-small-cell lung cancer proliferation.* J Clin Invest, 2015. **125**(2): p. 687-98.
44. DeBerardinis, R.J., et al., *Beyond aerobic glycolysis: transformed cells can engage in glutamine metabolism that exceeds the requirement for protein and nucleotide synthesis.* Proc Natl Acad Sci U S A, 2007. **104**(49): p. 19345-50.
45. Wang, R., et al., *The transcription factor Myc controls metabolic reprogramming upon T lymphocyte activation.* Immunity, 2011. **35**(6): p. 871-82.
46. Watmough, N.J. and F.E. Frerman, *The electron transfer flavoprotein: ubiquinone oxidoreductases.* Biochim Biophys Acta, 2010. **1797**(12): p. 1910-6.
47. Wilson, B.A., J.C. Schisler, and M.S. Willis, *Sir Hans Adolf Krebs: Architect of Metabolic Cycles.* Laboratory Medicine, 2010. **41**(6): p. 377-380.
48. Dupuy, J., et al., *Crystal structure of human iron regulatory protein 1 as cytosolic aconitase.* Structure, 2006. **14**(1): p. 129-39.
49. Johnson, J.D., W.W. Muhonen, and D.O. Lambeth, *Characterization of the ATP- and GTP-specific succinyl-CoA synthetases in pigeon. The enzymes incorporate the same alpha-subunit.* J Biol Chem, 1998. **273**(42): p. 27573-9.

50. Vinogradov, A.D., D. Winter, and T.E. King, *The binding site for oxaloacetate on succinate dehydrogenase.* Biochem Biophys Res Commun, 1972. **49**(2): p. 441-4.
51. Martinez-Reyes, I. and N.S. Chandel, *Mitochondrial TCA cycle metabolites control physiology and disease.* Nat Commun, 2020. **11**(1): p. 102.
52. Hatzivassiliou, G., et al., *ATP citrate lyase inhibition can suppress tumor cell growth.* Cancer Cell, 2005. **8**(4): p. 311-21.
53. Owen, O.E., S.C. Kalhan, and R.W. Hanson, *The key role of anaplerosis and cataplerosis for citric acid cycle function.* J Biol Chem, 2002. **277**(34): p. 30409-12.
54. Carrer, A., et al., *Acetyl-CoA Metabolism Supports Multistep Pancreatic Tumorigenesis.* Cancer Discov, 2019. **9**(3): p. 416-435.
55. Peng, M., et al., *Aerobic glycolysis promotes T helper 1 cell differentiation through an epigenetic mechanism.* Science, 2016. **354**(6311): p. 481-484.
56. Infantino, V., et al., *ATP-citrate lyase is essential for macrophage inflammatory response.* Biochem Biophys Res Commun, 2013. **440**(1): p. 105-11.
57. Michelucci, A., et al., *Immune-responsive gene 1 protein links metabolism to immunity by catalyzing itaconic acid production.* Proc Natl Acad Sci U S A, 2013. **110**(19): p. 7820-5.
58. Noushmehr, H., et al., *Identification of a CpG island methylator phenotype that defines a distinct subgroup of glioma.* Cancer Cell, 2010. **17**(5): p. 510-22.
59. Fan, J., et al., *Human phosphoglycerate dehydrogenase produces the oncometabolite D-2-hydroxyglutarate.* ACS Chem Biol, 2015. **10**(2): p. 510-6.
60. Zhu, J., K.R. Vinothkumar, and J. Hirst, *Structure of mammalian respiratory complex I.* Nature, 2016. **536**(7616): p. 354-358.
61. Zhang, X.C. and B. Li, *Towards understanding the mechanisms of proton pumps in Complex-I of the respiratory chain.* Biophysics Reports, 2019. **5**(5): p. 219-234.
62. Schultz, B.E. and S.I. Chan, *Structures and proton-pumping strategies of mitochondrial respiratory enzymes.* Annu Rev Biophys Biomol Struct, 2001. **30**: p. 23-65.
63. Cecchini, G., *Function and structure of complex II of the respiratory chain.* Annu Rev Biochem, 2003. **72**: p. 77-109.
64. Iwata, S., et al., *Complete structure of the 11-subunit bovine mitochondrial cytochrome bc1 complex.* Science, 1998. **281**(5373): p. 64-71.
65. Crofts, A.R., et al., *The Q-cycle reviewed: How well does a monomeric mechanism of the bc(1) complex account for the function of a dimeric complex?* Biochim Biophys Acta, 2008. **1777**(7-8): p. 1001-19.
66. Ow, Y.P., et al., *Cytochrome c: functions beyond respiration.* Nat Rev Mol Cell Biol, 2008. **9**(7): p. 532-42.
67. Kadenbach, B., *Regulation of Mammalian 13-Subunit Cytochrome c Oxidase and Binding of other Proteins: Role of NDUFA4.* Trends Endocrinol Metab, 2017. **28**(11): p. 761-770.
68. Zong, S., et al., *Structure of the intact 14-subunit human cytochrome c oxidase.* Cell Res, 2018. **28**(10): p. 1026-1034.
69. Wikstrom, M., K. Krab, and V. Sharma, *Oxygen Activation and Energy Conservation by Cytochrome c Oxidase.* Chem Rev, 2018. **118**(5): p. 2469-2490.
70. He, J., et al., *Assembly of the membrane domain of ATP synthase in human mitochondria.* Proc Natl Acad Sci U S A, 2018. **115**(12): p. 2988-2993.
71. Jonckheere, A.I., J.A. Smeitink, and R.J. Rodenburg, *Mitochondrial ATP synthase: architecture, function and pathology.* J Inherit Metab Dis, 2012. **35**(2): p. 211-25.
72. Walker, J.E., *The ATP synthase: the understood, the uncertain and the unknown.* Biochem Soc Trans, 2013. **41**(1): p. 1-16.
73. Turina, P., D. Samoray, and P. Graber, *H+/ATP ratio of proton transport-coupled ATP synthesis and hydrolysis catalysed by CF0F1-liposomes.* EMBO J, 2003. **22**(3): p. 418-26.
74. Petersen, J., et al., *Comparison of the H+/ATP ratios of the H+-ATP synthases from yeast and from chloroplast.* Proc Natl Acad Sci U S A, 2012. **109**(28): p. 11150-5.
75. Milenkovic, D., et al., *The Enigma of the Respiratory Chain Supercomplex.* Cell Metab, 2017. **25**(4): p. 765-776.
76. Schagger, H. and K. Pfeiffer, *Supercomplexes in the respiratory chains of yeast and mammalian mitochondria.* EMBO J, 2000. **19**(8): p. 1777-83.
77. Guo, R., et al., *Architecture of Human Mitochondrial Respiratory Megacomplex I2III2IV2.* Cell, 2017. **170**(6): p. 1247-1257 e12.
78. Acin-Perez, R., et al., *Respiratory complex III is required to maintain complex I in mammalian mitochondria.* Mol Cell, 2004. **13**(6): p. 805-15.

79. Calvaruso, M.A., et al., *Mitochondrial complex III stabilizes complex I in the absence of NDUFS4 to provide partial activity.* Hum Mol Genet, 2012. **21**(1): p. 115-20.
80. Greggio, C., et al., *Enhanced Respiratory Chain Supercomplex Formation in Response to Exercise in Human Skeletal Muscle.* Cell Metab, 2017. **25**(2): p. 301-311.
81. Letts, J.A., et al., *Structures of Respiratory Supercomplex I+III2 Reveal Functional and Conformational Crosstalk.* Mol Cell, 2019. **75**(6): p. 1131-1146 e6.
82. Strauss, M., et al., *Dimer ribbons of ATP synthase shape the inner mitochondrial membrane.* EMBO J, 2008. **27**(7): p. 1154-60.
83. Jang, S. and S. Javadov, *Elucidating the contribution of ETC complexes I and II to the respirasome formation in cardiac mitochondria.* Sci Rep, 2018. **8**(1): p. 17732.
84. Kovarova, N., et al., *High molecular weight forms of mammalian respiratory chain complex II.* PLoS One, 2013. **8**(8): p. e71869.
85. Lenaz, G. and M.L. Genova, *Kinetics of integrated electron transfer in the mitochondrial respiratory chain: random collisions vs. solid state electron channeling.* Am J Physiol Cell Physiol, 2007. **292**(4): p. C1221-39.
86. Thunberg, T., *Studien über die Beeinflussung des Gasaustausches des überlebenden Froschmuskels durch verschiedene Stoffe.* Skandinavisches Archiv Für Physiologie, 1909. **22**(2): p. 430-436.
87. Hederstedt, L. and L. Rutberg, *Succinate dehydrogenase--a comparative review.* Microbiol Rev, 1981. **45**(4): p. 542-55.
88. Beinert, H., *Spectroscopy of succinate dehydrogenases, a historical perspective.* Biochim Biophys Acta, 2002. **1553**(1-2): p. 7-22.
89. Technische Universität Braunschweig, *Enzyme Database - BRENDA*.
90. Anderson, N.M., et al., *The emerging role and targetability of the TCA cycle in cancer metabolism.* Protein Cell, 2018. **9**(2): p. 216-237.
91. Sun, F., et al., *Crystal structure of mitochondrial respiratory membrane protein complex II.* Cell, 2005. **121**(7): p. 1043-57.
92. Van Vranken, J.G., et al., *Protein-mediated assembly of succinate dehydrogenase and its cofactors.* Crit Rev Biochem Mol Biol, 2015. **50**(2): p. 168-80.
93. Sharma, P., et al., *Crystal structure of an assembly intermediate of respiratory Complex II.* Nat Commun, 2018. **9**(1): p. 274.
94. Sharma, P., et al., *The roles of SDHAF2 and dicarboxylate in covalent flavinylation of SDHA, the human complex II flavoprotein.* Proc Natl Acad Sci U S A, 2020. **117**(38): p. 23548-23556.
95. Yankovskaya, V., et al., *Architecture of succinate dehydrogenase and reactive oxygen species generation.* Science, 2003. **299**(5607): p. 700-4.
96. Maklashina, E., et al., *The unassembled flavoprotein subunits of human and bacterial complex II have impaired catalytic activity and generate only minor amounts of ROS.* J Biol Chem, 2018. **293**(20): p. 7754-7765.
97. Chouchani, E.T., et al., *Ischaemic accumulation of succinate controls reperfusion injury through mitochondrial ROS.* Nature, 2014. **515**(7527): p. 431-435.
98. Bisbach, C.M., et al., *Succinate Can Shuttle Reducing Power from the Hypoxic Retina to the O2-Rich Pigment Epithelium.* Cell Rep, 2020. **31**(5): p. 107606.
99. Berman, H.M., et al., *The Protein Data Bank.* Nucleic Acids Res, 2000. **28**(1): p. 235-42.
100. Hadrava Vanova, K., et al., *Mitochondrial complex II and reactive oxygen species in disease and therapy.* Redox Rep, 2020. **25**(1): p. 26-32.
101. UniProt Consortium, *UniProt*. 2002 – 2021.
102. Sharma, P., et al., *Maturation of the respiratory complex II flavoprotein.* Curr Opin Struct Biol, 2019. **59**: p. 38-46.
103. Na, U., et al., *The LYR factors SDHAF1 and SDHAF3 mediate maturation of the iron-sulfur subunit of succinate dehydrogenase.* Cell Metab, 2014. **20**(2): p. 253-66.
104. Angerer, H., *Eukaryotic LYR Proteins Interact with Mitochondrial Protein Complexes.* Biology (Basel), 2015. **4**(1): p. 133-50.
105. Maio, N., et al., *Cochaperone binding to LYR motifs confers specificity of iron sulfur cluster delivery.* Cell Metab, 2014. **19**(3): p. 445-57.
106. Starbird, C.A., et al., *Structural and biochemical analyses reveal insights into covalent flavinylation of the Escherichia coli Complex II homolog quinol:fumarate reductase.* J Biol Chem, 2017. **292**(31): p. 12921-12933.
107. Giancaspero, T.A., et al., *Remaining challenges in cellular flavin cofactor homeostasis and flavoprotein biogenesis.* Front Chem, 2015. **3**: p. 30.

108. Kounosu, A., *Analysis of covalent flavinylation using thermostable succinate dehydrogenase from Thermus thermophilus and Sulfolobus tokodaii lacking SdhE homologs.* FEBS Lett, 2014. **588**(6): p. 1058-63.
109. Maher, M.J., et al., *Crystal structure of bacterial succinate:quinone oxidoreductase flavoprotein SdhA in complex with its assembly factor SdhE.* Proc Natl Acad Sci U S A, 2018. **115**(12): p. 2982-2987.
110. Hao, H.X., et al., *SDH5, a gene required for flavination of succinate dehydrogenase, is mutated in paraganglioma.* Science, 2009. **325**(5944): p. 1139-42.
111. Bezawork-Geleta, A., et al., *Mitochondrial matrix proteostasis is linked to hereditary paraganglioma: LON-mediated turnover of the human flavinylation factor SDH5 is regulated by its interaction with SDHA.* FASEB J, 2014. **28**(4): p. 1794-804.
112. Belt, K., et al., *An Assembly Factor Promotes Assembly of Flavinated SDH1 into the Succinate Dehydrogenase Complex.* Plant Physiol, 2018. **177**(4): p. 1439-1452.
113. Van Vranken, J.G., et al., *SDHAF4 promotes mitochondrial succinate dehydrogenase activity and prevents neurodegeneration.* Cell Metab, 2014. **20**(2): p. 241-52.
114. Boniecki, M.T., et al., *Structure and functional dynamics of the mitochondrial Fe/S cluster synthesis complex.* Nat Commun, 2017. **8**(1): p. 1287.
115. Kim, H.J., et al., *Flavinylation and assembly of succinate dehydrogenase are dependent on the C-terminal tail of the flavoprotein subunit.* J Biol Chem, 2012. **287**(48): p. 40670-9.
116. Grimm, S., *Respiratory chain complex II as general sensor for apoptosis.* Biochim Biophys Acta, 2013. **1827**(5): p. 565-72.
117. Vanova, K.H., et al., *Novel Germline SUCLG2 Mutations in Patients With Pheochromocytoma and Paraganglioma.* Journal of the Endocrine Society, 2021. **5**(Supplement_1): p. A168-A169.
118. Bezawork-Geleta, A., et al., *Alternative assembly of respiratory complex II connects energy stress to metabolic checkpoints.* Nat Commun, 2018. **9**(1): p. 2221.
119. Gill, A.J., *Succinate dehydrogenase (SDH) and mitochondrial driven neoplasia.* Pathology, 2012. **44**(4): p. 285-92.
120. Silver, N., et al., *Selection of housekeeping genes for gene expression studies in human reticulocytes using real-time PCR.* BMC Mol Biol, 2006. **7**: p. 33.
121. Tan, A.S., et al., *Mitochondrial genome acquisition restores respiratory function and tumorigenic potential of cancer cells without mitochondrial DNA.* Cell Metab, 2015. **21**(1): p. 81-94.
122. Joshi, A., et al., *The mitochondrial HSP90 paralog TRAP1 forms an OXPHOS-regulated tetramer and is involved in mitochondrial metabolic homeostasis.* BMC Biol, 2020. **18**(1): p. 10.
123. Guzzo, G., et al., *Inhibition of succinate dehydrogenase by the mitochondrial chaperone TRAP1 has anti-oxidant and anti-apoptotic effects on tumor cells.* Oncotarget, 2014. **5**(23): p. 11897-908.
124. Liu, Y., et al., *Cryo-EM reveals the dynamic interplay between mitochondrial Hsp90 and SdhB folding intermediates.* bioRxiv, 2020: p. 2020.10.06.327627.
125. Sciacovelli, M., et al., *The mitochondrial chaperone TRAP1 promotes neoplastic growth by inhibiting succinate dehydrogenase.* Cell Metab, 2013. **17**(6): p. 988-999.
126. Cimen, H., et al., *Regulation of succinate dehydrogenase activity by SIRT3 in mammalian mitochondria.* Biochemistry, 2010. **49**(2): p. 304-11.
127. Finley, L.W., et al., *Succinate dehydrogenase is a direct target of sirtuin 3 deacetylase activity.* PLoS One, 2011. **6**(8): p. e23295.
128. Salvi, M., et al., *Identification of the flavoprotein of succinate dehydrogenase and aconitase as in vitro mitochondrial substrates of Fgr tyrosine kinase.* FEBS Lett, 2007. **581**(29): p. 5579-85.
129. Acin-Perez, R., et al., *ROS-triggered phosphorylation of complex II by Fgr kinase regulates cellular adaptation to fuel use.* Cell Metab, 2014. **19**(6): p. 1020-33.
130. Murphy, M.P., *How mitochondria produce reactive oxygen species.* Biochem J, 2009. **417**(1): p. 1-13.
131. Kluckova, K., et al., *Ubiquinone-binding site mutagenesis reveals the role of mitochondrial complex II in cell death initiation.* Cell Death Dis, 2015. **6**: p. e1749.
132. Ishii, T., et al., *A Mutation in the SDHC Gene of Complex II Increases Oxidative Stress, Resulting in Apoptosis and Tumorigenesis.* Cancer Research, 2005. **65**(1): p. 203-209.
133. Scialo, F., D.J. Fernandez-Ayala, and A. Sanz, *Role of Mitochondrial Reverse Electron Transport in ROS Signaling: Potential Roles in Health and Disease.* Front Physiol, 2017. **8**: p. 428.
134. Mills, E.L., et al., *Succinate Dehydrogenase Supports Metabolic Repurposing of Mitochondria to Drive Inflammatory Macrophages.* Cell, 2016. **167**(2): p. 457-470 e13.

135. Grimolizzi, F. and L. Arranz, *Multiple faces of succinate beyond metabolism in blood.* Haematologica, 2018. **103**(10): p. 1586-1592.
136. Gilissen, J., et al., *Insight into SUCNR1 (GPR91) structure and function.* Pharmacol Ther, 2016. **159**: p. 56-65.
137. He, W., et al., *Citric acid cycle intermediates as ligands for orphan G-protein-coupled receptors.* Nature, 2004. **429**(6988): p. 188-93.
138. Reddy, A., et al., *pH-Gated Succinate Secretion Regulates Muscle Remodeling in Response to Exercise.* Cell, 2020. **183**(1): p. 62-75 e17.
139. Sapieha, P., et al., *The succinate receptor GPR91 in neurons has a major role in retinal angiogenesis.* Nat Med, 2008. **14**(10): p. 1067-76.
140. Park, J., et al., *SIRT5-mediated lysine desuccinylation impacts diverse metabolic pathways.* Mol Cell, 2013. **50**(6): p. 919-30.
141. Tretter, L., A. Patocs, and C. Chinopoulos, *Succinate, an intermediate in metabolism, signal transduction, ROS, hypoxia, and tumorigenesis.* Biochim Biophys Acta, 2016. **1857**(8): p. 1086-1101.
142. Lin, H., X. Su, and B. He, *Protein lysine acylation and cysteine succination by intermediates of energy metabolism.* ACS Chem Biol, 2012. **7**(6): p. 947-60.
143. Burgener, A.V., et al., *SDHA gain-of-function engages inflammatory mitochondrial retrograde signaling via KEAP1-Nrf2.* Nat Immunol, 2019. **20**(10): p. 1311-1321.
144. Gut, P., et al., *SUCLA2 mutations cause global protein succinylation contributing to the pathomechanism of a hereditary mitochondrial disease.* Nat Commun, 2020. **11**(1): p. 5927.
145. Yang, Y. and G.E. Gibson, *Succinylation Links Metabolism to Protein Functions.* Neurochem Res, 2019. **44**(10): p. 2346-2359.
146. Hakak, Y., et al., *The role of the GPR91 ligand succinate in hematopoiesis.* J Leukoc Biol, 2009. **85**(5): p. 837-43.
147. Rubic, T., et al., *Triggering the succinate receptor GPR91 on dendritic cells enhances immunity.* Nat Immunol, 2008. **9**(11): p. 1261-9.
148. Mills, E. and L.A. O'Neill, *Succinate: a metabolic signal in inflammation.* Trends Cell Biol, 2014. **24**(5): p. 313-20.
149. Dang, E.V., et al., *Control of T(H)17/T(reg) balance by hypoxia-inducible factor 1.* Cell, 2011. **146**(5): p. 772-84.
150. Nastasi, C., et al., *Inhibition of succinate dehydrogenase activity impairs human T cell activation and function.* Sci Rep, 2021. **11**(1): p. 1458.
151. Lampropoulou, V., et al., *Itaconate Links Inhibition of Succinate Dehydrogenase with Macrophage Metabolic Remodeling and Regulation of Inflammation.* Cell Metab, 2016. **24**(1): p. 158-66.
152. Tannahill, G.M., et al., *Succinate is an inflammatory signal that induces IL-1beta through HIF-1alpha.* Nature, 2013. **496**(7444): p. 238-42.
153. Jeanmonod, R., E. Asuka, and D. Jeanmonod, *Inborn Errors Of Metabolism*, in *StatPearls*. 2021: Treasure Island (FL).
154. Tavares, M.V., et al., *Antenatal manifestations of mitochondrial disorders.* J Inherit Metab Dis, 2013. **36**(5): p. 805-11.
155. Rustin, P., et al., *Inborn errors of the Krebs cycle: a group of unusual mitochondrial diseases in human.* Biochim Biophys Acta, 1997. **1361**(2): p. 185-97.
156. Briere, J.J., et al., *Succinate dehydrogenase deficiency in human.* Cell Mol Life Sci, 2005. **62**(19-20): p. 2317-24.
157. Jain-Ghai, S., et al., *Complex II deficiency--a case report and review of the literature.* Am J Med Genet A, 2013. **161A**(2): p. 285-94.
158. Renkema, G.H., et al., *SDHA mutations causing a multisystem mitochondrial disease: novel mutations and genetic overlap with hereditary tumors.* Eur J Hum Genet, 2015. **23**(2): p. 202-9.
159. Courage, C., et al., *SDHA mutation with dominant transmission results in complex II deficiency with ocular, cardiac, and neurologic involvement.* Am J Med Genet A, 2017. **173**(1): p. 225-230.
160. Baertling, F., et al., *A guide to diagnosis and treatment of Leigh syndrome.* J Neurol Neurosurg Psychiatry, 2014. **85**(3): p. 257-65.
161. Al Khazal, F., et al., *A conditional mouse model of complex II deficiency manifesting as Leigh-like syndrome.* FASEB J, 2019. **33**(12): p. 13189-13201.
162. Alston, C.L., et al., *Recessive germline SDHA and SDHB mutations causing leukodystrophy and isolated mitochondrial complex II deficiency.* J Med Genet, 2012. **49**(9): p. 569-77.

163. Jackson, C.B., et al., *Mutations in SDHD lead to autosomal recessive encephalomyopathy and isolated mitochondrial complex II deficiency.* J Med Genet, 2014. **51**(3): p. 170-5.
164. Ohlenbusch, A., et al., *Leukoencephalopathy with accumulated succinate is indicative of SDHAF1 related complex II deficiency.* Orphanet J Rare Dis, 2012. **7**: p. 69.
165. Ghezzi, D., et al., *SDHAF1, encoding a LYR complex-II specific assembly factor, is mutated in SDH-defective infantile leukoencephalopathy.* Nat Genet, 2009. **41**(6): p. 654-6.
166. Brahimi-Horn, M.C. and J. Pouyssegur, *HIF at a glance.* J Cell Sci, 2009. **122**(Pt 8): p. 1055-7.
167. Selak, M.A., et al., *Succinate links TCA cycle dysfunction to oncogenesis by inhibiting HIF-alpha prolyl hydroxylase.* Cancer Cell, 2005. **7**(1): p. 77-85.
168. Wilson, W.R. and M.P. Hay, *Targeting hypoxia in cancer therapy.* Nat Rev Cancer, 2011. **11**(6): p. 393-410.
169. Dahia, P.L., *Pheochromocytoma and paraganglioma pathogenesis: learning from genetic heterogeneity.* Nat Rev Cancer, 2014. **14**(2): p. 108-19.
170. Jochmanova, I., et al., *HIF signaling pathway in pheochromocytoma and other neuroendocrine tumors.* Physiol Res, 2014. **63**(Suppl 2): p. S251-62.
171. Xiao, M., et al., *Inhibition of alpha-KG-dependent histone and DNA demethylases by fumarate and succinate that are accumulated in mutations of FH and SDH tumor suppressors.* Genes Dev, 2012. **26**(12): p. 1326-38.
172. Clark, G.R., et al., *Germline FH mutations presenting with pheochromocytoma.* J Clin Endocrinol Metab, 2014. **99**(10): p. E2046-50.
173. Letouze, E., et al., *SDH mutations establish a hypermethylator phenotype in paraganglioma.* Cancer Cell, 2013. **23**(6): p. 739-52.
174. Sulkowski, P.L., et al., *Krebs-cycle-deficient hereditary cancer syndromes are defined by defects in homologous-recombination DNA repair.* Nat Genet, 2018. **50**(8): p. 1086-1092.
175. Guzy, R.D., et al., *Loss of the SdhB, but Not the SdhA, subunit of complex II triggers reactive oxygen species-dependent hypoxia-inducible factor activation and tumorigenesis.* Mol Cell Biol, 2008. **28**(2): p. 718-31.
176. Selak, M.A., R.V. Duran, and E. Gottlieb, *Redox stress is not essential for the pseudo-hypoxic phenotype of succinate dehydrogenase deficient cells.* Biochim Biophys Acta, 2006. **1757**(5-6): p. 567-72.
177. Liu, Y., et al., *Therapeutic Targeting of SDHB-Mutated Pheochromocytoma/Paraganglioma with Pharmacologic Ascorbic Acid.* Clin Cancer Res, 2020. **26**(14): p. 3868-3880.
178. Thomas, C., et al., *Hydroxyl radical is produced via the Fenton reaction in submitochondrial particles under oxidative stress: implications for diseases associated with iron accumulation.* Redox Rep, 2009. **14**(3): p. 102-8.
179. Smestad, J., et al., *Chromatin Succinylation Correlates with Active Gene Expression and Is Perturbed by Defective TCA Cycle Metabolism.* iScience, 2018. **2**: p. 63-75.
180. Matlac, D.M., et al., *Succinate Mediates Tumorigenic Effects via Succinate Receptor 1: Potential for New Targeted Treatment Strategies in Succinate Dehydrogenase Deficient Paragangliomas.* Front Endocrinol (Lausanne), 2021. **12**: p. 589451.
181. Swann, J.B. and M.J. Smyth, *Immune surveillance of tumors.* J Clin Invest, 2007. **117**(5): p. 1137-46.
182. Wang, Y.A., et al., *Effects of tumor metabolic microenvironment on regulatory T cells.* Mol Cancer, 2018. **17**(1): p. 168.
183. Westendorf, A.M., et al., *Hypoxia Enhances Immunosuppression by Inhibiting CD4+ Effector T Cell Function and Promoting Treg Activity.* Cell Physiol Biochem, 2017. **41**(4): p. 1271-1284.
184. Chanmee, T., et al., *Tumor-associated macrophages as major players in the tumor microenvironment.* Cancers (Basel), 2014. **6**(3): p. 1670-90.
185. Ke, X., et al., *Hypoxia modifies the polarization of macrophages and their inflammatory microenvironment, and inhibits malignant behavior in cancer cells.* Oncol Lett, 2019. **18**(6): p. 5871-5878.
186. Indio, V., et al., *Gene Expression Landscape of SDH-Deficient Gastrointestinal Stromal Tumors.* J Clin Med, 2021. **10**(5).
187. Wu, J.Y., et al., *Cancer-Derived Succinate Promotes Macrophage Polarization and Cancer Metastasis via Succinate Receptor.* Mol Cell, 2020. **77**(2): p. 213-227 e5.
188. Fischer, K., et al., *Inhibitory effect of tumor cell-derived lactic acid on human T cells.* Blood, 2007. **109**(9): p. 3812-9.
189. Nakagawa, Y., et al., *Effects of extracellular pH and hypoxia on the function and development of antigen-specific cytotoxic T lymphocytes.* Immunol Lett, 2015. **167**(2): p. 72-86.

190. Messai, Y., et al., *ITPR1 protects renal cancer cells against natural killer cells by inducing autophagy.* Cancer Res, 2014. **74**(23): p. 6820-32.
191. Labiano, S., et al., *Hypoxia-induced soluble CD137 in malignant cells blocks CD137L-costimulation as an immune escape mechanism.* Oncoimmunology, 2016. **5**(1): p. e1062967.
192. Pinato, D.J., et al., *Programmed cell death ligands expression in phaeochromocytomas and paragangliomas: Relationship with the hypoxic response, immune evasion and malignant behavior.* Oncoimmunology, 2017. **6**(11): p. e1358332.
193. Drusbosky, L., et al., *Tumor mutation burden and PD-L1 expression in SDH/FH mutated solid tumors.* Journal of Clinical Oncology, 2019. **37**(15_suppl): p. 1524-1524.
194. Rasheed, M. and G. Tarjan, *Succinate Dehydrogenase Complex: An Updated Review.* Arch Pathol Lab Med, 2018. **142**(12): p. 1564-1570.
195. Bausch, B., et al., *Max Schottelius: Pioneer in Pheochromocytoma.* J Endocr Soc, 2017. **1**(7): p. 957-964.
196. Welander, J., P. Soderkvist, and O. Gimm, *Genetics and clinical characteristics of hereditary pheochromocytomas and paragangliomas.* Endocr Relat Cancer, 2011. **18**(6): p. R253-76.
197. McNichol, A.M., *Differential diagnosis of pheochromocytomas and paragangliomas.* Endocr Pathol, 2001. **12**(4): p. 407-15.
198. Neumann, H.P., et al., *65 YEARS OF THE DOUBLE HELIX: Genetics informs precision practice in the diagnosis and management of pheochromocytoma.* Endocr Relat Cancer, 2018. **25**(8): p. T201-T219.
199. Neumann, H.P.H., W.F. Young, Jr., and C. Eng, *Pheochromocytoma and Paraganglioma.* N Engl J Med, 2019. **381**(6): p. 552-565.
200. Ghayee, H.K., et al., *Mediastinal paragangliomas: association with mutations in the succinate dehydrogenase genes and aggressive behavior.* Endocr Relat Cancer, 2009. **16**(1): p. 291-9.
201. Lenders, J.W., et al., *Phaeochromocytoma.* Lancet, 2005. **366**(9486): p. 665-75.
202. Lloyd, R.V., et al., *World Health Organization classification of tumours.* Pituitary Tumors: Introduction in Pathology and Genetics of Tumours of Endocrine Organs, 2004: p. 10-3.
203. Chrisoulidou, A., et al., *The diagnosis and management of malignant phaeochromocytoma and paraganglioma.* Endocr Relat Cancer, 2007. **14**(3): p. 569-85.
204. Adjalle, R., et al., *Treatment of malignant pheochromocytoma.* Horm Metab Res, 2009. **41**(9): p. 687-96.
205. Taieb, D., et al., *Molecular imaging and radionuclide therapy of pheochromocytoma and paraganglioma in the era of genomic characterization of disease subgroups.* Endocr Relat Cancer, 2019. **26**(11): p. R627-R652.
206. Ilanchezhian, M., et al., *Emerging Treatments for Advanced/Metastatic Pheochromocytoma and Paraganglioma.* Curr Treat Options Oncol, 2020. **21**(11): p. 85.
207. Neumann, H.P., et al., *Germ-line mutations in nonsyndromic pheochromocytoma.* N Engl J Med, 2002. **346**(19): p. 1459-66.
208. Baysal, B.E., et al., *Mutations in SDHD, a mitochondrial complex II gene, in hereditary paraganglioma.* Science, 2000. **287**(5454): p. 848-51.
209. Bayley, J.P., et al., *SDHAF2 mutations in familial and sporadic paraganglioma and phaeochromocytoma.* Lancet Oncol, 2010. **11**(4): p. 366-72.
210. Else, T., et al., *The clinical phenotype of SDHC-associated hereditary paraganglioma syndrome (PGL3).* J Clin Endocrinol Metab, 2014. **99**(8): p. E1482-6.
211. Eisenhofer, G., et al., *Measurements of plasma methoxytyramine, normetanephrine, and metanephrine as discriminators of different hereditary forms of pheochromocytoma.* Clin Chem, 2011. **57**(3): p. 411-20.
212. Jochmanova, I., et al., *SDHB-related pheochromocytoma and paraganglioma penetrance and genotype-phenotype correlations.* J Cancer Res Clin Oncol, 2017. **143**(8): p. 1421-1435.
213. Gimenez-Roqueplo, A.P., et al., *Mutations in the SDHB gene are associated with extra-adrenal and/or malignant phaeochromocytomas.* Cancer Res, 2003. **63**(17): p. 5615-21.
214. Loriot, C., et al., *Epithelial to mesenchymal transition is activated in metastatic pheochromocytomas and paragangliomas caused by SDHB gene mutations.* J Clin Endocrinol Metab, 2012. **97**(6): p. E954-62.
215. Jha, A., et al., *Clinical, Diagnostic, and Treatment Characteristics of SDHA-Related Metastatic Pheochromocytoma and Paraganglioma.* Front Oncol, 2019. **9**: p. 53.
216. Baysal, B.E., *Mitochondrial complex II and genomic imprinting in inheritance of paraganglioma tumors.* Biochim Biophys Acta, 2013. **1827**(5): p. 573-7.

217. Hensen, E.F., et al., *Somatic loss of maternal chromosome 11 causes parent-of-origin-dependent inheritance in SDHD-linked paraganglioma and phaeochromocytoma families.* Oncogene, 2004. **23**(23): p. 4076-83.
218. Wang, Y.M., M.L. Gu, and F. Ji, *Succinate dehydrogenase-deficient gastrointestinal stromal tumors.* World J Gastroenterol, 2015. **21**(8): p. 2303-14.
219. Killian, J.K., et al., *Recurrent epimutation of SDHC in gastrointestinal stromal tumors.* Sci Transl Med, 2014. **6**(268): p. 268ra177.
220. Nannini, M., et al., *Expression of IGF-1 receptor in KIT/PDGF receptor-alpha wild-type gastrointestinal stromal tumors with succinate dehydrogenase complex dysfunction.* Future Oncol, 2013. **9**(1): p. 121-6.
221. Neppala, P., et al., *Current management of succinate dehydrogenase-deficient gastrointestinal stromal tumors.* Cancer Metastasis Rev, 2019. **38**(3): p. 525-535.
222. McEvoy, C.R., et al., *SDH-deficient renal cell carcinoma associated with biallelic mutation in succinate dehydrogenase A: comprehensive genetic profiling and its relation to therapy response.* NPJ Precis Oncol, 2018. **2**: p. 9.
223. Gill, A.J., et al., *Succinate dehydrogenase (SDH)-deficient renal carcinoma: a morphologically distinct entity: a clinicopathologic series of 36 tumors from 27 patients.* Am J Surg Pathol, 2014. **38**(12): p. 1588-602.
224. Gill, A.J., et al., *Succinate dehydrogenase deficiency is rare in pituitary adenomas.* Am J Surg Pathol, 2014. **38**(4): p. 560-6.
225. Yao, L., et al., *Mutations of the metabolic genes IDH1, IDH2, and SDHAF2 are not major determinants of the pseudohypoxic phenotype of sporadic pheochromocytomas and paragangliomas.* J Clin Endocrinol Metab, 2010. **95**(3): p. 1469-72.
226. Ferreira, C.V., et al., *Role of VEGF-A and its receptors in sporadic and MEN2-associated pheochromocytoma.* Int J Mol Sci, 2014. **15**(4): p. 5323-36.
227. O'Kane, G.M., et al., *A phase 2 trial of sunitinib in patients with progressive paraganglioma or pheochromocytoma: the SNIPP trial.* Br J Cancer, 2019. **120**(12): p. 1113-1119.
228. Escudier, B., et al., *Sorafenib in advanced clear-cell renal-cell carcinoma.* N Engl J Med, 2007. **356**(2): p. 125-34.
229. Ben-Ami, E., et al., *Long-term follow-up results of the multicenter phase II trial of regorafenib in patients with metastatic and/or unresectable GI stromal tumor after failure of standard tyrosine kinase inhibitor therapy.* Ann Oncol, 2016. **27**(9): p. 1794-9.
230. Chou, A., et al., *Succinate dehydrogenase-deficient GISTs are characterized by IGF1R overexpression.* Mod Pathol, 2012. **25**(9): p. 1307-13.
231. Gualberto, A. and M. Pollak, *Emerging role of insulin-like growth factor receptor inhibitors in oncology: early clinical trial results and future directions.* Oncogene, 2009. **28**(34): p. 3009-21.
232. Pang, Y., et al., *Targeting NAD(+)/PARP DNA Repair Pathway as a Novel Therapeutic Approach to SDHB-Mutated Cluster I Pheochromocytoma and Paraganglioma.* Clin Cancer Res, 2018. **24**(14): p. 3423-3432.
233. Hadoux, J., et al., *SDHB mutations are associated with response to temozolomide in patients with metastatic pheochromocytoma or paraganglioma.* Int J Cancer, 2014. **135**(11): p. 2711-20.
234. Albayrak, T., et al., *The tumor suppressor cybL, a component of the respiratory chain, mediates apoptosis induction.* Mol Biol Cell, 2003. **14**(8): p. 3082-96.
235. Kluckova, K., et al., *Mitochondrial complex II, a novel target for anti-cancer agents.* Biochim Biophys Acta, 2013. **1827**(5): p. 552-64.
236. Jimenez, C., *Treatment for Patients With Malignant Pheochromocytomas and Paragangliomas: A Perspective From the Hallmarks of Cancer.* Front Endocrinol (Lausanne), 2018. **9**: p. 277.
237. Fanciulli, G., et al., *Emerging Therapies in Pheochromocytoma and Paraganglioma: Immune Checkpoint Inhibitors in the Starting Blocks.* J Clin Med, 2020. **10**(1).
238. Greene, L.A. and A.S. Tischler, *Establishment of a noradrenergic clonal line of rat adrenal pheochromocytoma cells which respond to nerve growth factor.* Proc Natl Acad Sci U S A, 1976. **73**(7): p. 2424-8.
239. Powers, J.F., et al., *Pheochromocytoma cell lines from heterozygous neurofibromatosis knockout mice.* Cell Tissue Res, 2000. **302**(3): p. 309-20.
240. Martiniova, L., et al., *Characterization of an animal model of aggressive metastatic pheochromocytoma linked to a specific gene signature.* Clin Exp Metastasis, 2009. **26**(3): p. 239-50.

241. Pfragner, R., et al., *First continuous human pheochromocytoma cell line: KNA. Biological, cytogenetic and molecular characterization of KNA cells.* J Neurocytol, 1998. **27**(3): p. 175-86.
242. Ghayee, H.K., et al., *Progenitor cell line (hPheo1) derived from a human pheochromocytoma tumor.* PLoS One, 2013. **8**(6): p. e65624.
243. Zetsche, B., et al., *Multiplex gene editing by CRISPR-Cpf1 using a single crRNA array.* Nat Biotechnol, 2017. **35**(1): p. 31-34.
244. Safari, F., et al., *CRISPR Cpf1 proteins: structure, function and implications for genome editing.* Cell Biosci, 2019. **9**: p. 36.
245. Concordet, J.P. and M. Haeussler, *CRISPOR: intuitive guide selection for CRISPR/Cas9 genome editing experiments and screens.* Nucleic Acids Res, 2018. **46**(W1): p. W242-W245.
246. Bardella, C., P.J. Pollard, and I. Tomlinson, *SDH mutations in cancer.* Biochim Biophys Acta, 2011. **1807**(11): p. 1432-43.
247. Schmitt, S., et al., *A semi-automated method for isolating functionally intact mitochondria from cultured cells and tissue biopsies.* Anal Biochem, 2013. **443**(1): p. 66-74.
248. Vondrusova, M., et al., *The effect of mitochondrially targeted anticancer agents on mitochondrial (super)complexes.* Methods Mol Biol, 2015. **1265**: p. 195-208.
249. Wittig, I., M. Karas, and H. Schagger, *High resolution clear native electrophoresis for in-gel functional assays and fluorescence studies of membrane protein complexes.* Mol Cell Proteomics, 2007. **6**(7): p. 1215-25.
250. The Jackson Laboratory. *NSG-SGM3*. 2021 28. 07. 2021]; Available from: https://www.jax.org/strain/013062.
251. Dong, L., et al., *Mitocans Revisited: Mitochondrial Targeting as Efficient Anti-Cancer Therapy.* Int J Mol Sci, 2020. **21**(21).
252. Hubackova, S., et al., *Selective elimination of senescent cells by mitochondrial targeting is regulated by ANT2.* Cell Death Differ, 2019. **26**(2): p. 276-290.
253. Neuzil, J., et al., *Alpha-tocopheryl succinate, an agent with in vivo anti-tumour activity, induces apoptosis by causing lysosomal instability.* Biochem J, 2002. **362**(Pt 3): p. 709-15.
254. Neuzil, J., *Vitamin E succinate and cancer treatment: a vitamin E prototype for selective antitumour activity.* Br J Cancer, 2003. **89**(10): p. 1822-6.
255. Neuzil, J., et al., *Selective cancer cell killing by alpha-tocopheryl succinate.* Br J Cancer, 2001. **84**(1): p. 87-9.
256. Dong, L.F., et al., *Alpha-tocopheryl succinate induces apoptosis by targeting ubiquinone-binding sites in mitochondrial respiratory complex II.* Oncogene, 2008. **27**(31): p. 4324-35.
257. Dong, L.F., et al., *Suppression of tumor growth in vivo by the mitocan alpha-tocopheryl succinate requires respiratory complex II.* Clin Cancer Res, 2009. **15**(5): p. 1593-600.
258. Maio, N., et al., *Disease-Causing SDHAF1 Mutations Impair Transfer of Fe-S Clusters to SDHB.* Cell Metab, 2016. **23**(2): p. 292-302.
259. Wang, J. and K. Pantopoulos, *Regulation of cellular iron metabolism.* Biochem J, 2011. **434**(3): p. 365-81.
260. Zhou, L., et al., *Alterations in Cellular Iron Metabolism Provide More Therapeutic Opportunities for Cancer.* Int J Mol Sci, 2018. **19**(5).
261. Qin, J.Y., et al., *Systematic comparison of constitutive promoters and the doxycycline-inducible promoter.* PLoS One, 2010. **5**(5): p. e10611.
262. Fiala, G.J., W.W. Schamel, and B. Blumenthal, *Blue native polyacrylamide gel electrophoresis (BN-PAGE) for analysis of multiprotein complexes from cellular lysates.* J Vis Exp, 2011(48).
263. Kolaj-Robin, O., et al., *Biochemical and biophysical characterization of succinate: quinone reductase from Thermus thermophilus.* Biochim Biophys Acta, 2011. **1807**(1): p. 68-79.
264. COSMIC – the Catalogue of Somatic Mutations in Cancer, *SDHAF4 Gene*. 2021.
265. National Cancer Institute, *TCGA - SDHAF4 Gene*.
266. Kudryavtseva, A.V., et al., *Mutation profiling in eight cases of vagal paragangliomas.* BMC Med Genomics, 2020. **13**(Suppl 8): p. 115.